NASA ROSES 2008 A.28
NASA Contract Number: NNX09AR68G

High-Resolution Subsurface Physical and Optical Property Fields in the Gulf of Mexico: Establishing Baselines and Assessment Tools for Resource Managers

Final Report, 1 May 2013

PI: Jason K. Jolliff
Naval Research Laboratory, Code 7331
Stennis Space Center, MS 39529
Phone: (228) 688-5587
FAX: (228) 688-4149
Email: jolliff@nrlssc.navy.mil

Co-I: Richard W. Gould, Jr.
Naval Research Laboratory, Code 7331
Stennis Space Center, MS 39529
Email: gould@nrlssc.navy.mil

Contributor: Sergio deRada
Naval Research Laboratory, Code 7331
Stennis Space Center, MS 39529

Contributor: Sherwin Ladner
Naval Research Laboratory, Code 7331
Stennis Space Center, MS 39529

Executive Summary

The goal of this project was to combine satellite data and state-of-the-art ocean models in a manner that provides subsurface material property climatologies that may be readily accessed by resource managers and decision-makers. This approach was applied to two key Gulf of Mexico habitats: (1) the coral reef communities of the Flower Garden Banks National Marine Sanctuary (FGBNMS); and (2) the bays and estuaries of the northern Gulf of Mexico. A 9-year hindcast ocean simulation was used to estimate monthly climatological conditions for coral reef communities within FGBNMS and surrounding habitat areas of particular concern (HAPCs). Input to these calculations made extensive use of NASA sensors and reanalysis products (MERRA, OASIM, EOS). These subsurface material property estimates compare favorably with in situ observations and bolster confidence that the datasets offer a robust estimate of subsurface marine environmental conditions for the first decade of the 21st century. The datasets were transitioned to end-user (NOAA) through the National Coastal Data Development Center's (NCDDC) graphical user interface web portal for the FGBNMS: (http://www.ncddc.noaa.gov/website/google_maps/FGB/mapsFGB.htm). This portal provides a means for decision-makers and the general public to visualize and access the datasets provided.

With respect to northern Gulf bays and estuaries, a climatology of satellite ocean color imagery was constructed to provide baseline optical conditions and turbidity loads. The U.S. Army Corps of Engineers (USACE) is responsible for dredging operations along Alabama and Florida coasts. Baseline knowledge of background optical properties is required to assess the impact of dredging on the environment and it will help inform resource management decisions related to flood protection and coastal restoration. Thus, this component of the project developed time series of high-resolution remote sensing imagery covering the northern Gulf of Mexico in order to: 1) provide regional and local-scale characterization of bio-optical properties for coastal habitats, and 2) help assess natural variability of those properties. The Naval Research Laboratory at Stennis Space Center (NRL/SSC) has processed and archived five years (2005-2009) of satellite imagery from the Moderate Resolution Spectral Imager (MODIS) at 250m spatial resolution. Derived optical and biogeochemical properties include the diffuse attenuation coefficient at 488 nm (K_d488), the euphotic depth (Z_{eu}), and concentrations of total suspended solids (TSS) partitioned into particulate organic matter (POM) and particulate inorganic matter (PIM) components. All of the imagery (weekly and monthly composites), extracted data, analysis figures, and this report are available at the web site: http://www7331.nrlssc.navy.mil.

This work is consistent with the Gulf of Mexico Alliance's (GOMA's) partnership goal to "Identify, inventory, and assess the current state of and trends in priority coastal, estuarine, nearshore, and offshore Gulf of Mexico habitats to inform resource management decisions" [*GOMA,* 2006]. Collectively, our products establish a quantitative measure of baseline environmental variables relevant to the management of critical habitat areas.

1. Introduction

The Flower Garden Banks National Marine Sanctuary (FGBNMS) consists of three separate areas in the northwestern Gulf of Mexico where salt dome crests rise to within 18-meters of the surface from an outer-continental shelf relief of 100-150-meters [*Lugo-Fernandez et al.*, 2001]. The coral reefs that have developed on the top of these unusual topographic features are recognized the healthiest in United States waters [*Lang et al.*, 2001; *Rezak et al.*, 1985]. Since the original FGBNMS boundary designation in January 1992, high-resolution multibeam bathymetry surveys have revealed numerous other topographic features in the surrounding region capable of supporting biological communities designated by the FGBNMS managers as critical habitats. Within the FGBNMS management framework, it is now recognized that numerous geologic features throughout the region may support biological communities that are ecologically linked to one another [*FGBNMS*, 2008], and these communities may warrant protection through proposed boundary expansion of the FGBNMS. Habitat identification and characterization is an objective of the Gulf of Mexico Alliance [*GOMA*, 2006] that must directly inform and guide the FGBNMS boundary expansion process.

Accordingly, our first set of objectives for this project was to establish baseline environmental conditions for the FGBNMS and adjacent benthic habitats where high-resolution bathymetry surveys have been performed. This high-resolution subsurface characterization was to serve two purposes (1) establish a baseline record of environmental conditions that may be compared to continuing survey work by FGBNMS staff and other researchers, and (2) establish baseline environmental conditions for areas that have been mapped by habitat type designation via Remotely Operated Vehicle (ROV) and diver surveys so that potential projections of habitat type may be made where no such detailed surveys have been performed. Working with our end-users at NOAA's National Coastal Data Development Center (NCDDC), we have thusly incorporated our baseline environmental climatologies into their web-based mapping portal (the end-user environment). These data are available to researchers and resource managers and may serve additional purposes not enumerated above or herein.

The second decision-making activity our project addressed concerned USACE dredging operations along coastal regions in the northern Gulf of Mexico. During these projects, the disposal of the dredge spoils generates turbidity plumes that must be monitored in both upstream and downstream directions to ensure that suspended sediment loads to don't exceed allowable state thresholds. Different thresholds are enforced in different states. For example, Mississippi and Alabama allow turbidity levels up to 50 NTU, whereas the threshold in Florida is lower (29 NTU, or lower near aquatic reserves). These discrepancies appear to arise over different estimates concerning what constitutes a "natural" or "background" level of water column turbidity.

In order to provide a more comprehensive dataset to establish reference levels, time series of high-resolution ocean color imagery and products was constructed in northern Gulf Coast estuaries. Our high-resolution (250-meter) satellite sediment maps provide

climatological information to assess natural variability and will facilitate comparisons between current conditions (that result from the dredging) and historical baseline conditions.

As the project was pursued, the Flower Garden Banks (FGB) work was lead by the project Principal Investigator, Jason Jolliff. Section 2 describes the work completed in that task area. Co-Investigator, Richard W. Gould, Jr, completed the Gulf Coast estuary work using MODIS 250m resolution satellite products. The third section of this report describes those efforts. Additional inquiries regarding end-user support, data availability, and methods for Gulf Coast estuary sediment loads and optical properties should be directed to Co-I Richard W. Gould, Jr. (gould@nrlssc.navy.mil).

In both task areas, the common theme is that we are using NASA satellite resources and data products to provide a baseline for environmental variables that may be used by resource mangers as assessments tools that will inform their decision-making activities. The term "baseline" has particular emphasis here and is a reference to the shifting baselines concept first introduced in the early 1990's by fisheries biologists [*Sheppard*, 1995]. The concept is that over time the anthropogenic influence may slowly shift perception of what constitutes "natural" variably for environmental variables in marine systems. These anthropogenic influences are manifold: overfishing, climate change, increasing coastal populations, urban/agricultural runoff, eutrophication, ocean acidification, hypoxia, poor water quality, etc. Our purpose is not to establish "natural" or "pristine" environmental markers, but rather, to establish where the present state of the marine environment exists for the initial decade of the 21st century.

Section 2. Flower Garden Banks (FGB) Subsurface Property Fields

2.1. FGB Temperature Products

The essential task of this project is to combine satellite data with ocean models in order to establish baseline environmental conditions for coastal and shelf marine habitats and to communicate this information to decision-makers and environmental resource managers. This section focuses upon efforts dedicated to the FGBNMS and surrounding structures identified by FGBNMS staff as "Habitat Areas of Particular Concern" (HAPCs; Figure 2-1). Accordingly, our first step was to establish a nested ocean model hierarchy for the Gulf of Mexico in order to provide background and high-resolution blended model/data products to the end-user. We completed our nested numerical ocean model setup in the Gulf of Mexico with the Navy Coastal Ocean Model (NCOM; Figure 2-2) [*Barron et al.*, 2004; *Kara et al.*, 2006; *Martin*, 2000]. This particular NCOM configuration is also referred to herein as the Gulf of Mexico Modeling System (GOMMS) [*deRada et al.*, 2009, 2011]. NCOM is the main oceanographic forecasting system for nested numerical ocean modeling at the U.S. Naval Oceanographic Office [*Rhodes et al.*, 2002].

NCOM is, however, a stand-alone ocean model: i.e., it requires atmospheric forcing as boundary conditions (wind stress, air temperature, humidity, solar shortwave, etc.). In operational forecasting mode, Navy atmospheric models such as NOGAPS or COAMPS

may provide these forcing data. Herein we sought to execute the model in "hindcast" mode for 9-years of continuous simulation (2000-2008). To accomplish this task we utilized atmospheric reanalysis products from NASA's Modern-Era Retrospective Analysis for Research and Applications (MERRA):

"MERRA is a NASA reanalysis for the satellite era using a major new version of the Goddard Earth Observing System Data Assimilation System Version 5 (GEOS-5). The Project focuses on historical analyses of the hydrological cycle on a broad range of weather and climate time scales and places the NASA EOS suite of observations in a climate context." (http://gmao.gsfc.nasa.gov/merra/)

The MERRA products [*Rienecker et al.*, 2011] provided the atmospheric boundary conditions required for the extended hindcast NCOM simulations. We have completed 9-years of simulated ocean circulation and air/sea thermal exchange in the Gulf of Mexico utilizing the nested configuration shown in Figure 2-2. The inner nest resolution, down to nominally sub-kilometer, was constructed around the Flower Garden Banks National Marine Sanctuary and adjacent structures identified with high-resolution bathymetry surveys [*Gardner et al.*, 1998]. Bathymetry data for the GOMMS domain was obtained from the General Bathymetric Chart of the Oceans (GEBCO) 30-arc-second gridded bathymetry dataset (http://www.gebco.net/).

The long-term simulations utilizing numerical forecast models designed for much shorter durations (~ 2 – 30 days) require additional constraints. Our implementation of NCOM utilized a relaxation scheme to synthetic three-dimensional temperature fields provided by the Modular Ocean Data Assimilation System (MODAS) [*Fox et al.*, 2002]. MODAS synthetics have been previously used to examine three-dimensional temperature structure in the Gulf of Mexico [*Jolliff et al.*, 2008]. Briefly, MODAS uses a global grid (1/8°) subsurface climatology of temperature derived from the U.S. Navy's Master Ocean Observation Database (MOODS). MODAS then assimilates remotely-sensed sea surface temperature (SST) and sea surface height (SSH) data that have been optimally interpolated [*Bretherton, et al.*, 1976] onto a two-dimensional grid. Departure from the subsurface MOODS long-term climatology is then calculated based on regression coefficients that derive subsurface temperature from SSH and SST. The result is a synthetic three-dimensional temperature field.

Relaxation to MODAS synthetics constrained the model results to the satellite ocean temperature observations whilst still allowing the model to respond to the atmospheric forcing provided by the MERRA products. Following execution of the 9-year hindcast simulation utilizing the nested GOMMS domain, temperature and other physical data (salinity, current velocity) were further post-processed into monthly climatology products at the spatial resolution of the fine-scale bathymetry (nominal 5-meter horizontal resolution). These bathymetry products are available via the USGS (http://walrus.wr.usgs.gov/pacmaps/wg-index.html) and are a result of multibeam sonar surveys in the region [*Gardner et al.*, 1998]. The surveys were distributed into 10 main datasets encompassing 10 main banks or combined bank complexes (Figures 2-3 to 2-4):

1) East Flower Garden Bank
2) West Flower Garden Bank
3) Geyer Bank
4) Jakkula Bank
5) MacNeil Bank
6) Stetson Bank
7) Sonnier Bank
8) Bright and Rankin Banks
9) Alderdice Bank
10) McGrail, Bouma, Rezak, Sidner Banks

The final post-processing step was to perform a bilinear interpolation of the results from the inner ocean model nest down to the high-resolution bathymetry provided by the USGS. It was not feasible to perform hydrostatic ocean model calculations at the native high-resolution bathymetry (5-meters) due to both the computational resource limitations and the inherent presumptions of hydrostatic models. Herein, we perform the interpolative post-processing steps to render the model products at the fine-scale resolution of the bathymetry. An example of the results, mean bottom temperatures for August (derived from the entire 9 year simulation) are presented in Figure 2-5.

These products are being transitioned to our collaborating partners at the NOAA/NCDDC for integration into the GIS-based GUI available to the public at http://www.ncddc.noaa.gov/website/google_maps/FGB/mapsFGB.htm (POC – Rost Parsons, *National Coastal Data Development Center*, Stennis Space Center). As the data are transitioned on-line for public display, a test site is also available to preview the products: (http://www.ncddc.noaa.gov/website/AGSViewers/FGB/mapsFGB.htm).

As an example of the GUI via NCDDC, Figure 2-6 shows the data menu (at left) where the user may select the bank and monthly mean temperatures to display. The data are contoured at right. Other data may be superimposed upon the temperature maps. Monthly mean temperatures for each bank area enumerated above were transitioned to NCDDC. Daily means are also available but have not been transitioned due to storage/size limitations. Those data have been saved to removable Western Digital SATA hard disks (2 TB per unit). The data are available for distribution upon request.

2.2. FGB Temperature Verification

As transition of our products to the end-user occurred, we were able to leverage two additional NRL projects that were underway in the Flower Garden Banks: (1) NOAA-funded "Current-Topography Interaction and its Influence on Water Quality and Contaminant Transport over Shelf-Edge Banks: Currents over Banks (COB)" and (2) NRL-funded "Mixing Over Rough Topography (MORT)." The objective of these projects was to observe, understand, and quantify the mixing mechanisms that determine vertical transport and lateral spreading of mass, momentum and scalars over sub-mesoscale bathymetric features in the coastal environment. As an example of the data

provided, temperature comparisons have been made between our high-resolution inner ocean model nest and CTD casts made during the June 2011 research cruise to the Flower Garden Banks (Figure 2-7). The results confirm model fidelity to observations and were presented at the 2012 Ocean Sciences meeting [*deRada et al.*, 2012].

More specific product verification of bottom water temperatures over the banks was achieved via comparisons to data contained within the FGBNMS long-term monitoring reports (available at http://flowergarden.noaa.gov/document_library/scidocs/). Particularly the 2003, and 2004-2005 monitoring reports [*Precht et al.*, 2008; *Precht et al.*, 2006]. In both studies, continuously recording moored monitoring equipment (YSI Datasondes and HoboTemp Thermographs) were deployed and refurbished at intervals of ~3-4 months on the East and West Flower Garden Bank reef caps. Here we compare our daily high-resolution climatology to the temperature records in these reports. The HoboTemp thermograph recorded temperature every hour (to within 0.02 °C at 25.0 °C [*Precht et al.*, 2006]); we averaged these measurements over the 24-hour period to calculate a daily observed average. The comparison is made to the nearest corresponding location in the FGB temperature climatology.

At an approximate depth of 27 m over the West Flower Garden Bank reef cap, the daily climatology compares well with observations from 2003 and 2004 (Figure 2-8). We examine three aspects of statistical comparison: linear correlation of time series (r), the difference between the time series means (bias), and the root-mean-square error (RMSE). In 2003, the bias is below the instrument sensitivity and in both years the linear correlation is above .93 – suggesting the climatology gives reasonable fidelity to the annual temperature patterns on the reef caps. RMSE in both years is nominally just above 1 °C – a statistic likely representative of higher frequency variability in the observations not captured by climatological averaging.

Model-data comparison statistics over the West Flower Garden Bank are quite different in 2005 (Figure 2-9). Peak summer temperatures observed are well above the climatological calculation by as much as ~ 3 °C. However, we interpret this as a success of the climatology rather than a deficiency. The summer 2005 was a truly anomalous thermal stress/coral bleaching event for the Flower Garden Banks [*Precht et al.*, 2008] and for coral reef communities across the Caribbean [*Eakin et al.*, 2010]. This suggests the climatology succeeds in presenting a baseline condition against which anomalous events or longer-term trends may be assessed.

2.3. FGB Bottom Light (PAR) Products

In addition to temperature, coral reef communities are sensitive to the amount of penetrating Photosynthetically Available Radiation (PAR) [*Dustan*, 1982; *Frade et al.*, 2008; *M. P. Lesser*, 2004; *Michael P. Lesser et al.*, 2009; *Wyman et al.*, 1987]. Most zooxanthellate coral species are thus restricted to depths of ~ 60 m or less [*Lesser et al.*, 2009]. However, macroalgae and sponges harboring photosynthetic bacteria (important components of coral reef communities within FGBNMS [*DeBose et al.*, 2013]) are also sensitive to the light environment [*Gattuso et al.*, 2006]. It is theorized that the impact of

water quality upon light penetration may be a significant controlling factor for the ecological shifts in benthic communities observed recently in the FGBNMS and adjacent HAPCs [*DeBose et al.*, 2013].

Motivated by these facts, we sought to create a high-resolution climatology of incident PAR fields for the benthic habitats that would compliment the temperature climatology described above. The mechanistic structure required to create such a record consists of (3) key ingredients: (1) an estimate of the incident PAR at the air-sea interface (after transmission through the intervening atmosphere); (2) an estimate of the surface optical properties in the water column that will impact the depth of light penetration into the ocean; (3) a radiation transfer model to simulate the depth-dependent PAR penetration from just beneath the air-sea interface to the bottom. These components were addressed with the following corresponding models/data-products [*Jolliff et al*., 2010]:

(1) NASA's Ocean Atmosphere Spectral Irradiance Model (OASIM; http://gmao.gsfc.nasa.gov/research/oceanbiology/) and cloud data from the International Satellite Cloud Climatology Project (ISSCP; http://isccp.giss.nasa.gov/)
(2) Mapped -processed 8-day composite Sea-viewing Wide Field-of-view Sensor (SeaWiFS) mission record data from NASA's Ocean Color Group at GSFC (http://oceandata.sci.gsfc.nasa.gov/SeaWiFS/Mapped/)
(3) Penetrating/broadband PAR radiative transfer numerical model [*Lee et al.*, 2005] that approximates the more complex hyperspectral calculations of HYDROLIGHT [*Mobley*, 1994].

1- OASIM – This component is a spectrally/directionally decomposed atmospheric radiative transfer model that builds on earlier formulations [*Gregg and Carder*, 1990] specific to maritime conditions. The revised implementation, however, takes advantage of atmospheric and meteorological data from a variety of NASA missions [*Gregg and Casey*, 2009]. Briefly, atmospheric aerosol data are derived primarily from the Moderate Resolution Imaging Spectroradiometer (MODIS). Ozone data are from the Total Ozone Mapping Spectrometer (TOMS) on the Nimbus -7 and Earth Probe spacecraft. Cloud data are from the International Satellite Cloud Climatology Project (ISSCP). Additional atmospheric parameters are taken from the National Center for Environmental Prediction (NCEP) reanalysis products. An advantage of OASIM is that it calculates spectrally decomposed transmittance/reflectance at the air-sea interface whilst accounting for the impact of sea foam (rough seas) [*Frouin et al.*, 1996].

The OASIM data products are distributed via NASA's Global Modeling and Assimilation Office (GMAO). The data are spectrally and directionally (direct / diffuse) decomposed from 200 nm to 4000 nm and provided as monthly means. Herein the additional step was taken to integrate the decomposition:

$$PAR_d = 1/(hcN_a) \int_{350nm}^{700nm} \lambda_m [E_d(\lambda)] d\lambda \quad (1)$$

$$PAR_s = 1/(hcN_a) \int_{350nm}^{700nm} \lambda_m [E_s(\lambda)] d\lambda \quad (2)$$

$$PAR(0^-) = PAR_s(0^-) + PAR_d(0^-) \quad (3)$$

where c is the speed of light, h is Planck's constant, N_a is Avogadro's number, E_d is the direct planar downwelling irradiance (W m^{-2} nm^{-1}) and E_s is the diffuse planar downwelling irradiance (W m^{-2} nm^{-1}). The diffuse and direct components are calculated separately to consider the angular distributions (below). The spectral integration and energy conversion yield PAR just beneath the sea surface [PAR(0^-)] in units μmol photon m^{-2} s^{-1} as a monthly mean photon flux density on a 1° **x** 1° global grid. A similar procedure was used on Gregg and Casey [2009] to compare OASIM products against in situ data as well as SeaWiFS PAR products, as well as ISCCP-FD, NCEP, and ISLSCP-II reanalysis products.

Incident OASIM PAR was utilized at the given spatial resolution: further interpolation did not yield significantly different results – spatial values were assigned based on the nearest 1° **x** 1° degree node. A temporal interpolation was performed to transform monthly PAR to daily PAR assuming the monthly value was centered at mid-month. For each of the (10) FGB domains (Figure 2-3) we calculated a daily PAR time series beginning on 1 January 1998 to 31 December 2006. This is 2-years prior to the start of the temperature time series (2000-2008); it was required so that more of the SeaWiFS mission and the OASIM data records overlapped.

2-SeaWiFS – Global coverage, 9 km, 8-day composite, mapped, SeaWiFS products (OC4-chloorphyll-*a*) were downloaded directly from NASA's Ocean Color Web archive (http://oceandata.sci.gsfc.nasa.gov/SeaWiFS/Mapped/). The mapped latitude and longitude for each "node" were extracted from the HDF file and the 8-day composite images were interpolated to daily values. The goal was to match up the SeaWiFS OC4 daily time series with the OASIM data products.

Why not use daily images or higher spatial resolution satellite products? After some initial experimentation with different satellite data sources it was determined that the OC4-chlorophyll-*a* 8-day composites rendered the most consistent time series over the duration of the SeaWiFS mission record; i.e., the processed 8-day OC4 products appeared to be less contaminated with image artifacts associated with edge-of-cloud pixilation,

edge-of-swath contamination, and other known problems [*Hooker and McClain*, 2000; *O'Reilly et al.*, 1998; *Robinson and Wang*, 2000].

3 – Numerical Radiative Transfer – A network of nodes were mapped based on the SeaWiFS resolution and matched to the nearest OASIM grid point. The results were complimentary pairs of incident irradiance and surface satellite chlorophyll-*a* estimates (referenced herein as Csat) with daily values extending over 1998-2006. The first step was to implement the numerical radiative transfer model of Lee et al. [2005], or LE05, at the native SeaWiFS resolution. LE05 requires, as minimum input to the algorithm, the surface total absorption coefficient at 490-nm ($a490$; m^{-1}), the surface backscattering coefficient ($bb490$; m^{-1}), and the incident PAR (furnished via OASIM). Csat values were converted to the required optical properties via empirically derived relationships. For $a490$, modified third-order polynomial based first on other work [*Morel et al.*, 2007] and then modified to match Case-I *in situ* observations obtained by NRL researchers [*Jolliff et al.*, 2012a] was implemented:

$$\mathrm{Log}_{10}(a490) = (-0.0169)\mathrm{Clog}^3 + (0.0756)\mathrm{Clog}^2 + 0.5542\mathrm{Clog} - 1.1488 \quad (4)$$

where $\mathrm{Clog} = \mathrm{Log}_{10}(\mathrm{Csat})$. The conversion to backscattering is taken from literature for Case-I waters [*Morel and Maritorena*, 2001]:

$$\mathrm{bp550} = 0.416\mathrm{Csat}^{0.766} \quad (5)$$

$$\text{IF } \mathrm{Csat} < 2.0, \mathrm{v1} = 0.5(\mathrm{Clog} - 0.3);\ \text{ELSE } \mathrm{v1} = 0 \quad (6)$$

$$\mathrm{bb490} = [0.002 + 0.01(0.5 - 0.25\mathrm{Clog})]\left(\frac{490}{550}\right)^{v1} \mathrm{bp550} + 0.00012 \quad (7)$$

where bp550 is the particle scattering coefficient at 550 nm (m^{-1}). The remaining algorithm is drawn from LE05 and is computed for the direct and diffuse PAR components at each depth increment. The precise equations are given in LE05 (eq. 7-10). Using a solar period-weighted mean solar zenith angle for each day and applying this angle to the direct PAR attenuation accounted for the angular distribution. For the diffuse term we presume a maximum solar zenith. At each depth increment, the diffuse and direct components are added to yield a total PAR flux at the respective depth.

We performed a daily calculation for the entire combined OASIM-SeaWiFS time series at each SeaWiFS 9km node. For each node the depth resolution was 0.5 meters. The final

step consists of a spatial interpolation from the node values to the high-resolution bathymetry data. The computer code authored specifically for this task identifies the three nearest nodes to the high-resolution latitude/longitude point and provides a distance-weighted interpolation at the respective depth of interest.

The results of these computations are displayed and stored as annual and monthly means from the 1998-2006 daily time series. Daily means are also available. Examples of the annual mean climatologies are displayed in Figures 2-10 to 2-15. In general, the East and West Flower Garden Bank reef cap communities (depth interval ~ 18 – 35 meters) fall into an annual range of 8 – 10 mol photon m^{-2} d^{-1}. This is substantially higher than similar platforms found at midshelf and similar topographic features found elsewhere in the region. The differences arise from the optical properties of the surface waters over the Flower Garden Banks. Their position at the shelf-break (~200 meters depth) permits the clear waters of the pelagic Gulf of Mexico to prevail under most conditions. Towards midshelf, increasing water column turbidity from sediment resuspension, freshwater runoff, and biological productivity prohibit benthic PAR fluxes of similar range. Stetson Bank (Figure 2-15) is a suitable example: the background relief is ~60 meters, however, only small portions of the main platform exceed an annual mean of 5 mol photon m^{-2} d^{-1}. Other shelf break platforms, such as Geyer Bank (Figure 2-12), simply do not rise high enough in the water column to permit exposure to PAR fluxes similar in magnitude to those found on the Flower Garden Bank reef caps – likely prohibiting the colonization of reef building scleractinian coral communities.

2.4. FGB Light Verification

A 22-day survey cruise to the Flower Garden Banks was conducted in May-June 2011 wherein comprehensive optical data were collected. The cruise consisted of station sampling using NRL optics packages: an AC-9 spectrophotometer and a HyperPro hyperspectral downwelling irradiance sensor. The cruise also included the deployment of the ScanFish MK II ('SF') platform. The SF is a remotely operated and towed vehicle that is piloted in the water column from just below the surface to about 150 m depth. Multiple sensors were mounted on the SF platform: AC-9 spectrophotometer for the measurement of multi-spectral absorption, scattering, and beam attenuation coefficients; WET Labs Environmental Characterization Optics (ECO)-BB3 instrument used here for the retrieval of particle backscattering coefficients, Sea-Bird Electronics CTD, a WET Labs ECO chlorophyll fluorometer (Ex/Em 470/695 nm).

The data obtained from this cruise provided an opportunity to verify the calculations described in Section 2.3. First we examined results from the SF tows, particularly the processed AC-9 data. On 10 - 11 June 2011, the SF-mounted AC-9 recorded 206,575 observations of the total absorption coefficient (488 nm m^{-1}) over the East Flower Garden Bank: the mean total absorption coefficient value above 30 meters depth was 0.030 m^{-1}. Our mean satellite based estimate from the 1998-2006 SeaWiFS record (*a*-490) was 0.033 m^{-1}. These results suggest the satellite-based method of extracting water column optical properties was providing reasonable results.

A more rigorous test of our methods was made possible via the HyperPro hyperspectral downwelling irradiance sensor. The hyperspectral downwelling irradiance observations were post-processed via integration to yield downwelling PAR values. We first compared the downwelling PAR expressed as a percent of the surface PAR. The HyperPro instrument is deployed with a complimentary ship-board surface PAR sensor such that integrated in-water values may be expressed as a percent surface PAR. We then calculated the algorithm estimate of % surface PAR based on the methods described in Section 2.3. The results are shown in Figure 2-16: 72 HyperPro casts were performed over the East Flower Garden Bank and the model calculation falls squarely within the observations down to > 80 meters depth and < 1% surface PAR. This dataset thus verifies the specific algorithms used to simulate light propagation for these areas.

Verification of instantaneous PAR fluxes (iPAR - μmol photon m^{-2} s^{-1}) is more challenging. The instantaneous values observed via the HyperPro may be impacted by very high frequency events (such as a cloud passing through the direct solar beam) that are not resolved by our methods. To accommodate the comparison, the HyperPro iPAR data were binned to 0.5 m depth increments and averaged across individual cast observations for each depth-bin. The daily mean climatological photon flux values were then converted to a mean instantaneous value by distributing the daily flux over a primary solar period of 8 hours (neglecting oblique sun angles near dawn and dusk). The comparisons are shown in Figure 2-18: below 20 meters depth the root-mean-square-error (RMSE) between the model and data is < 10 μmol photon m^{-2} s^{-1}. Scaling the RMSE back up to a daily flux yields ±0.28 mol photon m^{-2} d^{-1}.

Our work on using the LE05 algorithm in conjunction with SeaWiFS data was leveraged together with another complimentary project, "Resolving Bio-Optical Feedbacks to Ocean/Atmosphere Dynamics" ONR/NRL, 6.1. This project involves inserting the PAR calculations described here into the numerical ocean circulation models, and coupled-ocean-atmosphere modeling systems. The results from this work were published in Geophysical Research Letters [Jolliff et al., 2012b], and this NASA project is acknowledged therein.

2.5. FGB Ancillary Products

The Gulf of Mexico NCOM configuration also rendered three-dimensional salinity and current fields (velocity components U [East/West], V [North/South] m s^{-1}). It is not presently feasible to transition these products at very high resolution to NCDDC due to storage requirements. NRL will retain these archived model results (2000 – 2008) at native resolution and will provide them upon end-user request or the request of potential end-users not specifically designated in this project. However, no verification of these products has been attempted for the inner model nest, so these products would be provided "as is" without any confidence estimates.

2.6. FGB Summary

Herein we have combined an extraordinary amount of cumulative satellite observations of the ocean and atmosphere as realized into data products, reanalysis products, and constraints on modeling systems. The end result is our best estimate of climatological conditions for temperature and light for benthic coral community habitats of the FGBNMS and adjacent areas at very high spatial resolution. To our knowledge, this is the first time such an undertaking has been synthesized in this manner.

These products have been transitioned into the NCDDC user interface to provide ease of access to NOAA FGBNMS staff, scientific researchers, and the general public. We note that continuing improvement of the products and methods developed will be sought through follow-on projects. We also note that the methods developed here may be applied to any other marine habitat where high-resolution bathymetry data are available.

Here we refrain from quantitative assessment of end-user impact until further time has elapsed to allow the wider dissemination of these data products. As these end-user data and feedback become available, we will gladly furnish NASA with all available information.

Section 3. Northern Gulf of Mexico: Five-Year Ocean Color Time Series

NRL has collected and processed high-resolution (250m) MODIS ocean color imagery covering selected bays in the northern Gulf of Mexico along the Alabama to Florida coast for a five year period from 1 January 2005 through 31 December 2009. Weekly and monthly composite images were created to reduce the effects of clouds. The specific bays of interest are: Mobile Bay, Pensacola Bay, Choctawhatchee Bay, and St. Andrews Bay (Figure 3-1). For each bay, multiple subregions within the bay were created to examine within-bay variability of bio-optical properties (Figures 3-2 to 3-5); pixel data were extracted from the weekly and monthly composite images and spatially averaged over the subregions shown in Figures 3-2 to 3-5.

<u>The goals of this project component were to:</u>

- Develop a 5-year time series of high-resolution satellite imagery covering the northern Gulf of Mexico.
- Use this image climatology to establish baseline bio-optical properties for coastal habitats in the Northern Gulf of Mexico.
- Provide regional and local-scale characterization of the bio-optical properties.
- Perform time-series analyses to help elucidate and assess natural variability of those properties.

All goals have been completed. These analyses provide insight into the magnitude, distribution, and variability of bio-optical properties in highly dynamic coastal estuaries and bays along the northern Gulf of Mexico coast. The 250m resolution MODIS optical products provide a capability to examine fine-scale distributions in coastal areas.

3.1. Sensor Data Processing

All MODIS ocean color imagery was processed using an Automated Processing System (APS) developed by NRL/SSC. APS is a powerful, extendable, image-processing tool that produces daily, near real time ocean color products from multiple satellite sensors (AVHRR, SeaWiFS, MODIS, MERIS, OCM, GOCI, and HICO). It is a complete end-to-end system that includes sensor calibration, atmospheric correction (with near-infrared correction for coastal waters), and bio-optical inversion. APS incorporates, and is consistent with, the latest NASA ocean color processing software (SeaDAS) and enables us to produce the NASA standard ocean color products, as well as Navy-specific products using NRL algorithms [Martinolich & Scardino, 2011]. This allows us to test and validate new products and algorithms, and to reprocess many data files (dozens of scenes/day). Furthermore, we can automatically extract image data from regions-of-interest to facilitate time-series analyses and from specific locations for match-ups with in situ data. APS is easily modified to process new geographic areas-of-interest. NRL/SSC is one of only a few institutions that has digested and implemented the complete MODIS processing code, and we have also implemented VIIRS processing. We maintain the code for compatibility with NASA/Goddard.

This work utilized a suite of bio-optical and biogeochemical products derived from MODIS-Aqua imagery: (1) Diffuse Attenuation coefficient at 488 nm (K_d488; m^{-1}); (2) Euphotic Depth (Z_{eu}, m); (3) Total Suspended Solids concentration (TSS, mg l^{-1}); (4) Particulate Organic Matter concentration (POM, mg l^{-1}); and (5) Particulate Inorganic Matter concentration (PIM, mg l^{-1}). Euphotic depth is the depth of the 1% light level. TSS is the sum of PIM + POM. The daily, level 1B MODIS imagery was obtained from the NASA LAADS website (http://ladsweb.nascom.nasa.gov), ingested into APS, processed with our latest atmospheric correction and bio-optical algorithms, and archived. $K_d(488)$ and Zeu were calculated using the algorithms described in Lee et al. [2005] and Lee et al. [2007]. For the PIM, POM, and TSS values, the absorption and backscattering coefficients were first calculated from the satellite water-leaving radiances[Lee et al., 2002]; these coefficients were then used in empirical relationships to estimate PIM, POM, and TSS following Gould at al. [2006]:

Input satellite chlorophyll, $a_t(412)$, $a_t(443)$, $b_b(555)$
Calculate b(555) from $b_b(555)$
Calculate a_{ph} from chlorophyll
Calculate a_p open-ocean (i.e., no sediment) from a_{ph}
Calculate $a_d = a_p$ open-ocean - a_{ph}
Calculate TSS from b555
Calculate POM from $a_{ph}(443)$
Calculate PIM = TSS - POM

3.2. Time-Series Analysis (Monthly Composites)

A climatology was created for the northern Gulf of Mexico, covering the coastal areas from eastern Louisiana to the west Florida panhandle. Monthly composite images from 2005-2009 were created for each of the 5 satellite-derived bio-optical properties

enumerated above, at 250 m spatial resolution. From the monthly composites, 12 "average" monthly images were created for each product. In other words, from the 5 January images from 2005-2009, an average image was created to represent "typical" January conditions. These images are shown in Figures 3-6 through 3-10 for $K_d(488)$, Z_{eu}, PIM, POM, and TSS, respectively. These monthly averages help visualize the seasonal cycles for each property. For example, for Mobile Bay the highest TSS values are observed in the Bay from December through April, with lower values in the summer and fall months (Figure 3-10). Since the diffuse attenuation coefficient, $K_d(488)$, is directly related to the suspended particulate load, the highest values of $K_d(488)$ are observed in the same months (Figure 3-6). The euphotic depth, Z_{eu}, however, is inversely related to the particulate load (i.e., higher suspended particles leads to reduced light penetration and thus a shallower 1% light level), so the seasonal pattern is reversed compared to TSS (lowest Z_{eu} values, shallowest light penetration in the winter and spring months, December through April; Figure 3-7).

3.3. Time-Series Analysis (5-Year Monthly Averages, Within-Bay Variability)

Pixel values were extracted from the monthly composite images and averaged for each subregion in each of the bays. Again, "average" monthly conditions were estimated by averaging all January values, all February values, etc., and annual plots were generated to facilitate monthly comparisons of within-bay variability. Figures 3-11 to 3-12 show the monthly average bio-optical values (and standard deviations) for each of the five satellite products for each of the three subregions in Mobile Bay: the plume, Lower Bay, and Upper Bay areas depicted in Figure 3-2. Each subregion is plotted in a separate color in Figures 3-11 to 3-12, so we can more easily examine differences in the properties between subregions within the same bay. For example, in Figure 3-11, there is a slight seasonal pattern for $K_d(488)$ in the plume (red points), but a more pronounced pattern in both the Upper and Lower Bay (green and blue points, respectively). Lowest values are observed in the July – September time frame in each region, and highest values in the winter and early spring. Euphotic depth is inversely related to $K_d(488)$, so the deepest light penetration is observed in the late-summer when the water is the clearest (Figure 3-11). Similar seasonal patterns are observed for PIM and TSS in Figure 3-12, suggesting that the inorganic component is more important than the organic component in controlling the seasonal pattern of the suspended particulate load in the Mobile Bay region. Both TSS and PIM have the highest values in the winter and early spring, demonstrating the tight coupling to $K_d(488)$. POM shows a spring peak, particularly in April in the Bay. Similar plots are shown for Pensacola, Choctawhatchee, and St. Andrews Bays in Figures 3-13 to 3-18.

3.4. Time-Series Analysis (Weekly Averages for 5-Years, Within-Bay Variability)

In addition to the extracted monthly averages, pixel values were also extracted from the weekly composite images and averaged for each subregion in each of the bays, to examine finer temporal-scale variability. Time-series plots were generated to facilitate comparisons of within-bay variability. Figures 3-19 to 3-20 show the weekly averages for the five-year period from 2005-2009 for each of the five satellite bio-optical products

for each of the three subregions in Mobile Bay: the plume, Lower Bay, and Upper Bay areas. Again, each subregion is plotted in a separate color. Kd(488) and Zeu are shown in Figure 3-19, and PIM, POM, and TSS are shown in Figure 3-20.

The ratio of the inorganic suspended material to the organic suspended material (PIM/POM) and the percent of the total suspended load due to the organic component (POM % of TSS) can be used to indicate the relative partitioning of the particulate load, and these time-series for Mobile Bay are shown in Figure 3-21. The organic component is highest in the Bay in mid-summer, with a less-pronounced seasonal pattern in the plume (Figure 3-21). Spikes of low % POM in the shallow areas of the Bay can be related to high wind/wave events that resuspend bottom sediments with a higher relative concentration of inorganic material [Gould et al., 2007], and these events are more frequent during winter months (Figure 3-21).

TSS, PIM, and POM are overlaid together for each subregion in Figure 3-22, to show how the particle composition changes over time in each subregion. In the Upper Bay, the organic load is fairly constant at around 1-2 mg/l (green curve in Figure 3-22), indicating that the variability in the total suspended sediment load is controlled by the inorganic component (red and blue curves in Figure 3-22).

Similar plots are shown for Pensacola, Choctawhatchee, and St. Andrews Bays in Figures 3-23 to 3-35.

3.5. Time-Series Analysis (Weekly Averages for 5-Years, Between-Bay Variability)

The extracted weekly averages for each bay and subregion were also used to examine between-bay variability. For example, the $K_d(488)$, TSS, and Z_{eu} time series for the plume subregions for each bay are compared in Figure 3-36. The Mobile Bay plume has higher $K_d(488)$ and TSS values and a shallower Z_{eu} than the plumes from Pensacola, Choctawhatchee, and St. Andrews Bay, for the entire 5-year period. The Z_{eu} for the Choctawhatchee Bay plume is the deepest, indicating the clearest waters of the four plume regions (green curve in Figure 3-36). The percent of organic matter is fairly constant in each plume, with the lowest values observed in the Mobile Bay plume (red curve, Figure 3-37); the aperiodic low spikes in the data record indicate episodic discharge events with higher inorganic loads.

Similar plots compare the bay subregions in Figures 3-38 to 3-39. For the bay subregions, Mobile Bay has the shallowest Z_{eu} at about 6 - 10 m (red curve in Figure 3-38); this is significantly shallower than the 15 – 30 m Z_{eu} in the Mobile Bay plume (red curve in Figure 3-36). St. Andrews Bay has the deepest Z_{eu} of the 4 bay subregions (cyan curve in Figure 3-38). The organic load is fairly constant at about 35% for the Pensacola, Choctawhatchee, and St. Andrews Bay subregions (POM % of TSS, Figure 3-39). The organic load in Mobile Bay exhibits a much more seasonal pattern, varying from about 10 - 35% of the total suspended particulate concentration, with the highest percentages observed in the mid-summer months (red curve in Figure 3-39).

3.6. Bio-Optical Property Relationships (Weekly Averages for 5-Years, Within-Bay Variability)

Using the extracted weekly average data we also created X/Y scatterplots using various combinations of the bio-optical properties to examine relationships in the bay subregions (within-bay variability). In Figure 3-40, we examine $K_d(488)$ vs. TSS, $K_d(488)$ vs. Z_{eu}, and Z_{eu} vs. TSS relationships in the three subregions in Mobile Bay. Each subregion in the bay is represented by a different color. In all three subregions, there is a linear relationship between $K_d(488)$ and TSS, and exponential relationships between $K_d(488)$ and Z_{eu}, and between Z_{eu} and TSS. A single relationship for each combination of properties seems to hold for all three locations in the bay (i.e., all the points fall along one curve). Similar plots for the other three bays and subregions highlight differences between different parts of the bays (Figures 3-41 to 3-43).

3.7. Bio-Optical Property Relationships (Weekly Averages for 5-Years, Between-Bay Variability)

Similar scatterplots were created using the weekly average data to highlight between-bay variability (Figure 3-44). In this figure, all data from all subregions within a bay are color coded as a single color. Again, a single relationship seems to hold for each bio-optical property pair, but there is more scatter about the relationship, particularly for $K_d(488)$ vs. TSS and Z_{eu} vs. TSS for St. Andrews Bay (cyan points in Figure 3-44). These relationships could be used to provide rough estimates of the bio-optical properties in the bays, if only one of the properties was measured. Furthermore, since the US Army Corps of Engineers frequently measure turbidity in Nephelometric Turbidity Units (NTU) rather than suspended sediment concentration (TSS in mg/l), we developed an equation to convert from TSS to NTU (Figure 3-45). This relationship was developed from *in situ* measurements collected during six cruises in Mississippi Bight and Mobile Bay. TSS was determined gravimetrically and NTU was measured with a Turner Aquafluor instrument.

3.8. High-Resolution, Hyperspectral Imagery

We also processed several high-resolution images collected by the Hyperspectral Imager for the Coastal Ocean (HICO). HICO is the first hyperspectral spaceborne imager specifically designed for environmental characterization of the coastal ocean. HICO has been operating aboard the International Space Station (ISS) since installation on 24 September 2009 [Lewis et al., 2009; Lucke et al., 2011] and provides high-resolution (100m), hyperspectral images over 128 contiguous spectral channels from 350 nm to 1070 nm range. However, it is most sensitive in the spectral wavelengths ranging from 400 nm to 900 nm, which are the most utilized spectral region for ocean color studies. A single HICO scene covers approximately 50 x 200km. Thus, HICO is an ideal tool for coastal studies. NRL is responsible for the HICO target selection, acquisition, data stream, and image processing. A limited set of HICO images covering smaller regions in the Gulf of Mexico was processed through APS to illustrate the high-resolution details of

the bio-optical properties in the coastal areas, and to augment the larger scale, coarser-resolution, multispectral data sets.

Figure 3-46 shows the HICO targets swaths covering the four bays of interest in the northern Gulf of Mexico. A true color HICO image of Mobile Bay on 5 December 2009 is shown in Figure 3-47; the sediment plumes and fronts are clearly visible. The corresponding TSS image derived from the same scene is shown in Figure 3-48, with a zoomed image of the Bay mouth shown in Figure 3-49. Note the areas of high sediment load (dark red colors) in the mid-bay and areas near the coast and Petit Bois Island.

In order to compare the HICO bio-optical property values to those derived from the coarser-resolution (1km) MODIS imagery, we created blotch areas for the HICO scene that roughly corresponded to the 3 Mobile Bay subregions used in the MODIS time-series analysis (Figure 3-50). Pixel values for the five HICO-derived bio-optical properties were extracted from the 9 December 2009 image for each of the three blotch areas and compared to the MODIS-derived values from the weekly composite image corresponding to the same time frame (12/3/2009 – 12/10/2009) as the HICO image. In general, there is good agreement between the HICO and MODIS values, although the differences increase somewhat moving northward from the plume, through the Lower Bay to the Upper Bay (Figure 3-51).

A HICO scene covering Pensacola Bay on 11 September 2011shows the details of coastal features in that area (Figures 3-52 to 3-54).

3.9. Northern Gulf Coast Summary

- MODIS imagery covering the northern Gulf of Mexico from 2005-2009 was acquired and processed through the NRL APS.
- Bio-optical products were produced at 250m resolution for 4 bays: Mobile, Pensacola, Choctawhatchee, and St. Andrews.
- Bio-optical products included: K_d488, Z_{eu}, TSS, POM, and PIM.
- Weekly and monthly composite images for each product and bay were created.
- Time-series analyses were performed to examine within-bay and between-bay bio-optical variability.
- Several high-resolution, hyperspectral images from HICO were also processed and analyzed, to provide examples of more detailed distributions of the optical properties in and around the bays.
- MODIS imagery and extracted data are available at: http://www7331.nrlssc.navy.mil/view_project.php?project=jolliff2

4. ACKNOWLEDGMENTS

This research was supported by NASA grant NNX09AR68G under the NASA ROSES 2008 A.28 Program, Earth Science for Decision Making: Gulf of Mexico Region.

5. REFERENCES

Barron, C. N., A. B. Kara, H. E. Hurlburt, C. Rowley, and L. F. Smedstad (2004), Sea surface height predictions from the Global Navy Coastal Ocean Model (NCOM) during 1998-2001, *Journal of Atmospheric and Oceanic Technology*, *21*, 1876-1894.

Bretherton, F. P., R. E. Davis, and C. B. Fandry (1976), A technique for objective analysis and design of oceanographic experiments applied to MODE-73, *Deep Sea Research*, *23*, 559-582.

DeBose, J. L., M. F. Nuttall, E. L. Hickerson, and G. P. Schmahl (2013), A high-latitude coral community with an uncertain future: Stetson Bank, northwestern Gulf of Mexico, *Coral Reefs*, *32*(1), 255-267.

deRada, S., R.A. Arnone, S. Anderson, 2009. Bio-physical ocean modeling in the Gulf of Mexico. OCEANS 2009, MTS/IEEE Biloxi - Marine Technology for Our Future: Global and Local Challenges, ISBN: 978-1-4244-4960-6, pp.1-7, 26-29 Oct. 2009 URL: http://ieeexplore.ieee.org/stamp/stamp.jsp?tp=&arnumber=5422217&isnumber=5422059

deRada, S., S. Ladner, B. Casey, R.A. Arnone, J.K. Jolliff, Using Numerical Ocean Models to Test and Validate Empirical Forecasting Systems. ASLO 2011 Aquatic Sciences Meeting, 13-18 February, San Juan, Puerto Rico.

deRada, S., J. Jolliff, R.A. Arnone, J.T. Fasullo, H. Wijesekera, and W.J. Teague (2012), Decadal-scale ocean model simulations in the Gulf of Mexico reveal increasing trends in ocean heat content and seasonal temperature extremes, AGU/ASLO Ocean Sciences Meeting, 20-24 February, Salt Lake City, Utah, USA.

Dustan, P. (1982), Depth-dependent photoadaption by zooxanthellae of the reef coral Montastrea annularis, *Marine Biology*, *68*(3), 253-264.
Eakin, C. M., et al. (2010), Caribbean Corals in Crisis: Record Thermal Stress, Bleaching, and Mortality in 2005, *PLoS ONE*, *5*(11), e13969.

FGBNMS (2008), Draft Options Document for the Flower Garden Banks National Marine Sncuary Management Plan Revision *Rep.*, 12 pp, NOAA-FGBNMS, Galveston, TX.

Fox, D. N., W. J. Teague, C. N. Barron, M. R. Carnes, and C. M. Lee (2002), The Modular Ocean Data Assimilation System (MODAS), *Journal of Atmospheric and Oceanic Technology*, *19*, 240-252.

Frade, P. R., P. Bongaerts, A. J. S. Winkelhagen, L. Tonk, and R. P. M. Bak (2008), In situ photobiology of corals over large depth ranges: A multivariate analysis on the roles of environment, host, and algal symbiont, *Limnology and Oceanography*, *53*(6), 2711-2723.

Frouin, R., M. Schwindling, and P. Y. Deschamps (1996), Spectral reflectance of sea foam in the visible and near-infrared: In situ measurements and remote sensing implications, *Journal of Geophysical Research C: Oceans*, *101*(C6), 14361-14371.

Gardner, J. V., J. D. Beaudoin, J. E. H. Clarke, and P. Dartnell (1998), Multibeam Mapping of Selected Areas of the Outer Continental Shelf, Northwestern Gulf of Mexico--Data, Images, and GIS, *U.S. Geological Survey Open-File Report 02-41*, U.S. Geological Survey, Menlo Park, CA.

Gattuso, J. P., B. Gentili, C. M. Duarte, J. A. Kleypas, J. J. Middelburg, and D. Antoine (2006), Light availability in the coastal ocean: Impact on the distribution of benthic photosynthetic organisms and their contribution to primary production, *Biogeosciences*, *3*(4), 489-513.

Gould, R.W., R.E. Green, P.M. Martinolich, R.A. Arnone. 2006. Physical/Optical Relationships in the Northern Gulf of Mexico. NASA Ocean Color Research Team Meeting, Newport, RI, April 2006.

Gould, R.W., Jr., R.E. Green, P.M. Martinolich, R.A. Arnone. Spatial and Temporal Optical Variability in the Northern Gulf of Mexico. 2007. NASA Ocean Color Science Team Meeting, Seattle, WA, 11-13 April 2007.

Gregg, W. W., and K. L. Carder (1990), A simple spectral solar irradiance model for cloudless maritime atmospheres, *Limnology and Oceanography*, *35*(8), 1657-1675.

Gregg, W. W., and N. W. Casey (2009), Skill assessment of a spectral ocean–atmosphere radiative model, *Journal of Marine Systems*, *76*(1–2), 49-63, doi:http://dx.doi.org/10.1016/j.jmarsys.2008.05.007.

GOMA, Gulf of Mexico Alliance (2006), Governor's Action Plan for Healthy and Resilient Coasts. Electronic Document, (http://www.gulfofmexicoalliance.org/pdfs/gap_final2.pdf); NOAA, U.S. Department of Commerce, 34 pp.

Hooker, S. B., and C. R. McClain (2000), The calibration and validation of SeaWiFS data, *Progress in Oceanography*, *45*, 427-465.

Jolliff, J.K., Richard Gould, Sergio deRada. Establishing Baseline Subsurface Light Fields for the Flower Garden Banks National Marine Sanctuary. Proceedings, Ocean Optics 2010. Anchorage, Alaska. 27 September – 1 October.

Jolliff, J. K., R. W. Gould, Jr., B. Penta, W. J. Teague, S. DeRada, F. P. Chavez, and R. A. Arnone (2012a), Water mass bio-optical properties in the Monterey Bay region: Fluorescence-based inference of shifts in phytoplankton photophysiology, *J. Geophys. Res.*, *117*(C7), C07019, doi:10.1029/2011jc007568.

Jolliff, J.K., T. Smith, S. deRada, R.W. Gould, S. Cayulas, R.A. Arnone, and C. Barron (2012b), The impact of coastal phytoplankton blooms on ocean-atmosphere thermal energy exchange: Evidence from a two-way coupled numerical modeling system. *Geophysical Research Letters*. doi: 10.1029/2012GL053634.

Jolliff, J. K., J. C. Kindle, B. Penta, R. Helber, Z. Lee, I. Shulman, R. A. Arnone, and C. Rowley (2008), On the relationship between satellite-estimated bio-optical and thermal properties in the Gulf of Mexico *Journal of Geophysical Research, Biogeosciences*, *113*, G010204, doi:010210.011029/012006JG000373.

Kara, A. B., C. N. Barron, P. J. Martin, L. F. Smedstad, and R. C. Rhodes (2006), Validation of interannual simulations from the 1/8^{o} global Navy Coastal Ocean Model (NCOM), *Ocean Modelling*, *11*, 376-398.

Lang, J. C., K. J. P. Deslarez, and G. P. Schmal (2001), The Flower Garden Banks: remarkable reefs in the NW Gulf of Mexico, *Coral Reefs*, *23*, 192-194.

Lee, Z., K. Du, R. A. Arnone, S. Liew, and B. Penta (2005), Penetration of solar radiation in the upper ocean: a numerical model for oceanic and coastal waters, *Journal of Geophysical Research*, *110*(C09019, doi:10.1029/2004JC002780).

Lee, Z.P., A. Weidemann, J. Kindle, R. Arnone, K.L. Carder, and C. Davis. 2007. Euphotic zone depth: Its derivation and implication to ocean-color remote sensing. *JGR-Oceans*, 112, C03009, doi:10.1029/2006JC003802.

Lee, Z.P., K.L. Carder, and R.A. Arnone. 2002. Deriving inherent optical properties from water color: a multiband quasi-analytical algorithm for optically deep waters. *Appl. Opt*. 41 (27): 5755-5772.

Lesser, M. P. (2004), Experimental biology of coral reef ecosystems, *Journal of Experimental Marine Biology and Ecology*, *300*(1-2), 217-252.

Lesser, M. P., M. Slattery, and J. J. Leichter (2009), Ecology of mesophotic coral reefs, *Journal of Experimental Marine Biology and Ecology*, *375*(1–2), 1-8, doi:http://dx.doi.org/10.1016/j.jembe.2009.05.009.

Lewis, M.D., R.W. Gould, Jr., R.A. Arnone, P.E. Lyon, P.M. Martinolich, R. Vaughan, A. Lawson, T. Scardino, W. Hou, W. Snyder, R. Lucke, M. Corson, M. Montes, C. Davis. 2009. The Hyperspectral Imager for the Coastal Ocean (HICO): Sensor and Data Processing Overview. Proceedings, Oceans 09 Conference, Biloxi, MS, 26-29 October 2009.

Lucke, R.L., M. Corson, N. R. McGlothlin, S. D. Butcher, D. L. Wood, D. R. Korwan, R. R. Li, W. A. Snyder, C. O. Davis, and D. T. Chen. 2011. The Hyperspectral Imager for the Coastal Ocean (HICO): Instrument Description and First Images, *Appl. Opt.* 50, 1501-1516.

Lugo-Fernandez, A., K. J. P. Deslarzes, J. M. Price, G. S. Boland, and M. V. Morin (2001), Inferring probable dispersal of Flower Garden Banks Coral Larvae (Gulf of Mexico) using observed and simulated drifter trajectories, *Continental Shelf Research*, *21*(1), 47-67.

Martin, P. J. (2000), Description of the Navy Coastal Ocean Model 1.0, NRL Report No. NRL/FR/7322/00/9962, 45 pp.

Martinolich, P. and T. Scardino. 2011. Automated Processing System User's Guide Version 4.2," http://www7333.nrlssc.navy.mil/docs/aps_v4.2/html/user/aps_chunk/index.xhtml, NRL, Washington, D.C.

Mobley, C. D. (1994), *Light and Water*, 595 pp., Academic Press, San Diego, CA.

Morel, A., Y. Huot, B. Gentili, P. J. Werdell, S. B. Hooker, and B. A. Franz (2007), Examining the consistency of products derived from various ocean color sensors in open ocean (Case 1) waters in the perspective of a multi-sensor approach, *Remote Sensing of Environment*, *111*(1), 69-88, doi:DOI: 10.1016/j.rse.2007.03.012.

Morel, A., and S. Maritorena (2001), Bio-optical properties of oceanic waters: A reappraisal, *Journal of Geophysical Research*, *106*(C4), 7163-7180.

O'Reilly, J. E., S. Maritourena, B. G. Mitchell, D. A. Siegal, K. L. Carder, S. A. Garver, M. Kahru, and C. McClain (1998), Ocean color algorithms for SeaWiFS, *Jounal of Geophysical Research*, *103*(C11), 24937-24953.

Precht, W. F., R. B. Aronson, K. J. P. Deslarez, M. L. Robbart, D. J. Evans, B. Zimmer, and L. Duncan (2008), Long-term monitoring at the East and West Flower Garden Banks, 2004-2005 - Interim report. Volume I: Technical Report.*Rep.*, 123 pp, U.S. Dept. of Interior, Minerals Management Service, Gulf of Mexico OCS Rregion, New Orleans, LA.
Precht, W. F., R. B. Aronson, K. J. P. Deslarez, M. L. Robbart, T. J. T. Murdoch, A. Gelber, D. J. Evans, B. Gearheart, and B. Zimmer (2006), Long-term monitoring at the East and West Flower Garden Banks, 2002-2003: Final Report. *Rep.*, 182 pp, U.S. Dept.

of Interior, Minerals Management Service, Gulf of Mexico OCS Region, New Orleans, LA.

Rezak, R., T. J. Bright, and D. W. McGrail (1985), *Reefs and Banks of the northwestern Gulf of Mexic: Their geological, biological, and physical dynamics*, 259 pp., John Wiley and Sons, Inc., New York, NY.

Rhodes, R. C., H. E. Hurlburt, A. J. Wallcraft, C. N. Barron, P. J. Martin, O. M. Smedstad, S. L. Cross, and A. B. Kara (2002), Navy Real-time Global Modeling Systems, *Oceanography*, *15*(1), 29-43.

Rienecker, M. M., et al. (2011), MERRA: NASA's Modern-Era Retrospective Analysis for Research and Applications, *Journal of Climate*, *24*(14), 3624-3648, doi:10.1175/JCLI-D-11-00015.1.

Robinson, W. D., and M. Wang (2000), SeaWiFS Postlaunch Calibration and Validation Analysis, Part I, *"*Vicarious Calibration of SeaWiFS Band 7" **(**/http://seawifs.gsfc.nasa.gov/SeaWiFS/).

Sheppard, C. (1995), The shifting baseline syndrome, *Marine Pollution Bulletin*, *30*(12), 766-767, doi:http://dx.doi.org/10.1016/0025-326X(95)90079-Q.

Wyman, K. D., Z. Dubinsky, J. W. Porter, and P. G. Falkowski (1987), Light absorption and utilization among hermatypic corals: a study in Jamaica, West Indies, *Marine Biology*, *96*(2), 283-292.

6. FIGURES

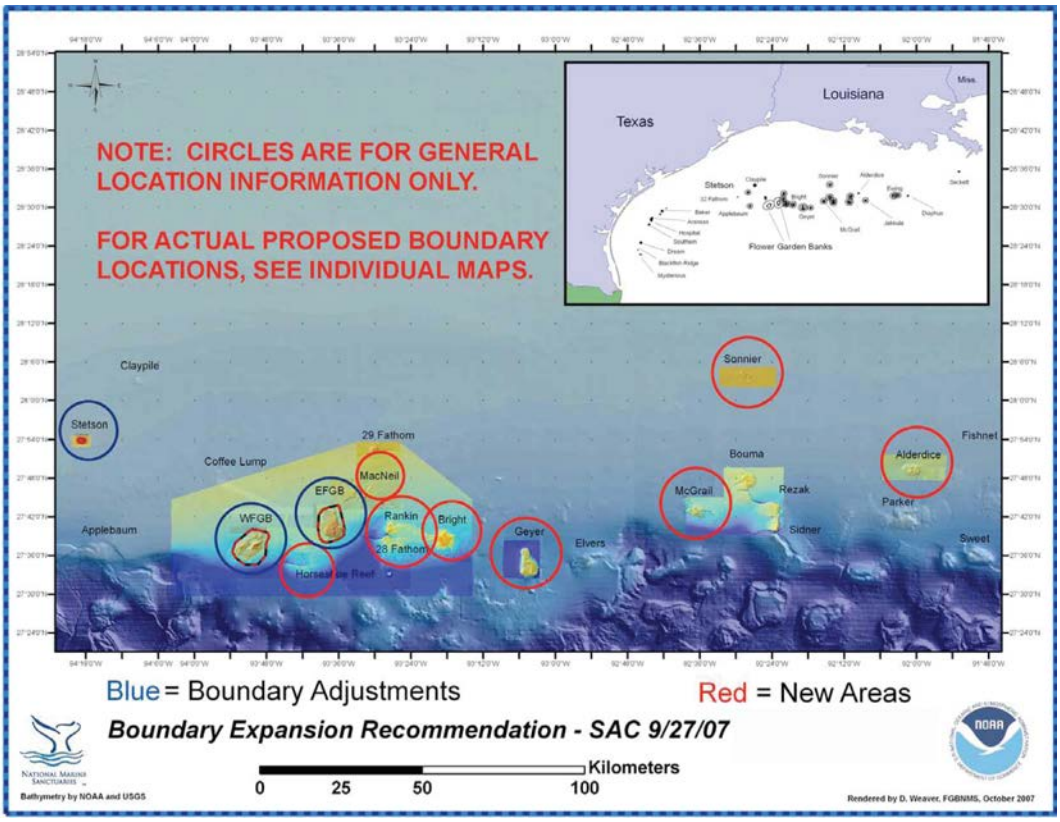

Figure 2-1. Location of FGBNMS and surrounding features shown with high-resolution, multibeam bathymetry. Proposed features considered by the Sanctuary Advisory Council for FGBNMS boundary expansion are shown in red. Reprinted from FGBNMS Sanctuary Advisory Council Boundary Expansion Recommendation Report, 2007. http://flowergarden.noaa.gov

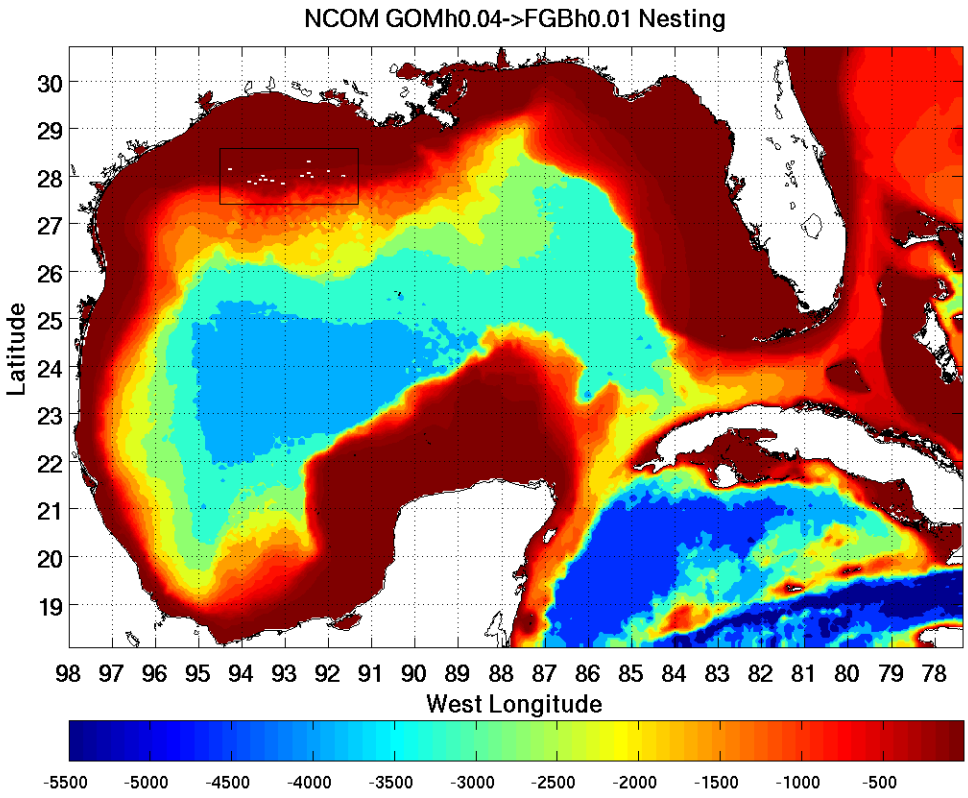

Figure 2-2. NCOM nested model configuration. Outer domain is 4 km, outer Caribbean Sea and Atlantic Ocean boundary conditions are provided by NCOM Global Ocean Model (1/8 °). The inner ocean nest (black lines) is constructed in the northwest Gulf of Mexico around the FGBNMS at higher resolution (almost 1 km horizontal). White patches indicate the bank structures references in the text.

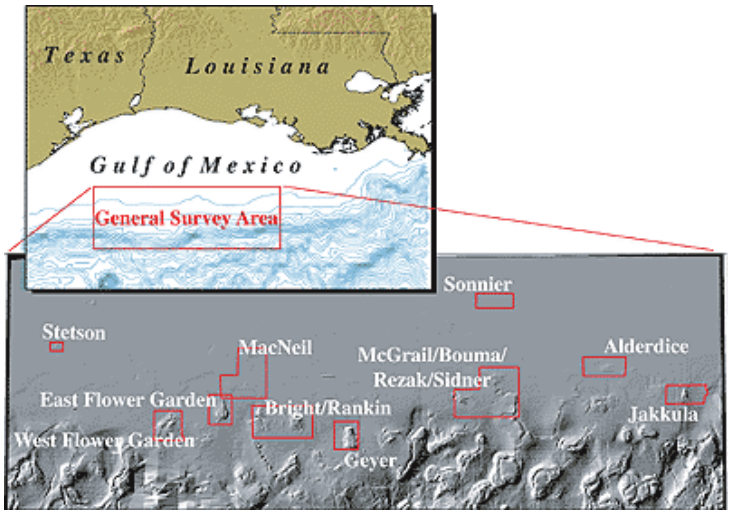

Figure 2-3. Survey areas where high-resolution (5-meter) bathymetry data are available (http://walrus.wr.usgs.gov/pacmaps/wg-index.html).

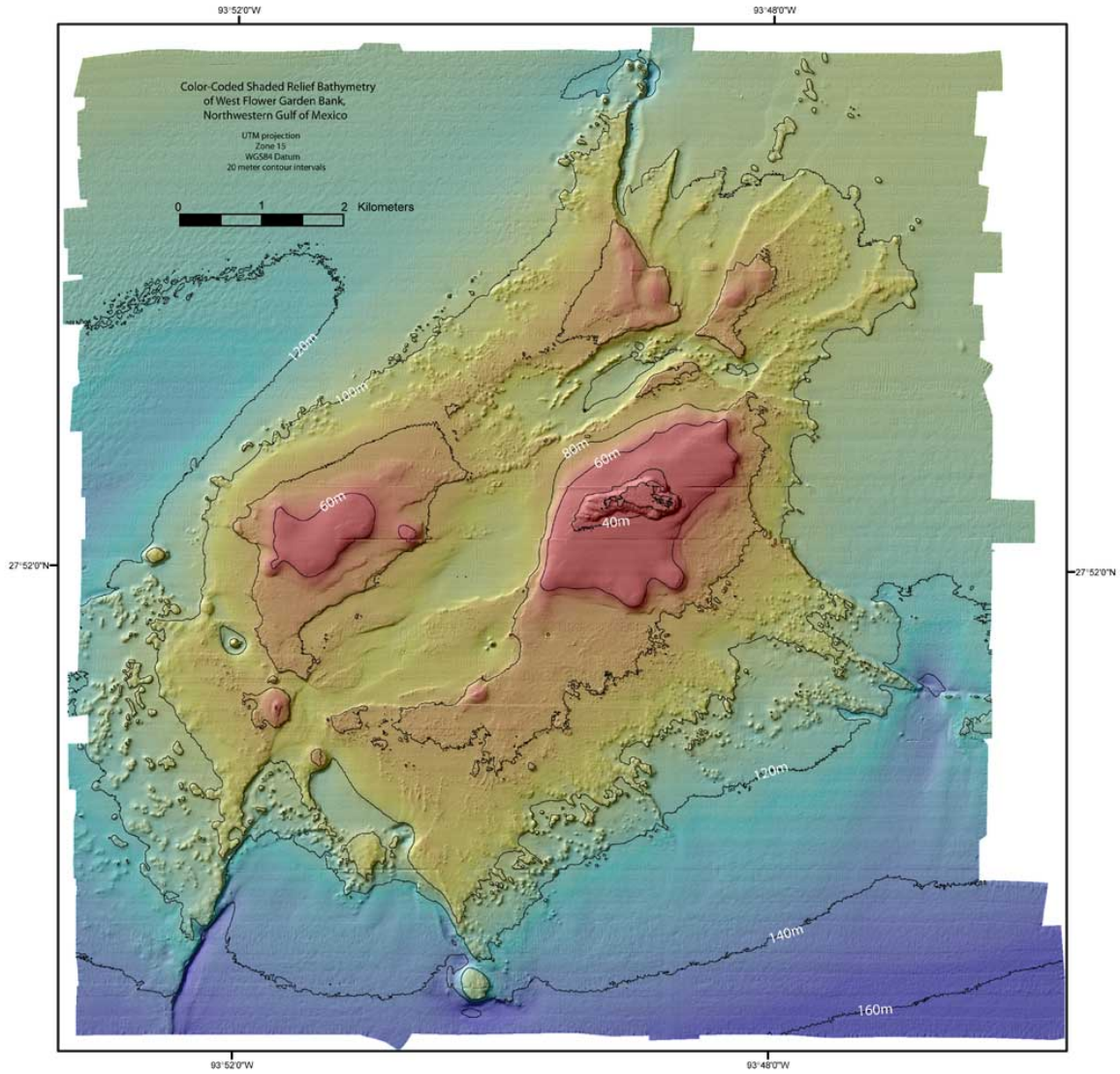

Figure 2-4. Example high-resolution bathymetry for the West Flower Garden Bank. Source: http://walrus.wr.usgs.gov/pacmaps/wg-index.html.

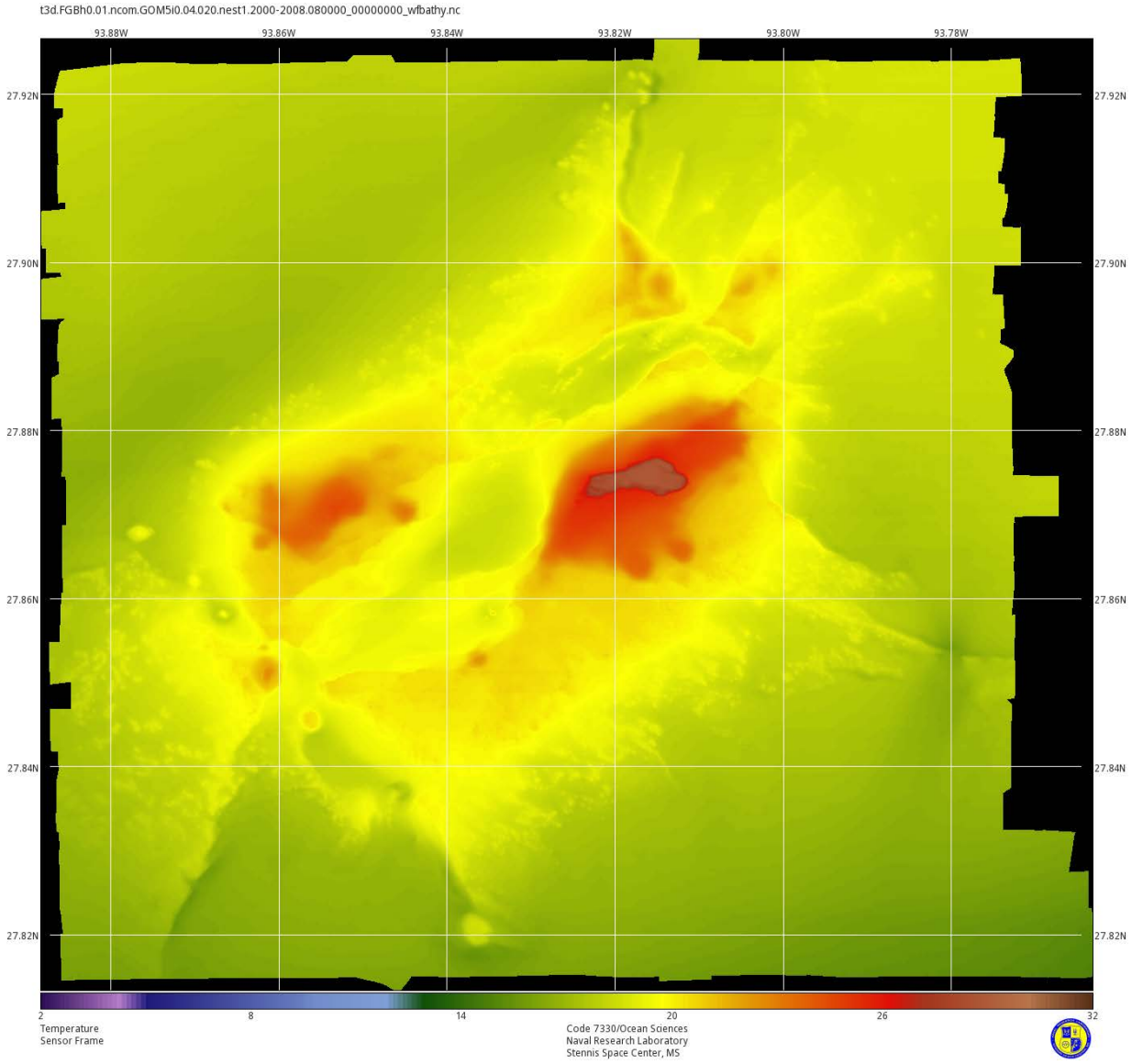

Figure 2-5. Monthly mean bottom temperature (August, 2000-2008) for the West Flower Garden Bank at 5-meter horizontal resolution.

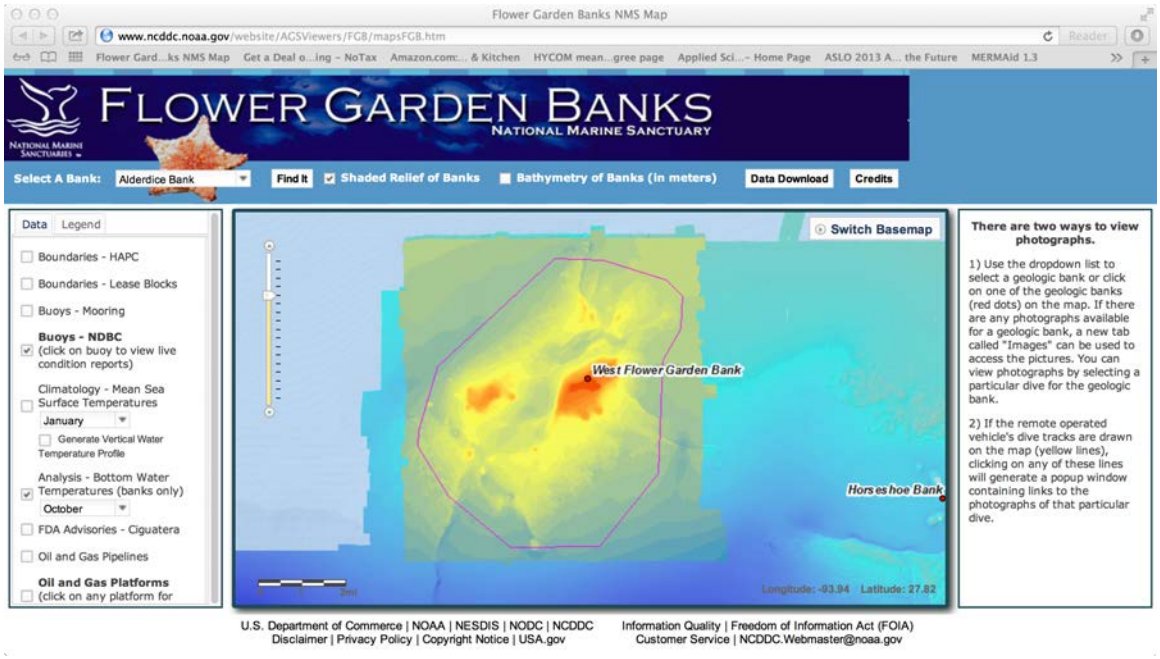

Figure 2-6. Example of monthly mean bottom temperature display via NCDDC. The data display menu at right allows users to access the data via "Analysis – Bottom Water Temperatures (banks only)" – the box allows users to select the month of interest.

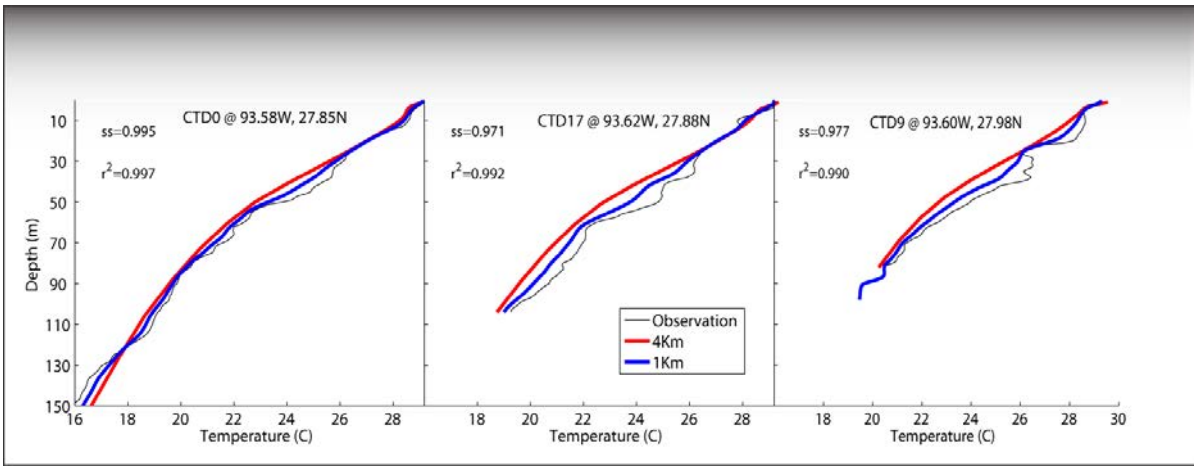

Figure 2-7. A comparison of the model fields (red=4Km GOM, blue=1Km inner nest) to selected CTD casts (black) taken during the MORT June 2011 field program in the FGBMS. In general (not all CTD casts shown), the model reproduces the vertical temperature gradient well. The higher horizontal resolution (both GOM and its inner nest have the same vertical structure) has better skill.

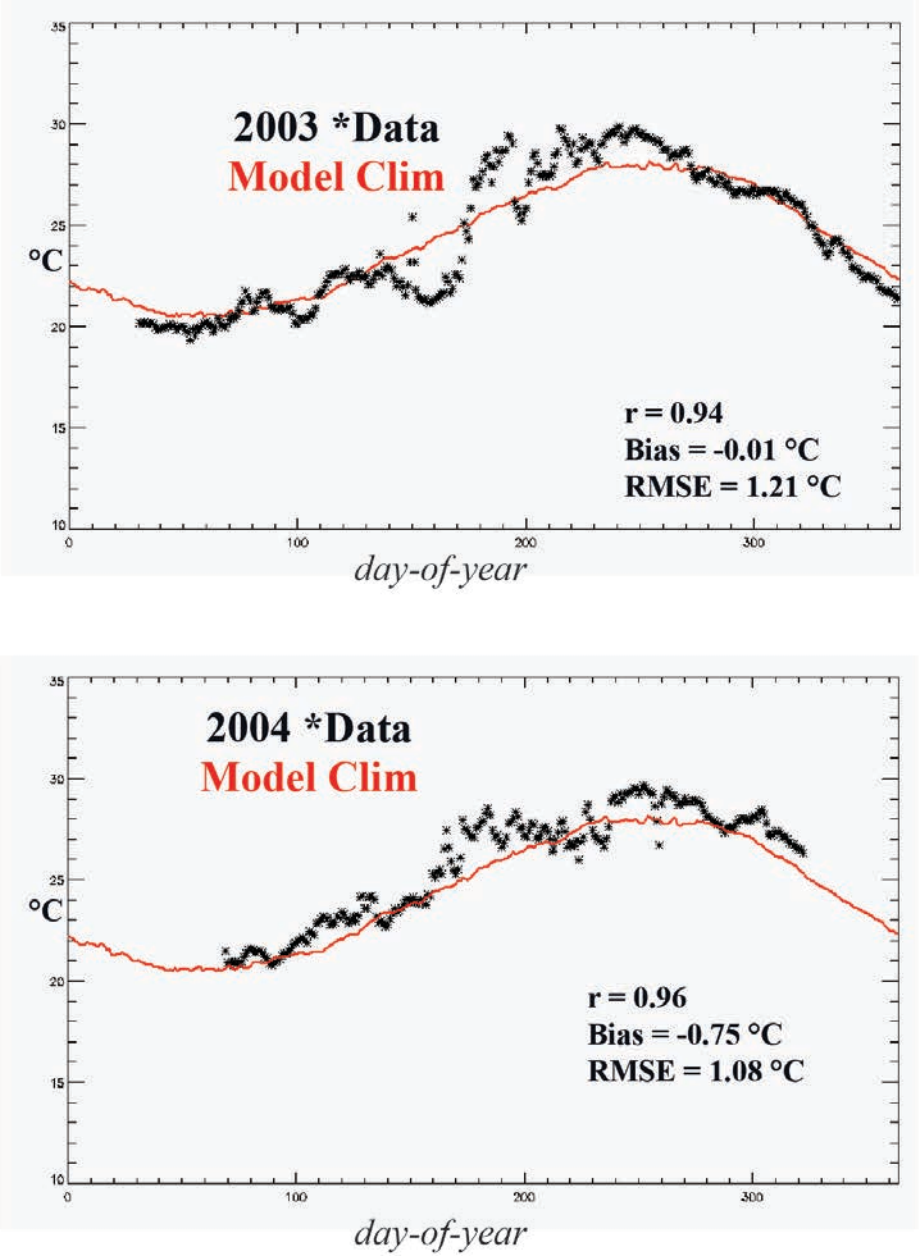

Figure 2-8. Comparison of long-term monitoring data at West Flower Garden Bank with FGB daily temperature climatology.

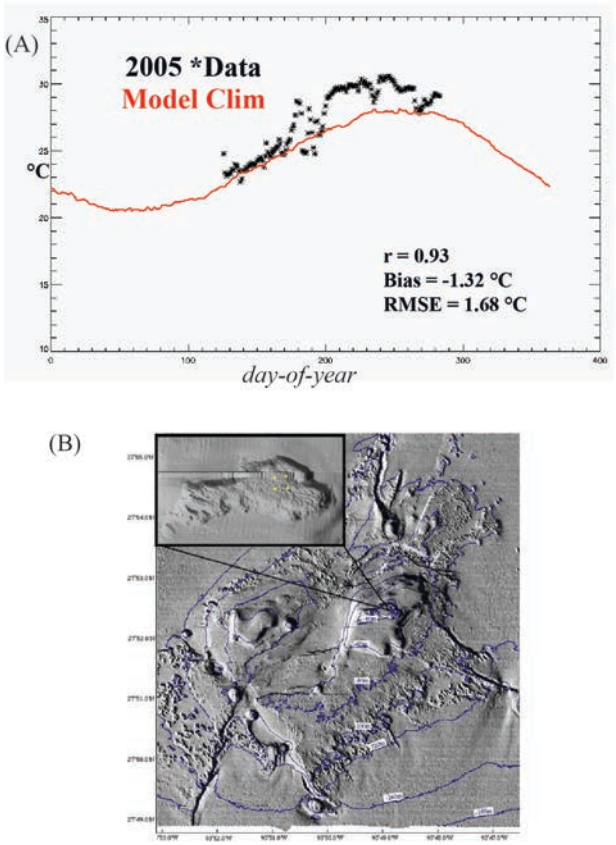

Figure 2-9. (A) Comparison of long-term monitoring data at West Flower Garden Bank (2005) with climatology. (B) Location of long-term monitoring equipment deployment on WFGB [Precht et al., 2008].

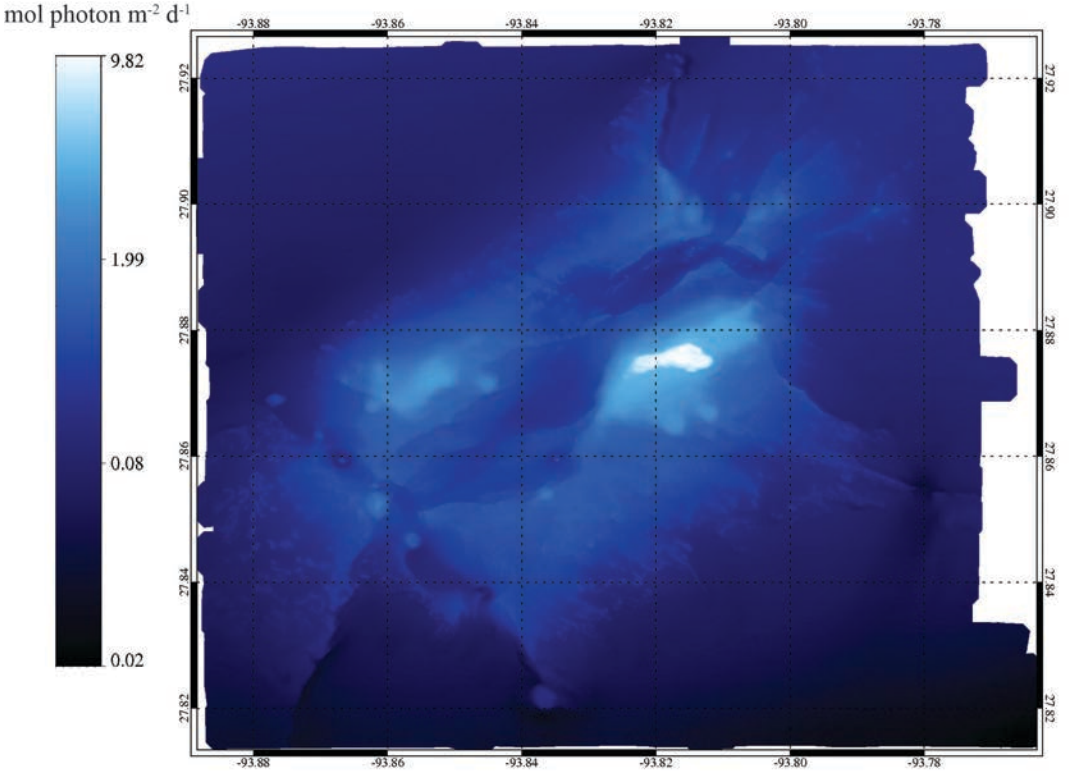

Figure 2-10. Annual Mean bottom PAR for the West Flower Garden Bank at high spatial resolution.

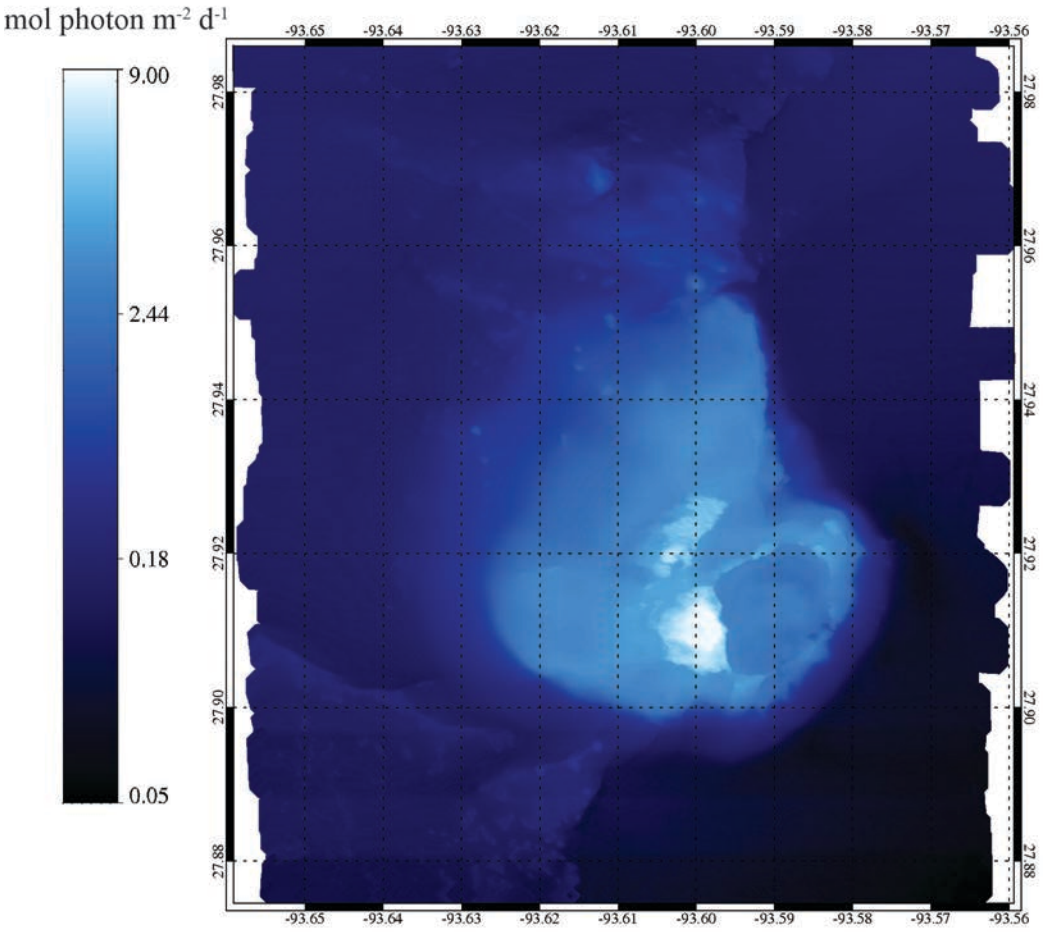

Figure 2-11. Annual Mean bottom PAR for the East Flower Garden Bank at high spatial resolution.

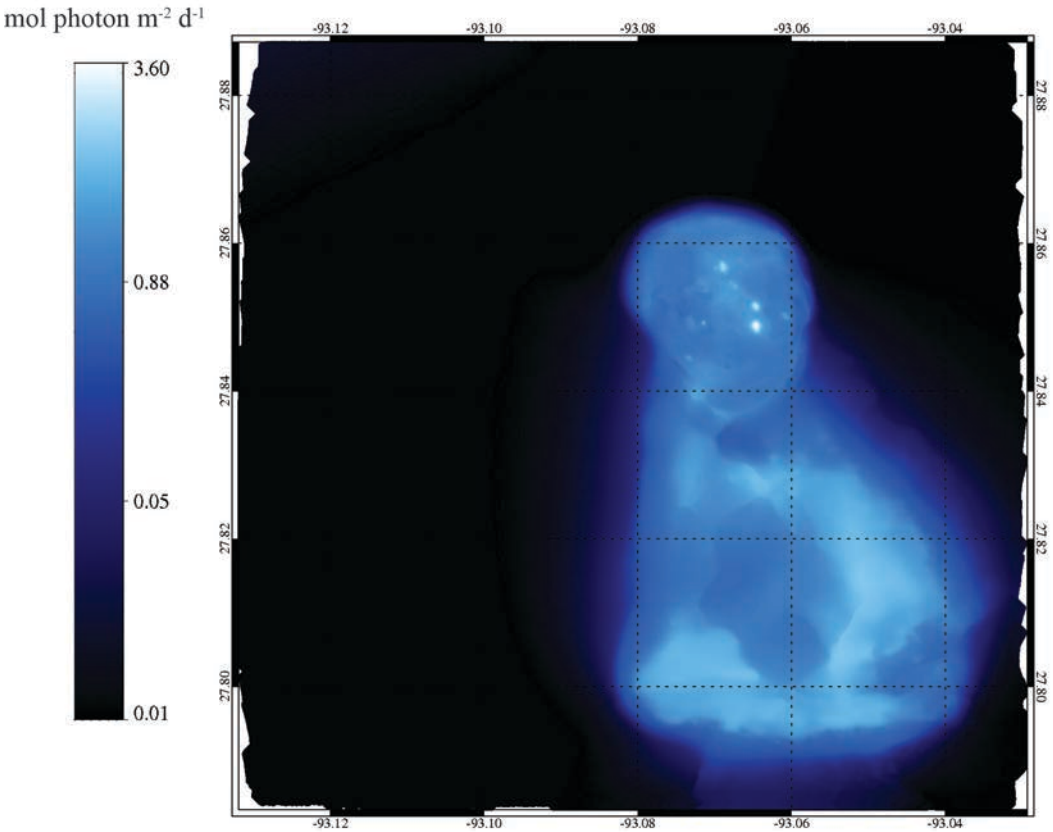

Figure 2-12. Annual Mean bottom PAR for Geyer Bank at high spatial resolution.

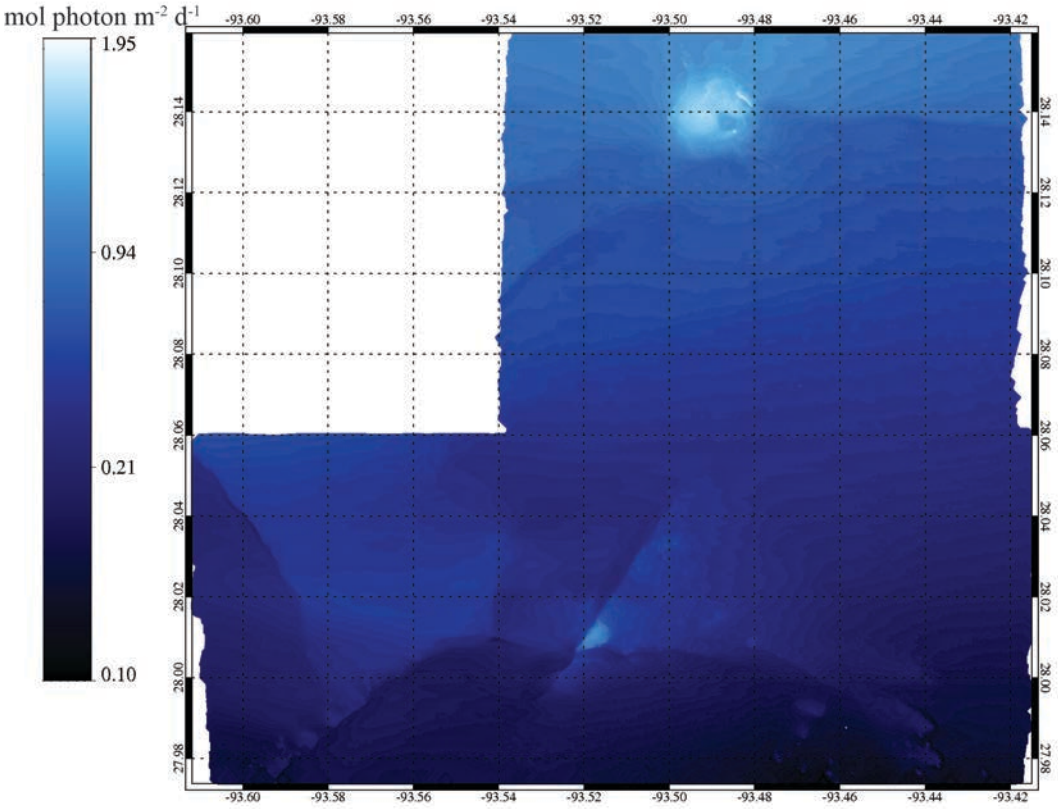

Figure 2-13. Annual Mean bottom PAR for MacNeil Bank at high spatial resolution.

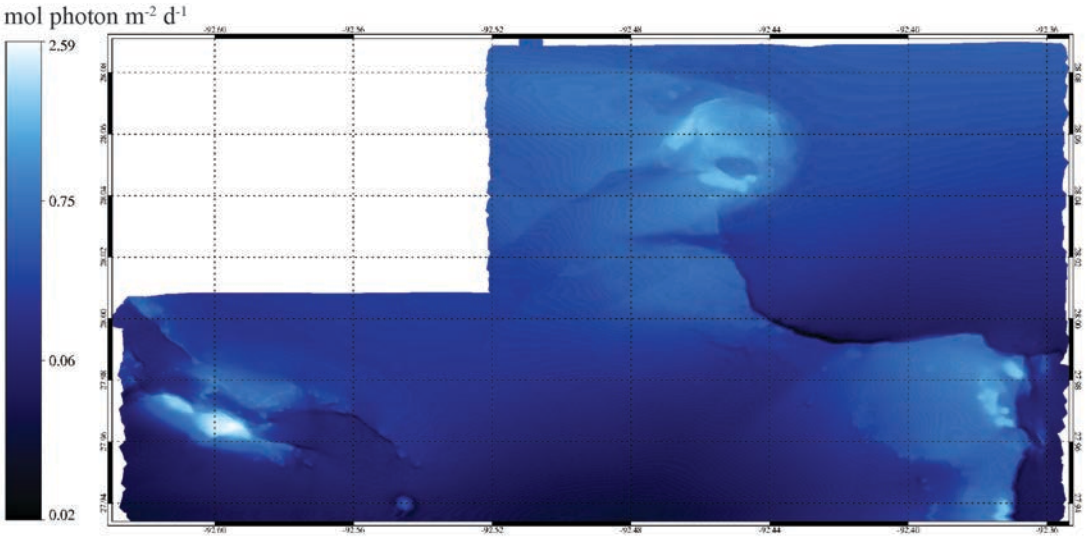

Figure 2-14. Annual Mean bottom PAR for the McGrail, Bouma, Rezak, and Sidner Bank complex at high spatial resolution.

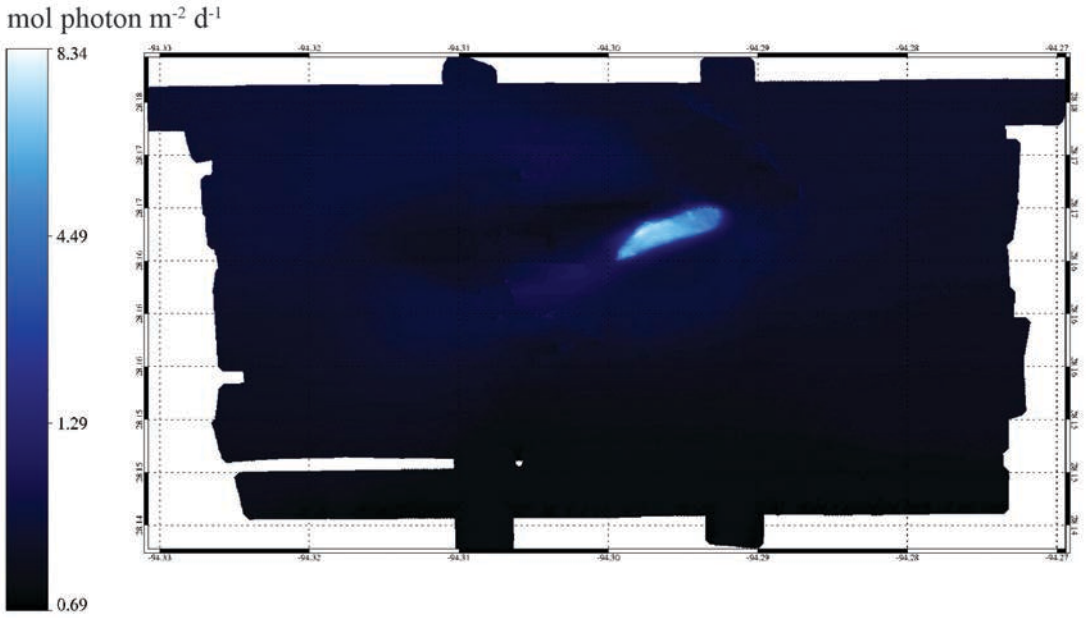

Figure 2-15. Annual Mean bottom PAR for Stetson Bank.

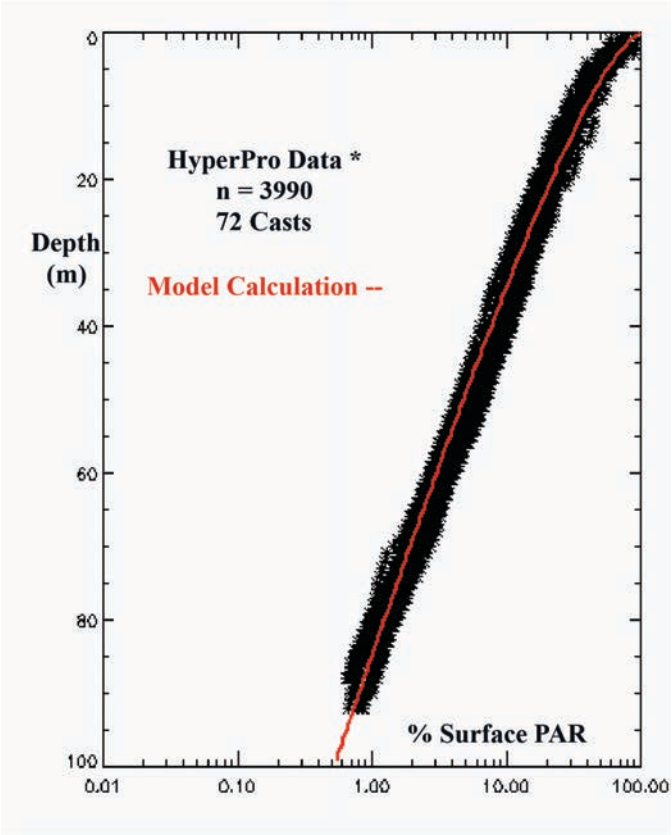

Figure 2-16. Comparison of Model Calculation with HyperPro free-falling Hyperspectral Radiometer data -- % surface PAR.

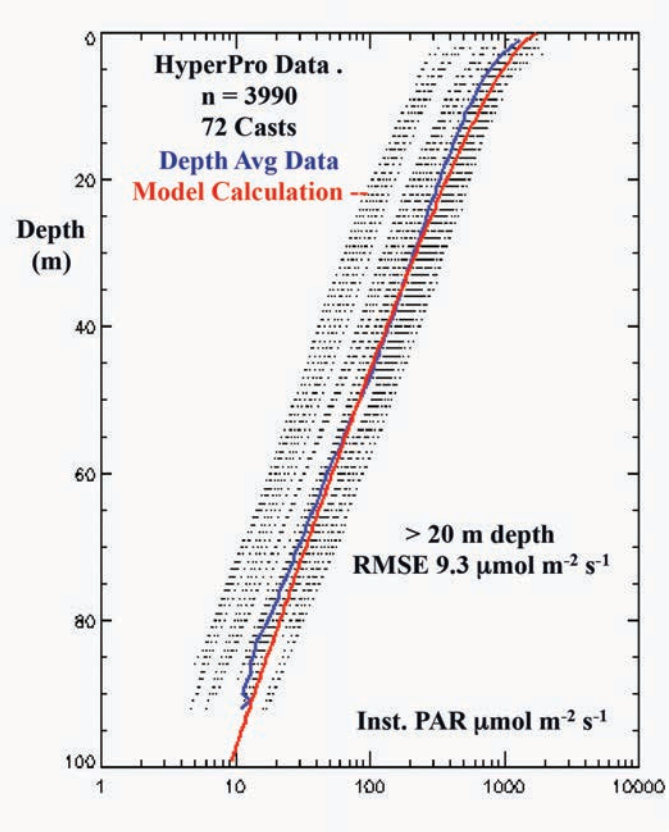

Figure 2-17. Comparison of Model Calculation with HyperPro free-falling Hyperspectral Radiometer data – instantaneous PAR.

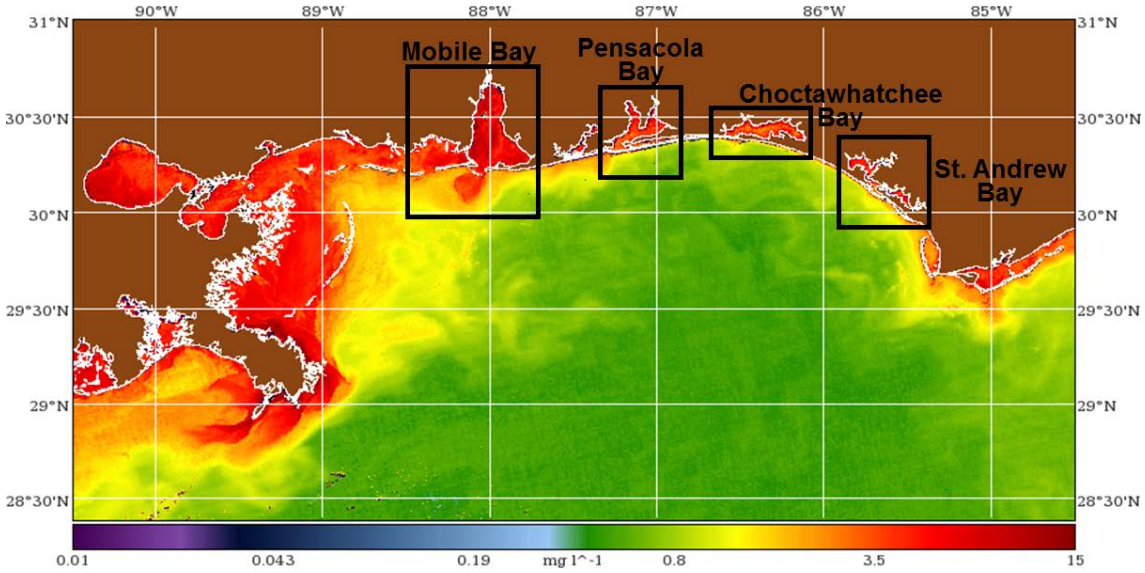

Figure 3-1. The four bays studied as part of this project. The image shown is chlorophyll a concentration.

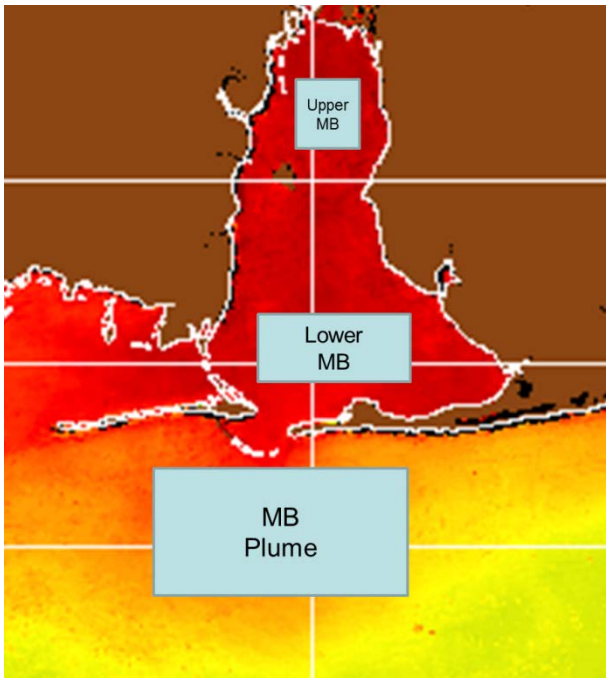

Figure 3-2. Mobile Bay subregions: Upper Mobile Bay, Lower Mobile Bay, Mobile Bay Plume.

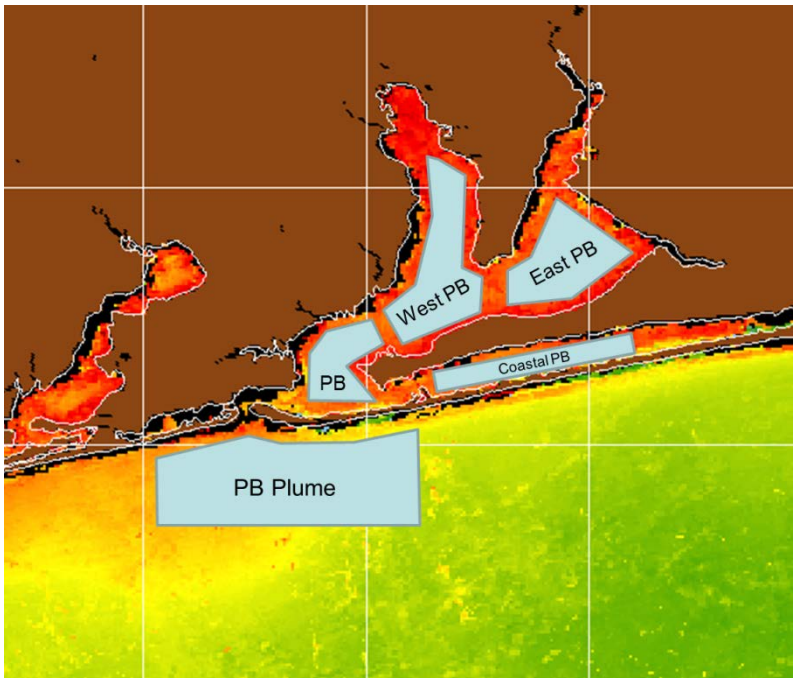

Figure 3-3. Pensacola Bay subregions: Pensacola Bay, West Pensacola Bay, East Pensacola Bay, Coastal Pensacola Bay, Pensacola Bay Plume.

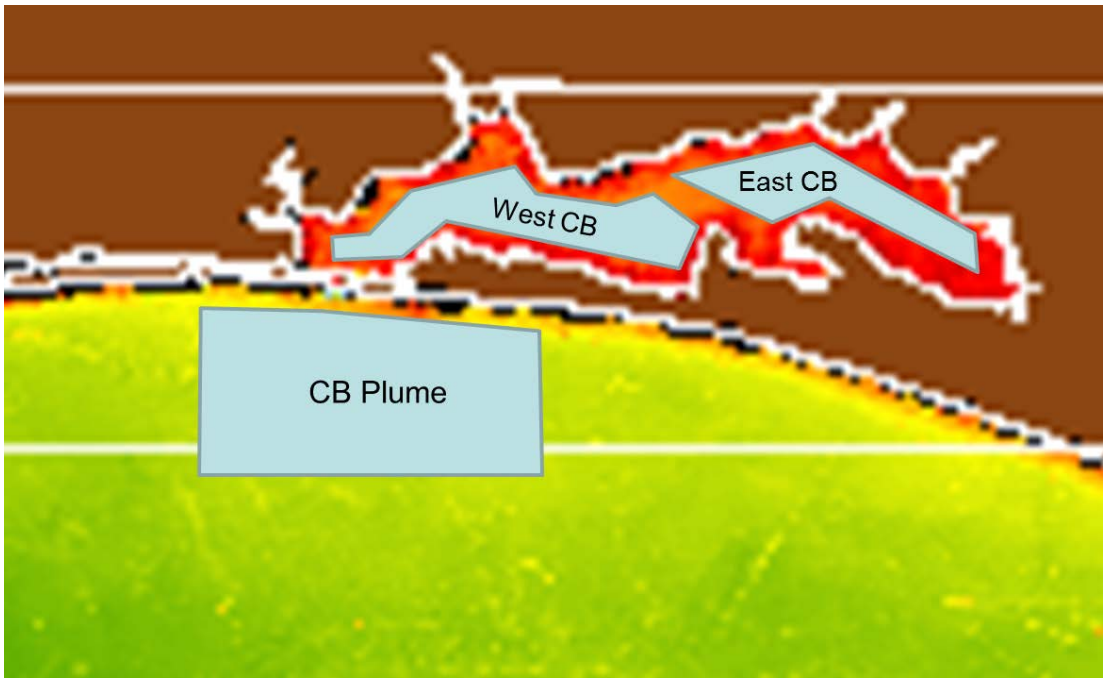

Figure 3-4. Choctawhatchee Bay subregions: West Choctawhatchee Bay, East Choctawhatchee Bay, Choctawhatchee Bay Plume.

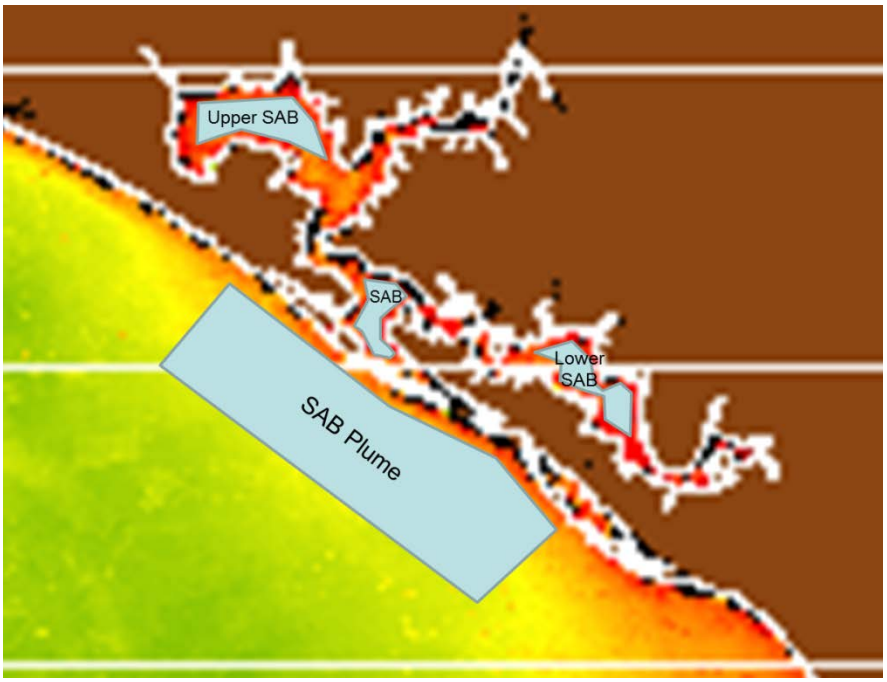

Figure 3-5. Choctawhatchee Bay subregions: West Choctawhatchee Bay, East Choctawhatchee Bay, Choctawhatchee Bay Plume.

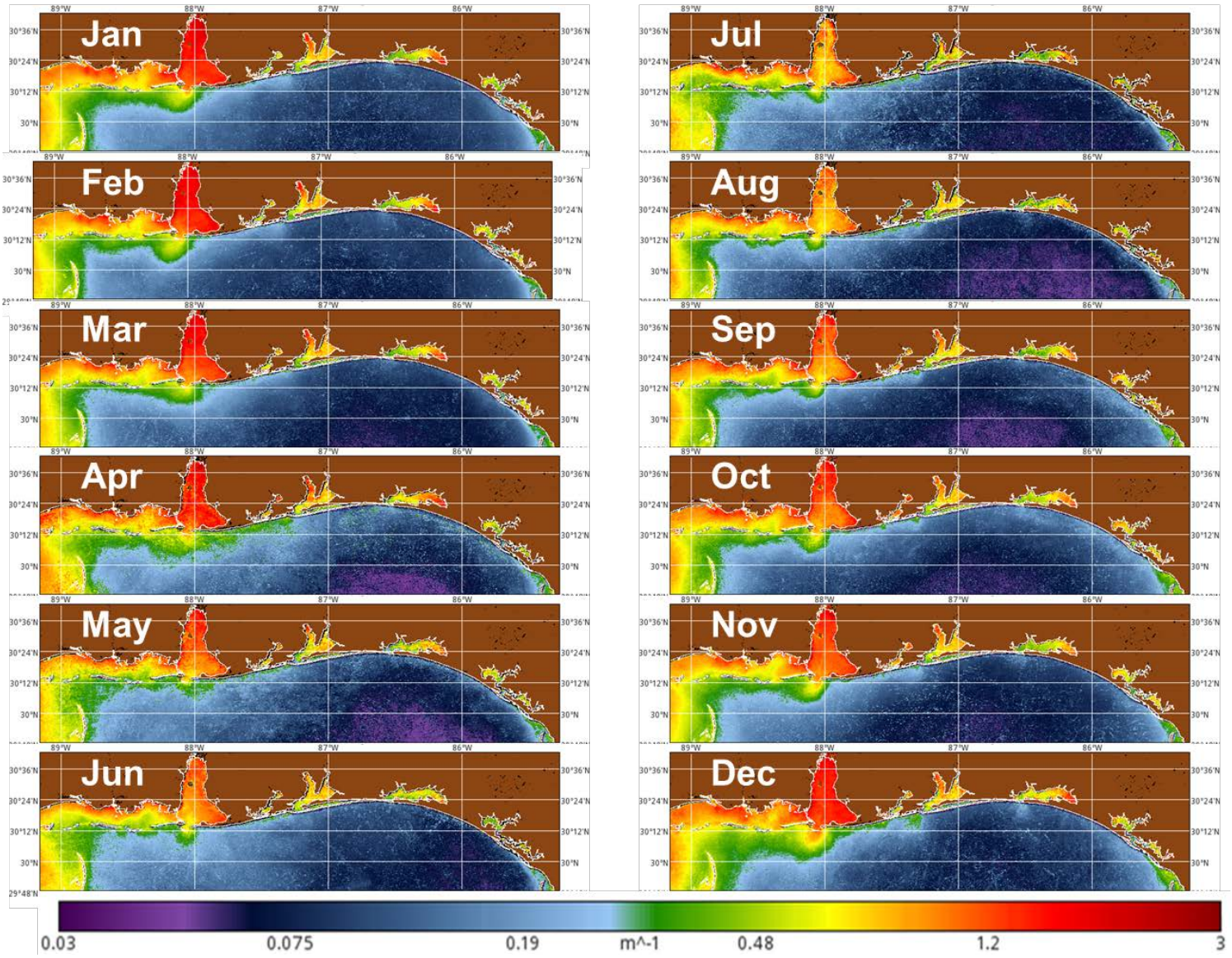

Figure 3-6. Northern Gulf of Mexico, 5-year (2005-2009) monthly average diffuse attenuation coefficient, $K_d(488)$.

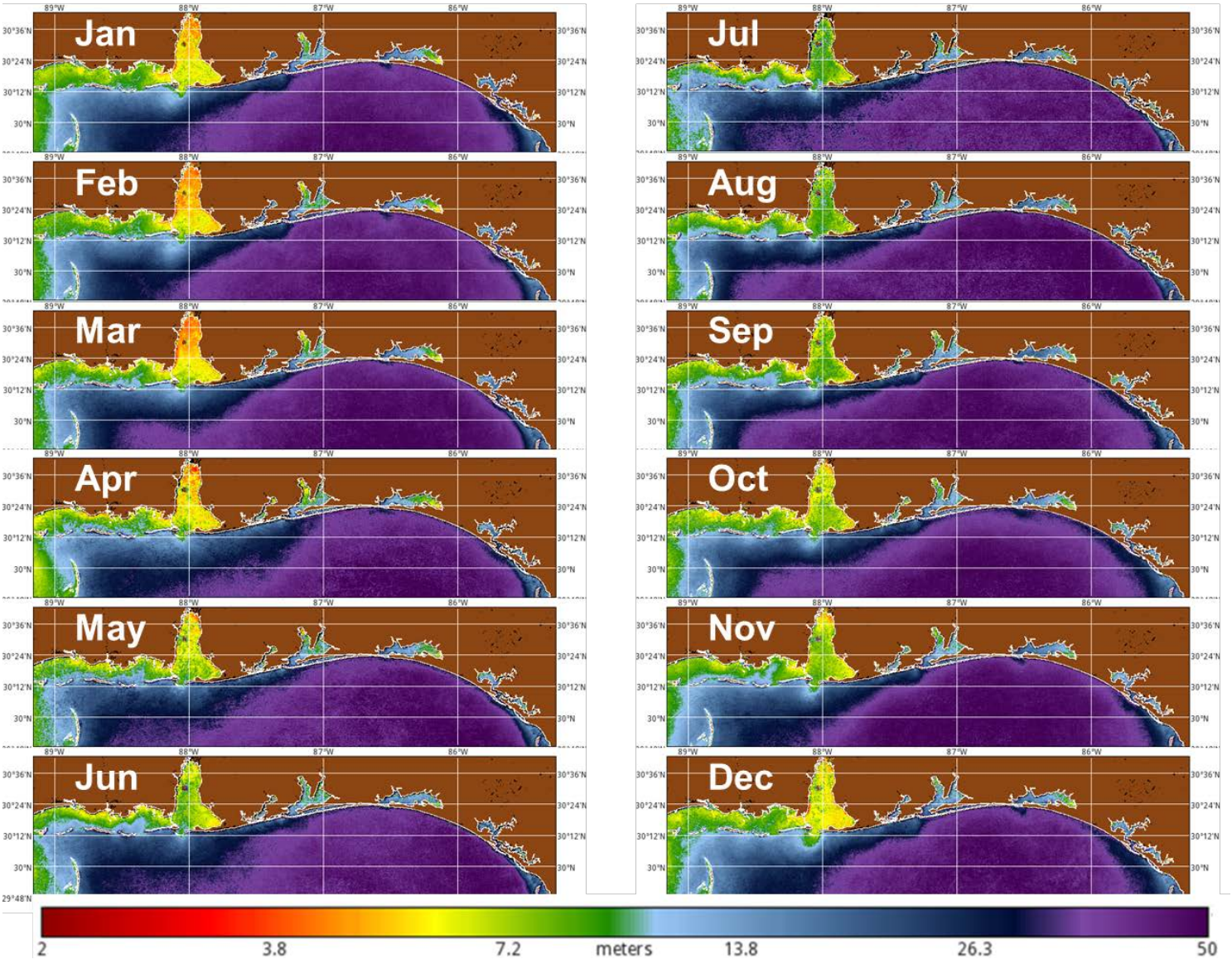

Figure 3-7. Northern Gulf of Mexico, 5-year (2005-2009) monthly average euphotic zone depth, Z_{eu}.

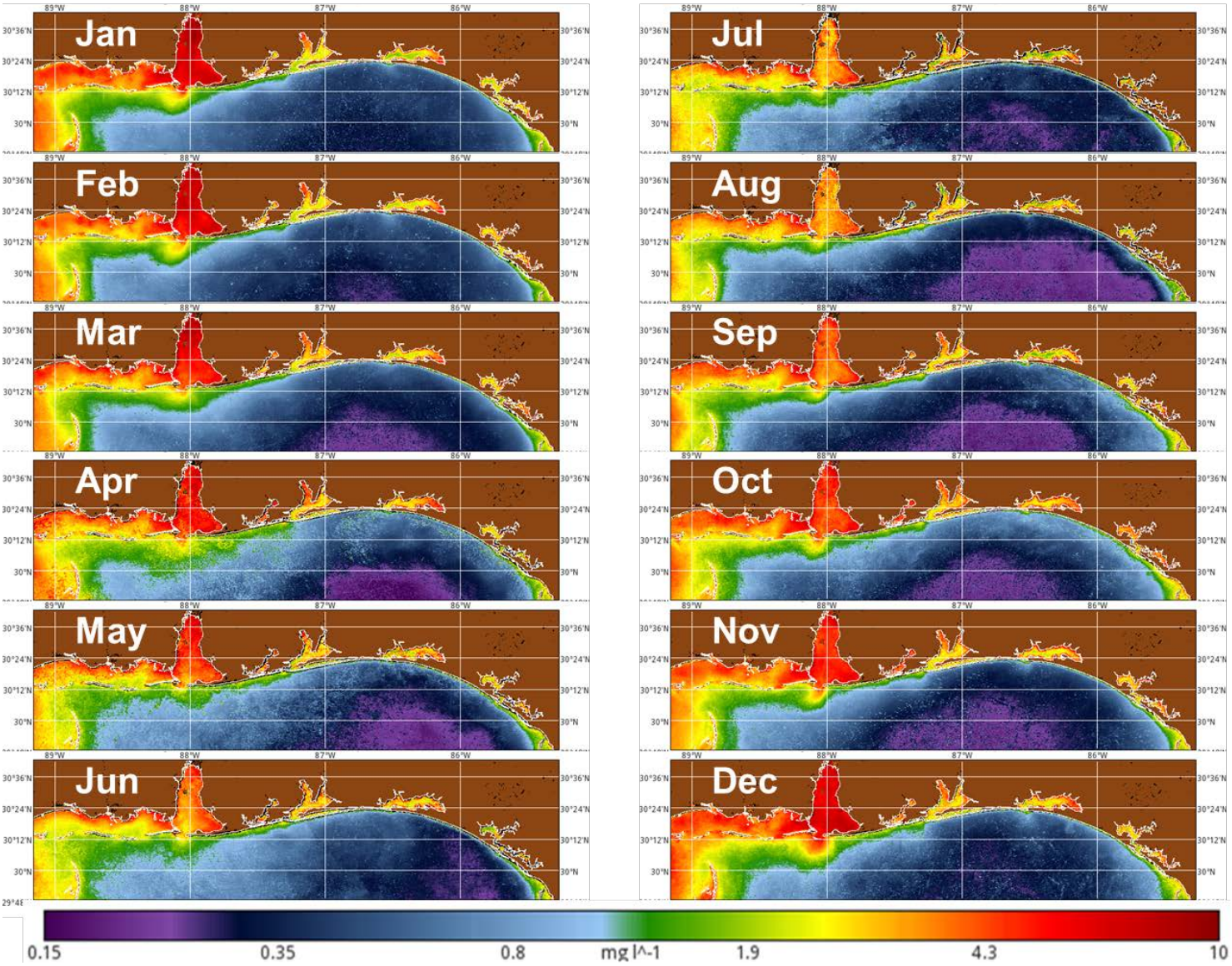

Figure 3-8. Northern Gulf of Mexico, 5-year (2005-2009) monthly average Particulate Inorganic Matter concentration (PIM).

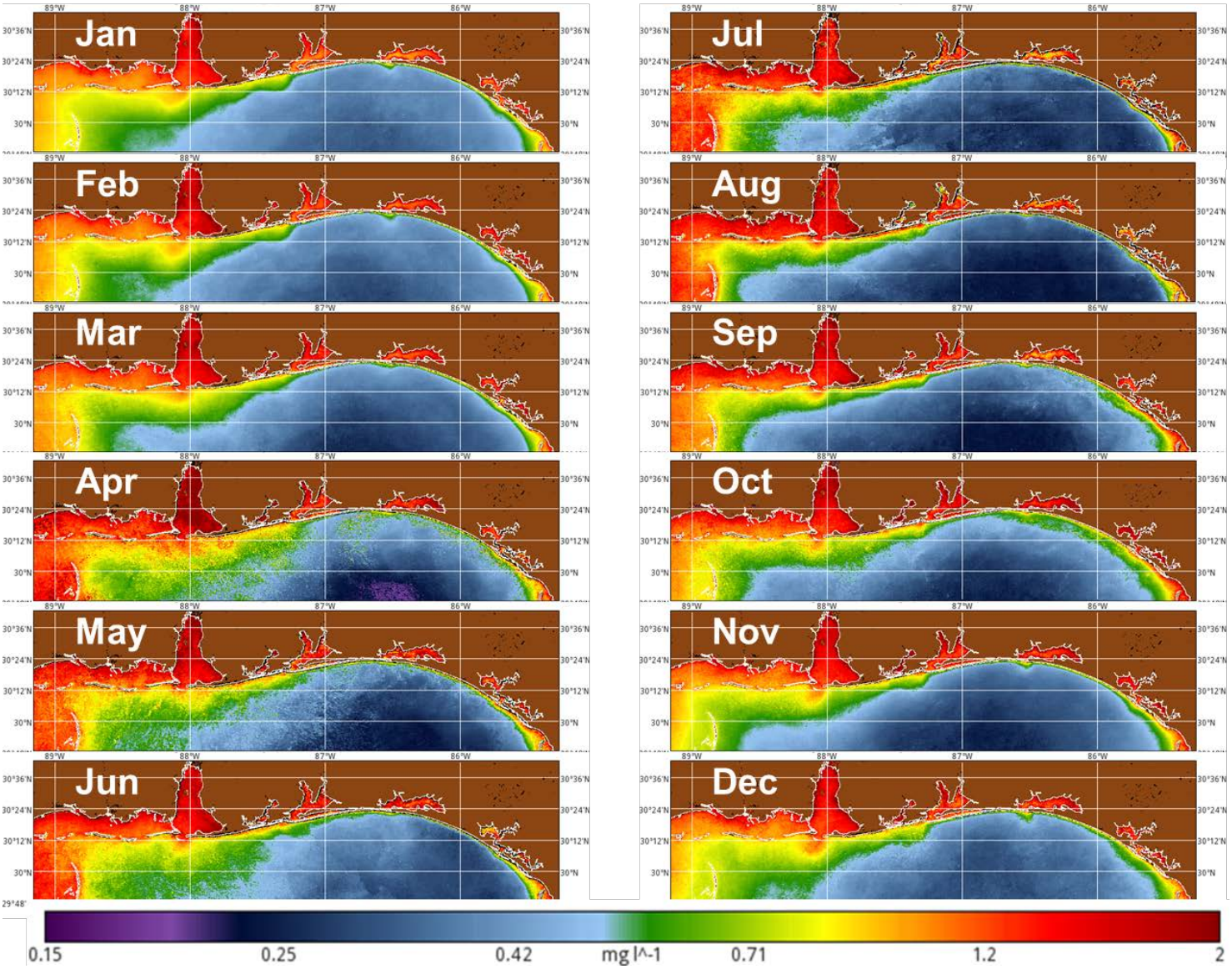

Figure 3-9. Northern Gulf of Mexico, 5-year (2005-2009) monthly average Particulate Organic Matter concentration (POM).

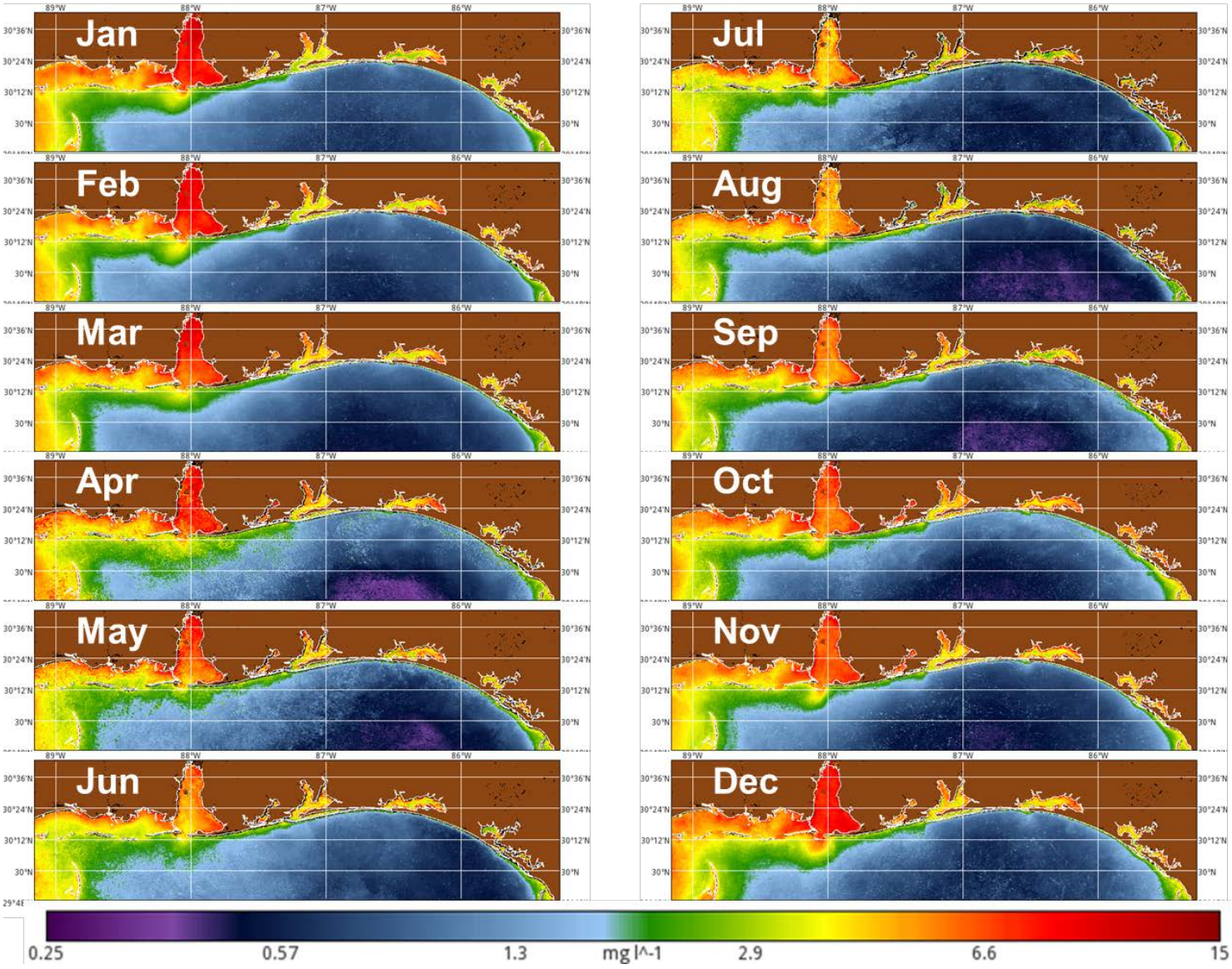

Figure 3-10. Northern Gulf of Mexico, 5-year (2005-2009) monthly average Total Suspended Solids concentration (TSS).

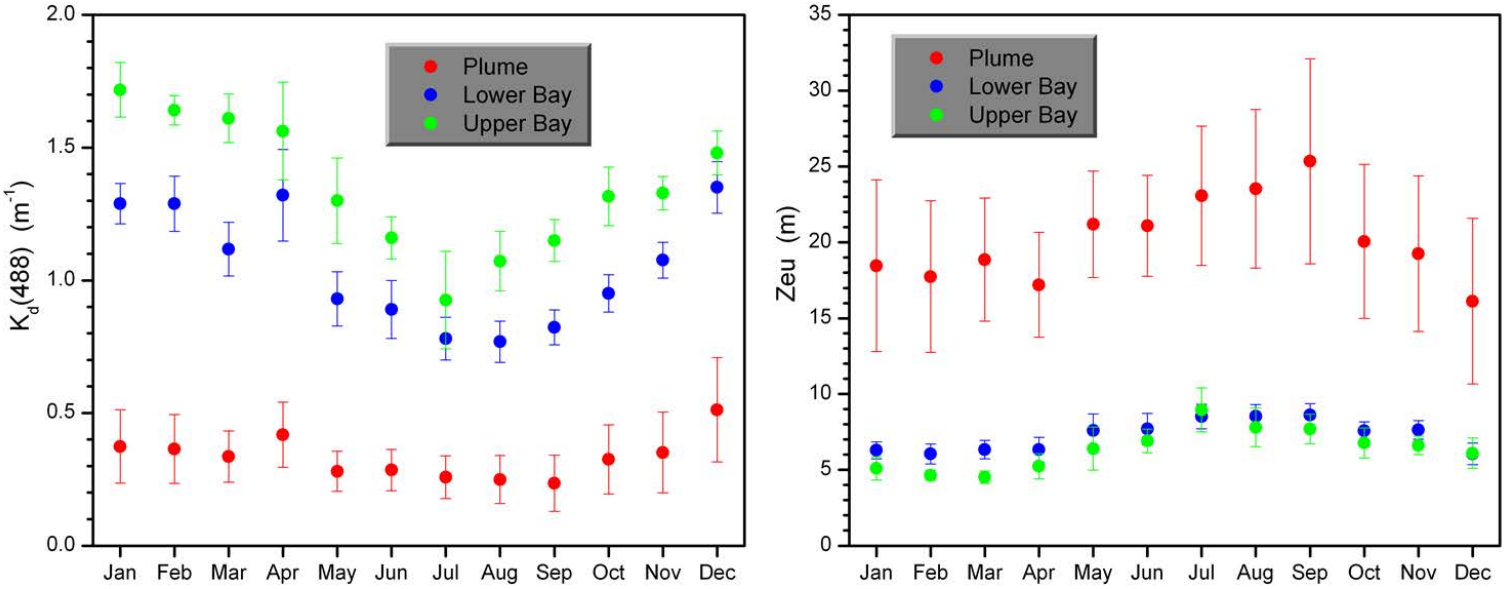

Figure 3-11. Time-series analysis. 5-year monthly averages, within-bay variability, Mobile Bay. Diffuse attenuation coefficient, $K_d(488)$ and euphotic depth, Z_{eu}.

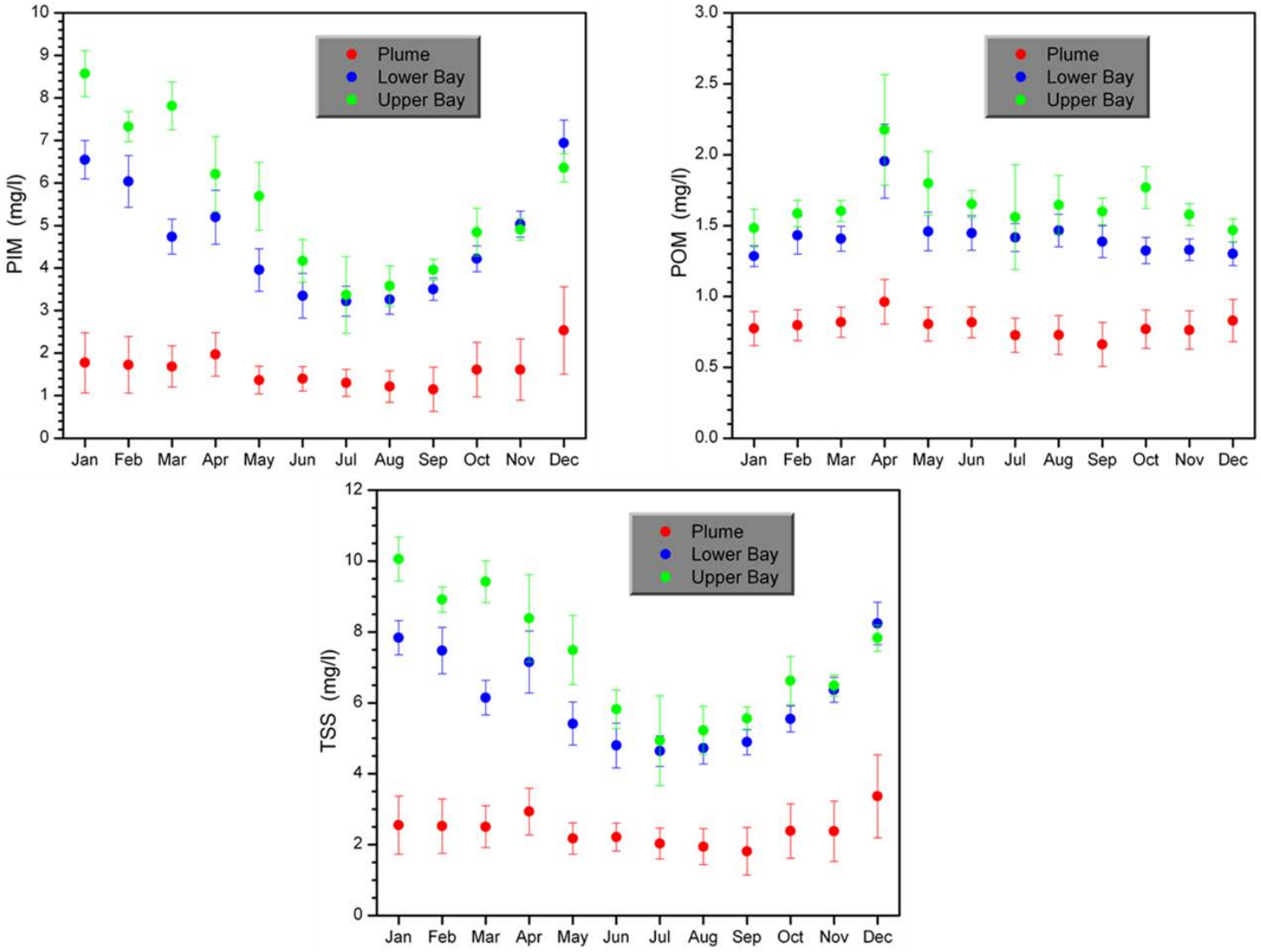

Figure 3-12. Time-series analysis. 5-year monthly averages, within-bay variability, Mobile Bay. Particulate Inorganic Matter (PIM), Particulate Organic Matter (POM), and Total Suspended Solids (TSS) concentrations.

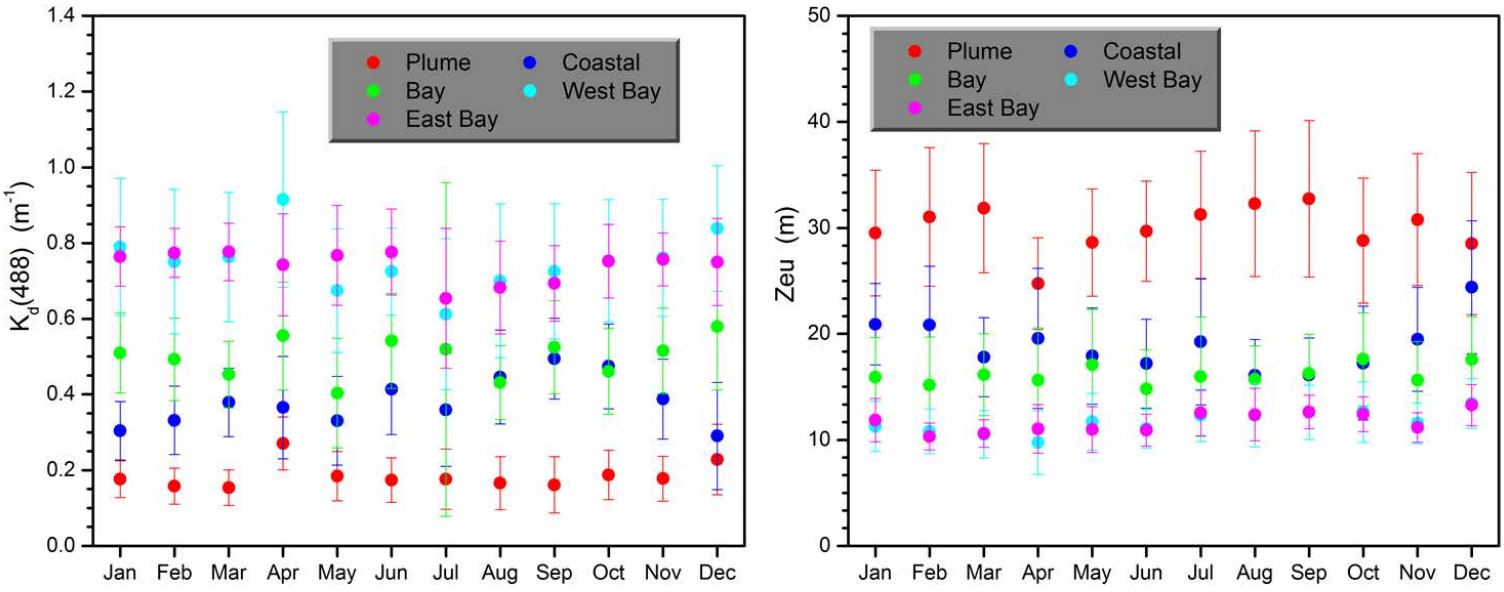

Figure 3-13. Time-series analysis. 5-year monthly averages, within-bay variability, Pensacola Bay. Diffuse attenuation coefficient, $K_d(488)$ and euphotic depth, Z_{eu}.

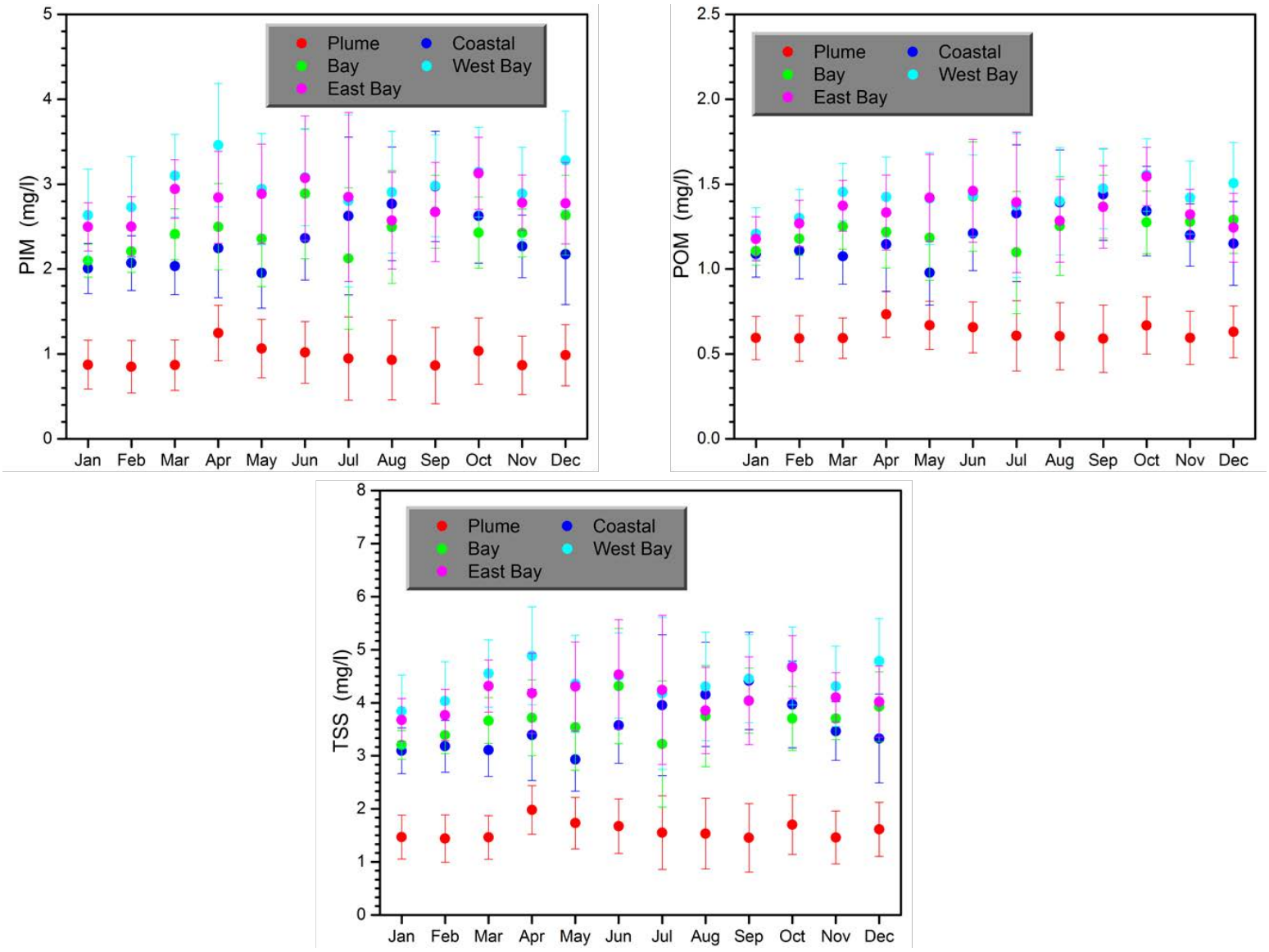

Figure 3-14. Time-series analysis. 5-year monthly averages, within-bay variability, Pensacola Bay. Particulate Inorganic Matter (PIM), Particulate Organic Matter (POM), and Total Suspended Solids (TSS) concentrations.

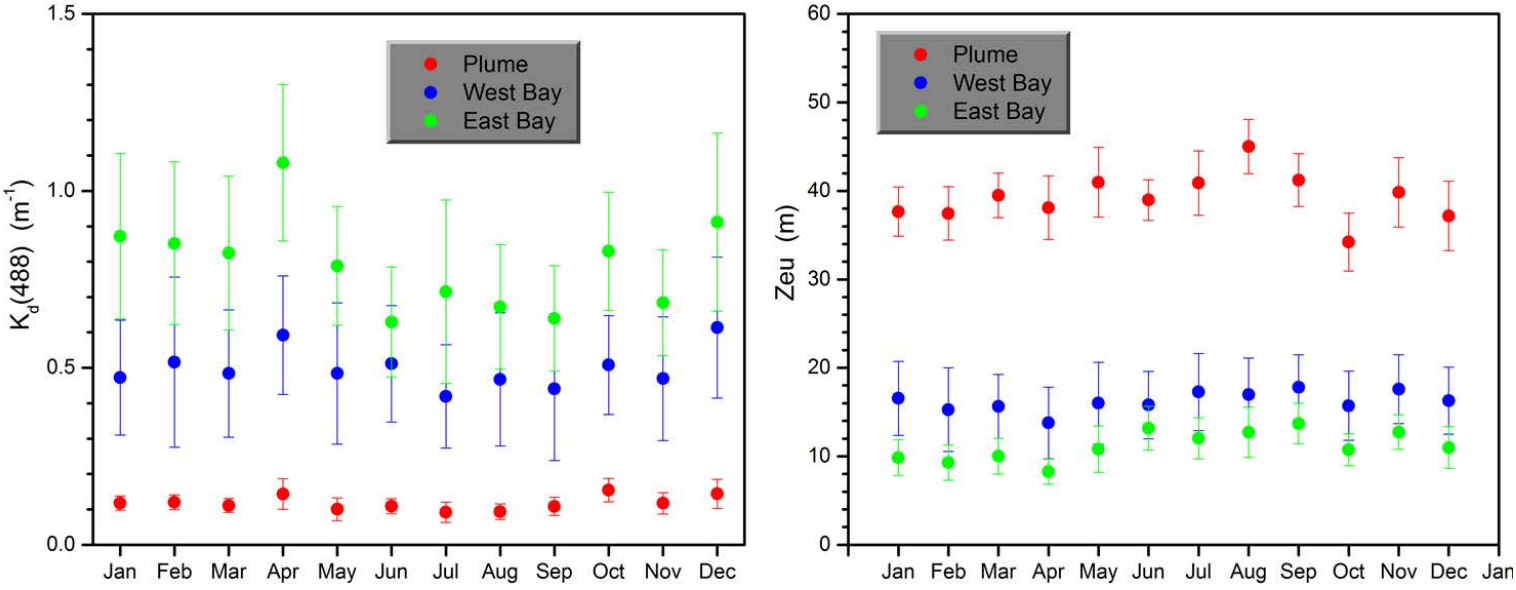

Figure 3-15. Time-series analysis. 5-year monthly averages, within-bay variability, Choctawhatchee Bay. Diffuse attenuation coefficient, $K_d(488)$ and euphotic depth, Z_{eu}.

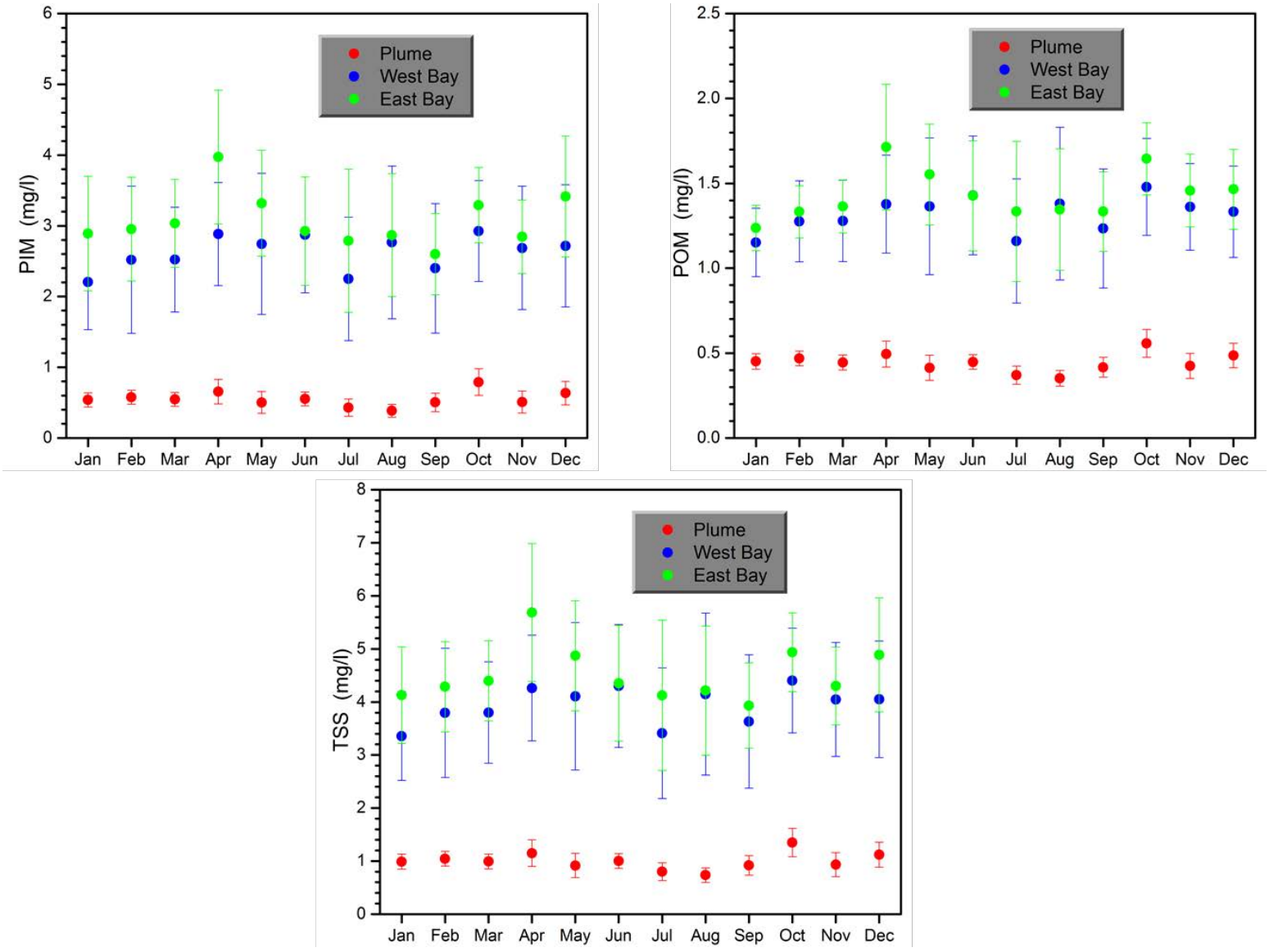

Figure 3-16. Time-series analysis. 5-year monthly averages, within-bay variability, Choctawhatchee Bay. Particulate Inorganic Matter (PIM), Particulate Organic Matter (POM), and Total Suspended Solids (TSS) concentrations.

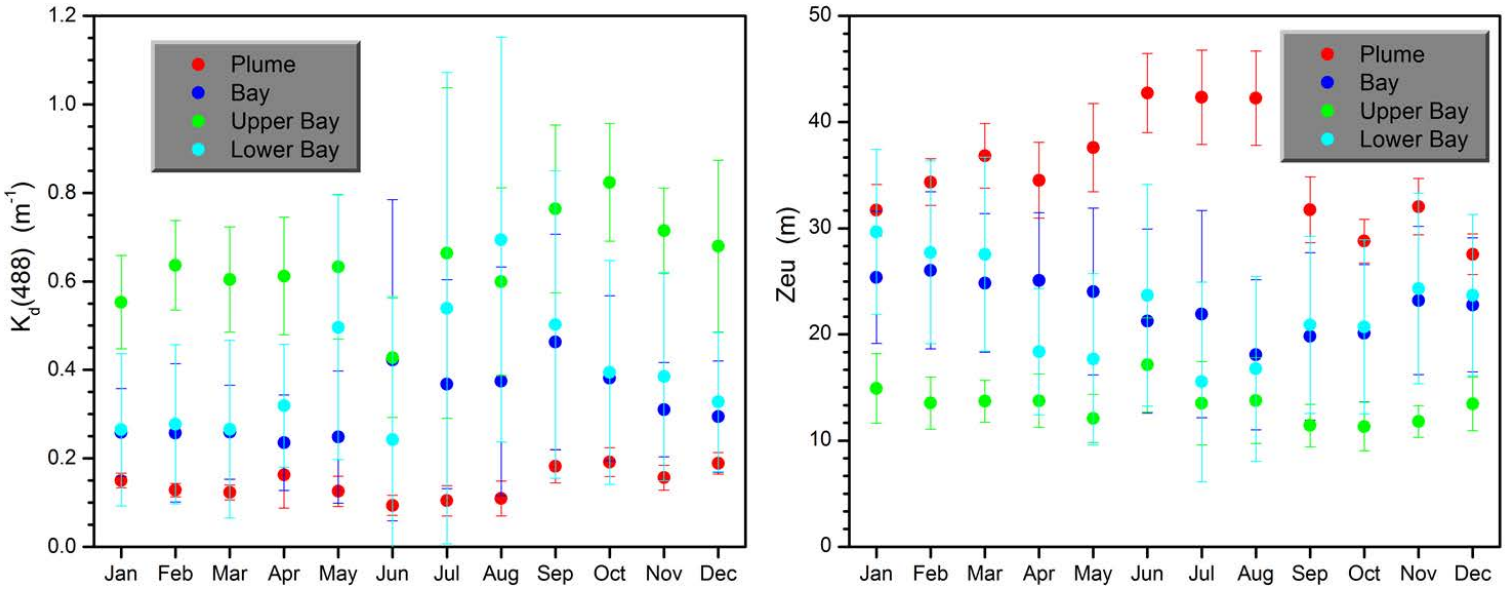

Figure 3-17. Time-series analysis. 5-year monthly averages, within-bay variability, St. Andrews Bay. Diffuse attenuation coefficient, $K_d(488)$ and euphotic depth, Z_{eu}.

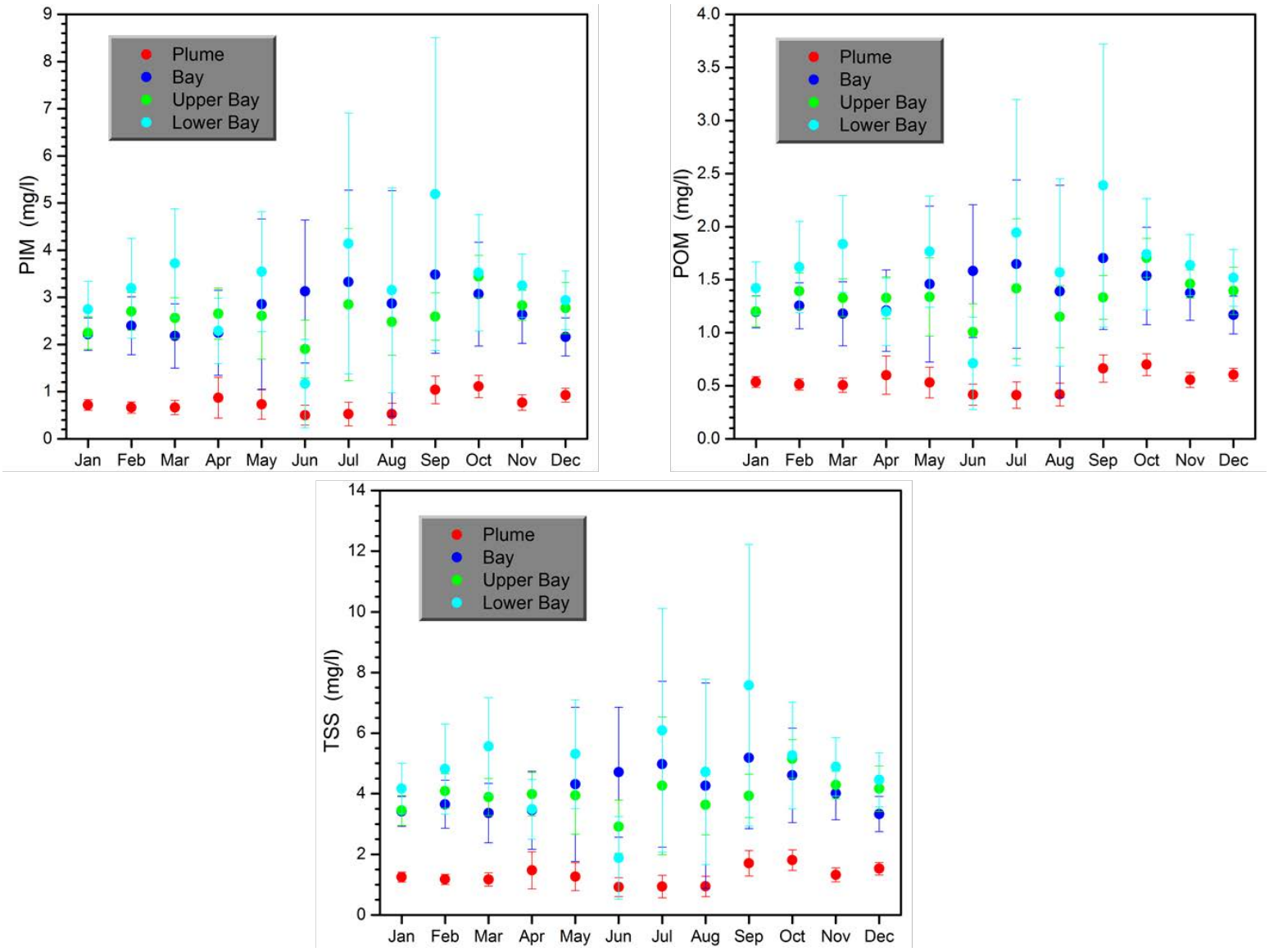

Figure 3-18. Time-series analysis. 5-year monthly averages, within-bay variability, St. Andrews Bay. Particulate Inorganic Matter (PIM), Particulate Organic Matter (POM), and Total Suspended Solids (TSS) concentrations.

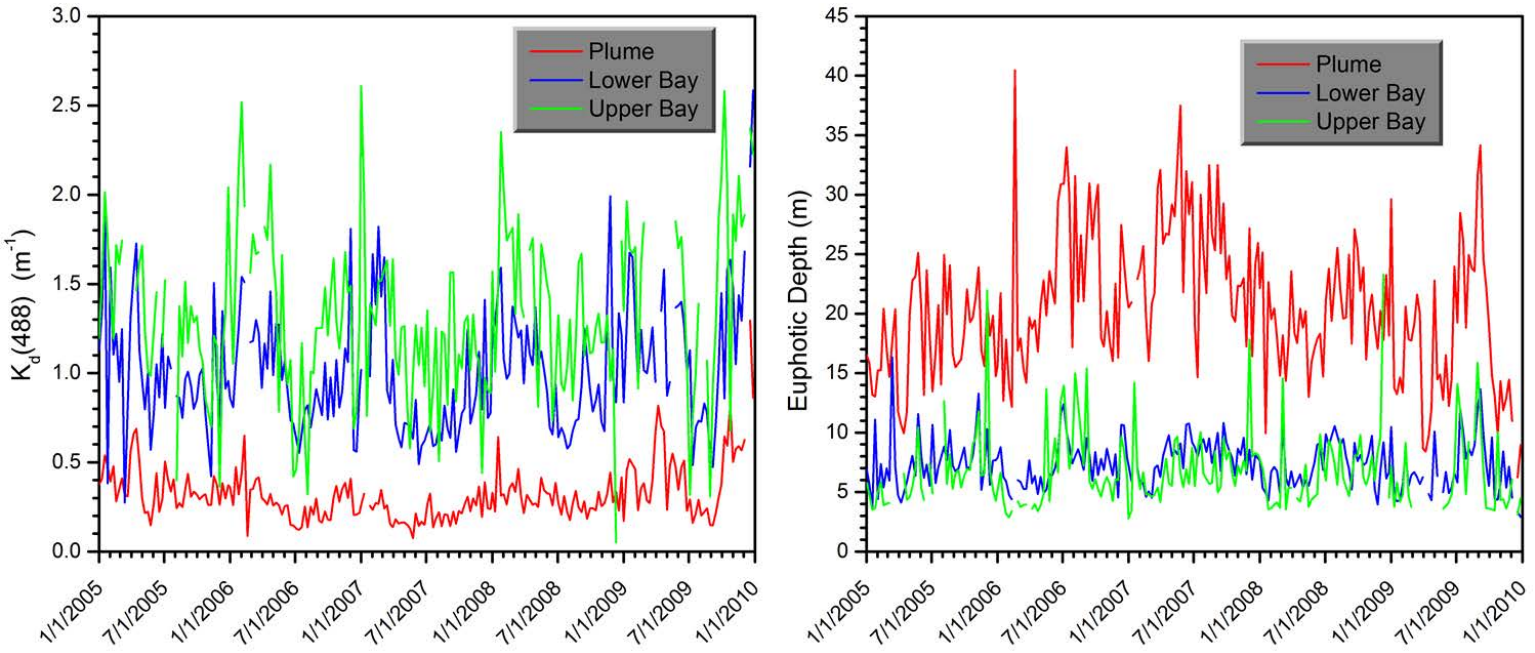

Figure 3-19. Time-series analysis. Weekly averages for 5-years, within-bay variability, Mobile Bay. Diffuse attenuation coefficient, $K_d(488)$ and euphotic depth, Z_{eu}.

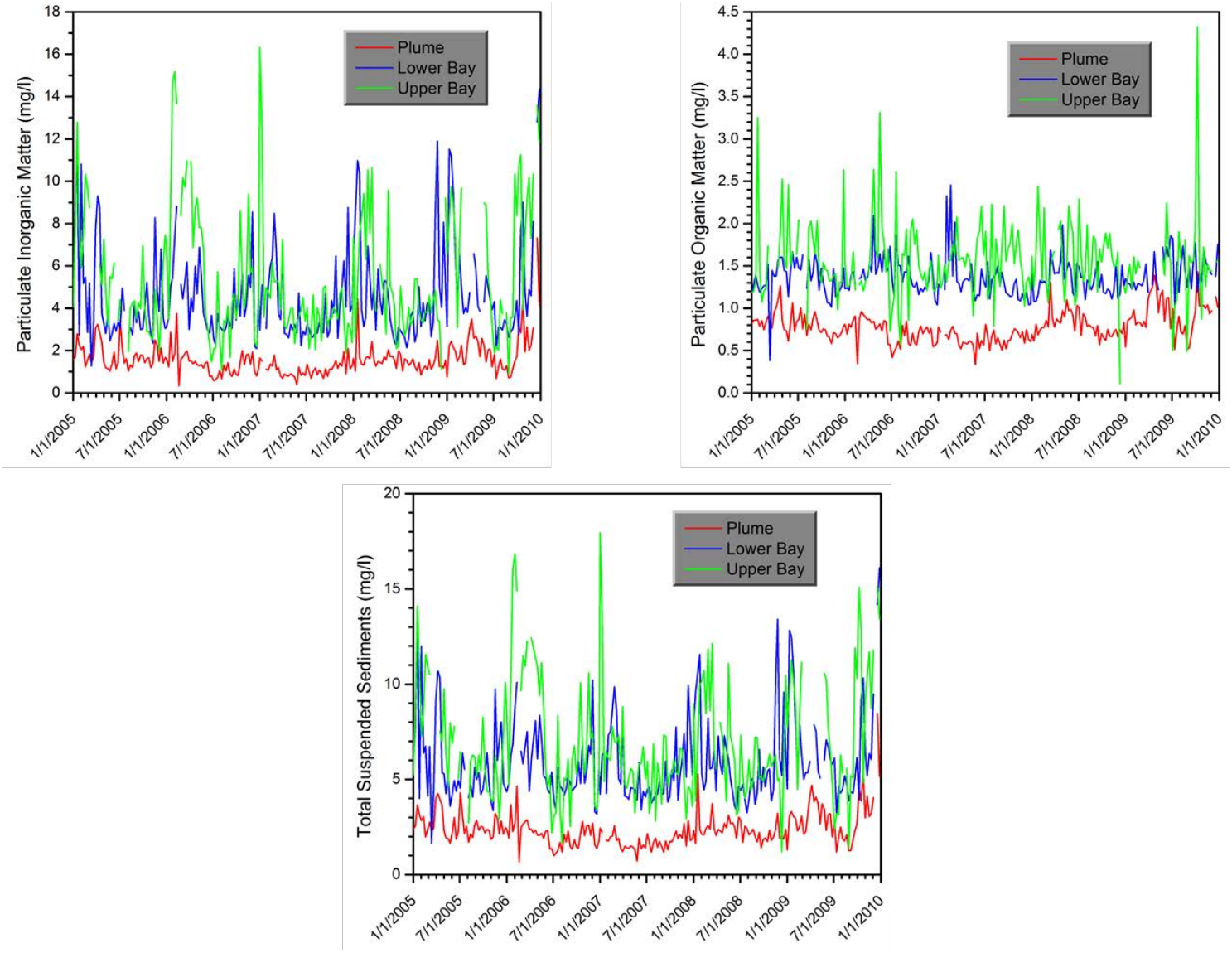

Figure 3-20. Time-series analysis. Weekly averages for 5-years, within-bay variability, Mobile Bay. Particulate Inorganic Matter (PIM), Particulate Organic Matter (POM), and Total Suspended Solids (TSS) concentrations.

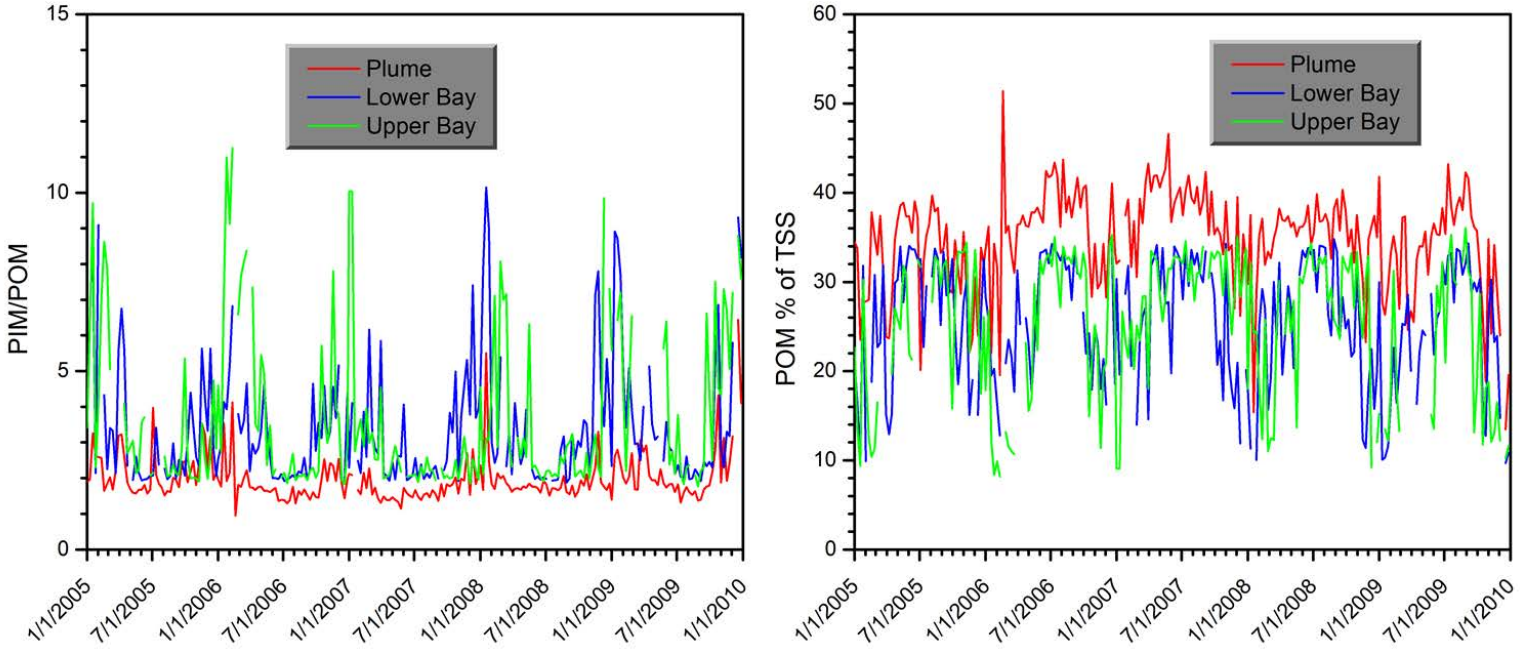

Figure 3-21. Time-series analysis. Weekly averages for 5-years, within-bay variability, Mobile Bay. PIM/POM ratio and % of TSS represented by organic matter (POM % of TSS).

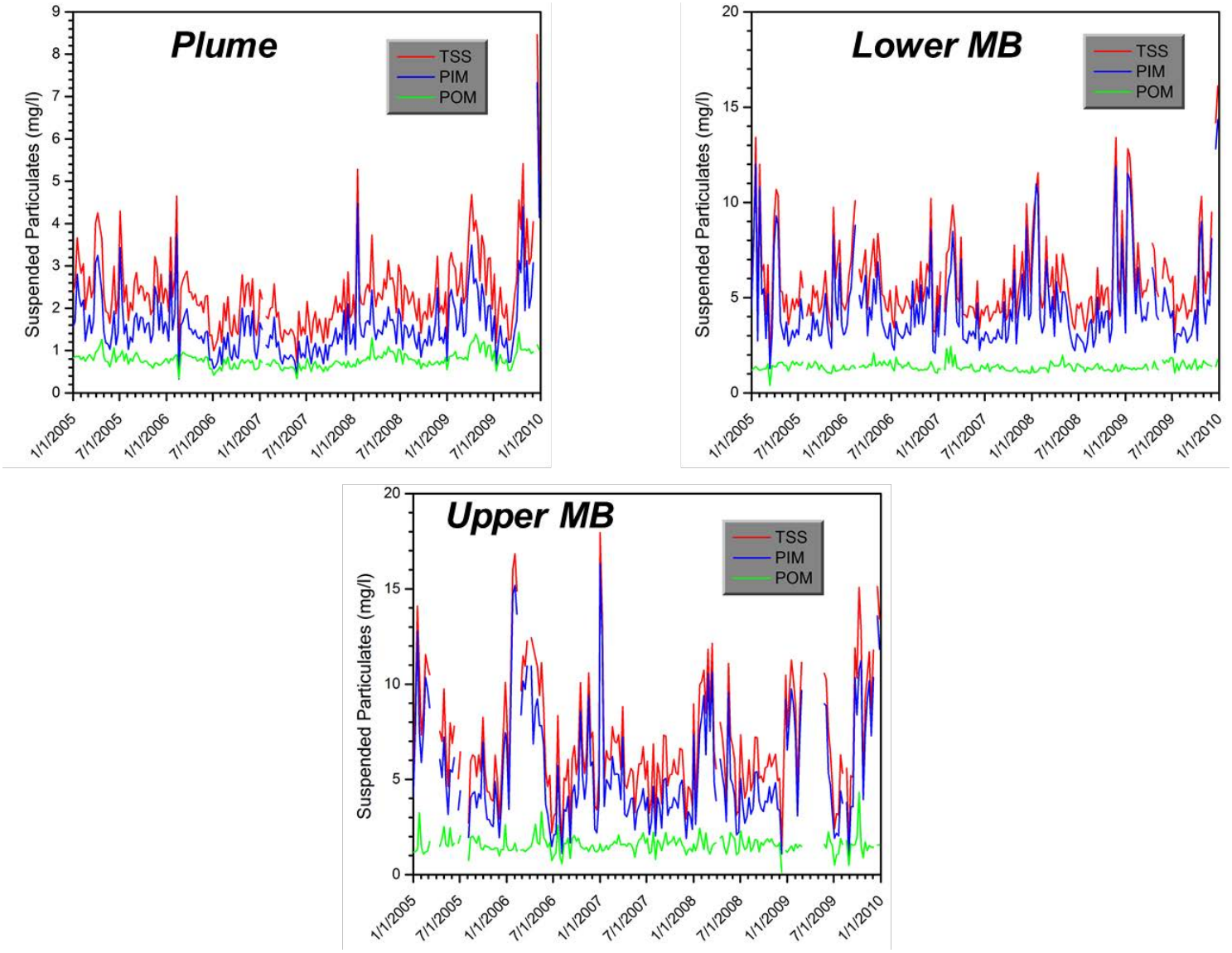

Figure 3-22. Time-series analysis. Weekly averages for 5-years, within-bay variability, Mobile Bay. Comparison of suspended particulate loads in the plume, Lower Bay, and Upper Bay.

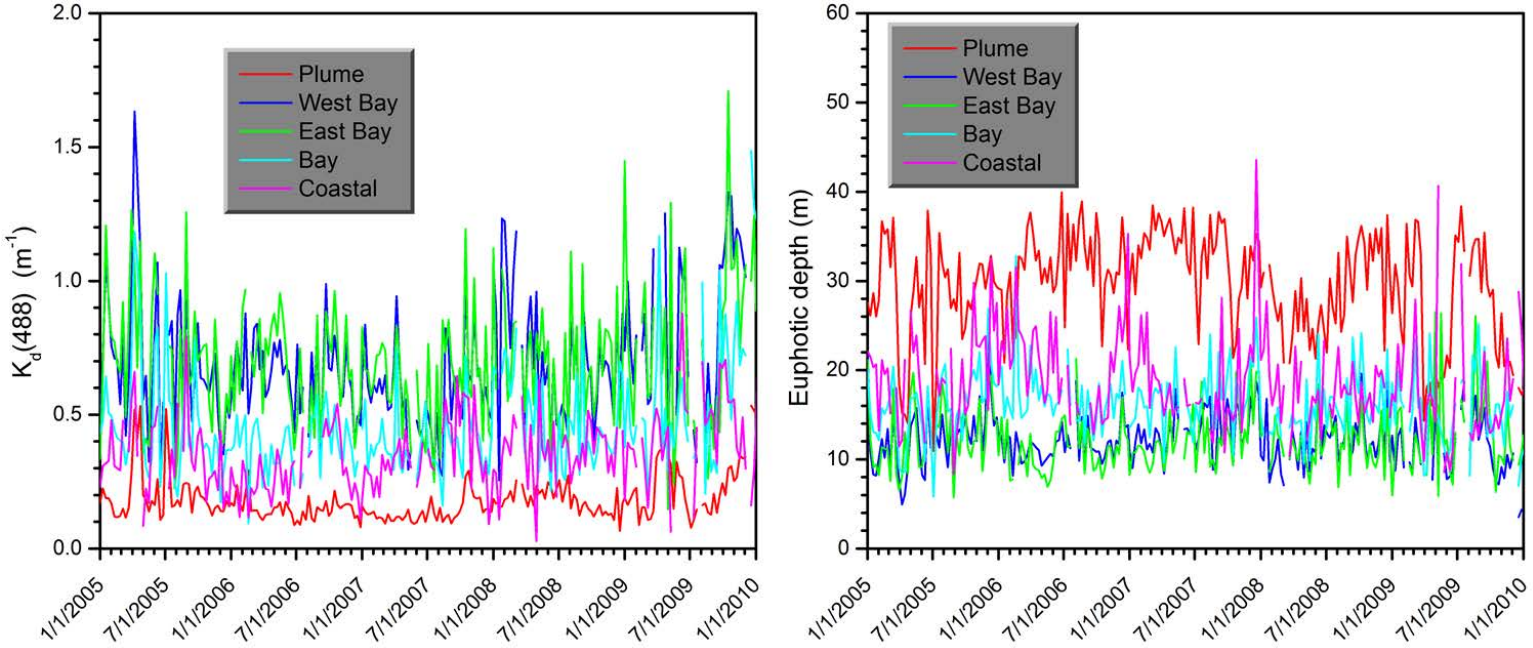

Figure 3-23. Time-series analysis. Weekly averages for 5-years, within-bay variability, Pensacola Bay. Diffuse attenuation coefficient, $K_d(488)$ and euphotic depth, Z_{eu}.

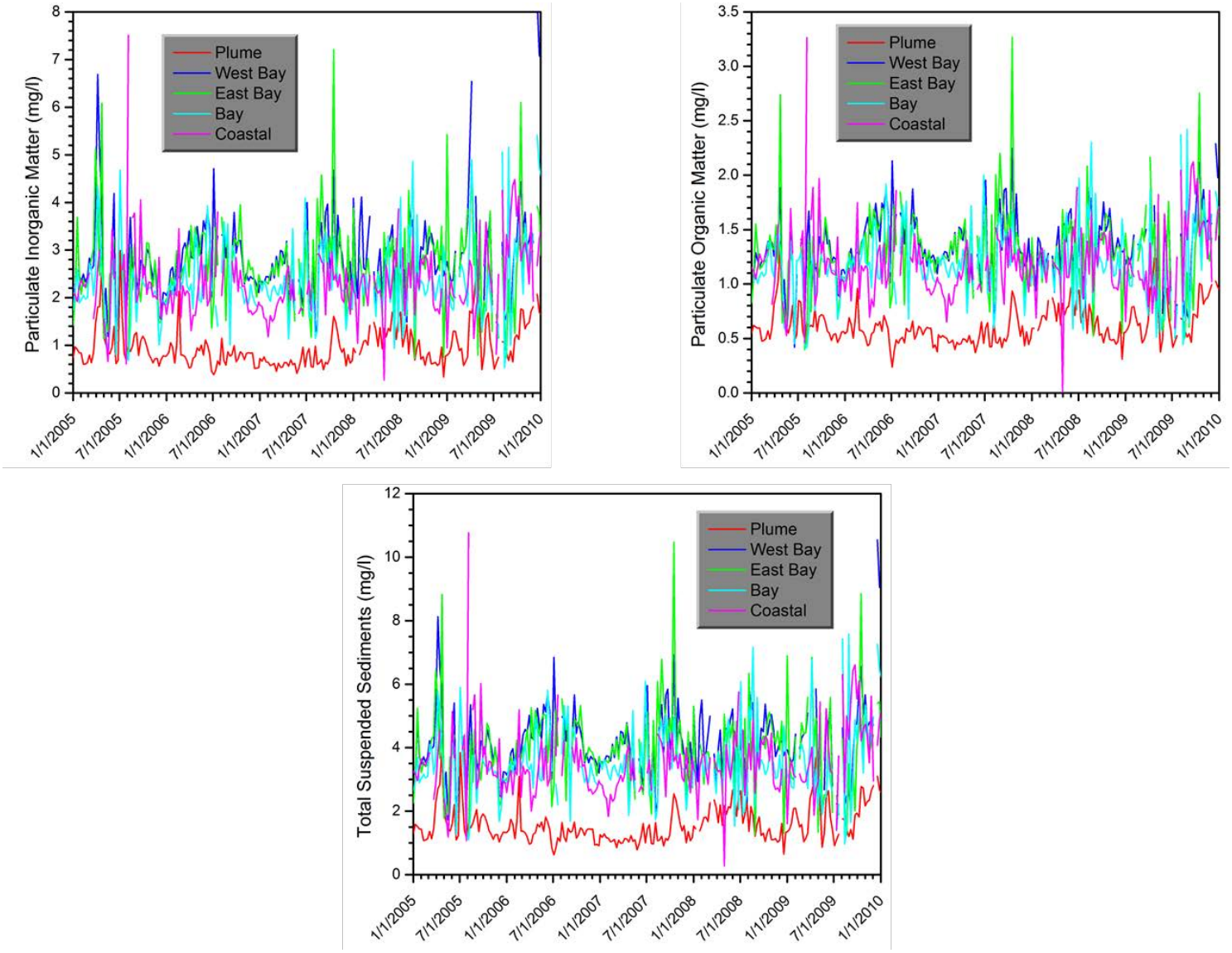

Figure 3-24. Time-series analysis. Weekly averages for 5-years, within-bay variability, Pensacola Bay. Particulate Inorganic Matter (PIM), Particulate Organic Matter (POM), and Total Suspended Solids (TSS) concentrations.

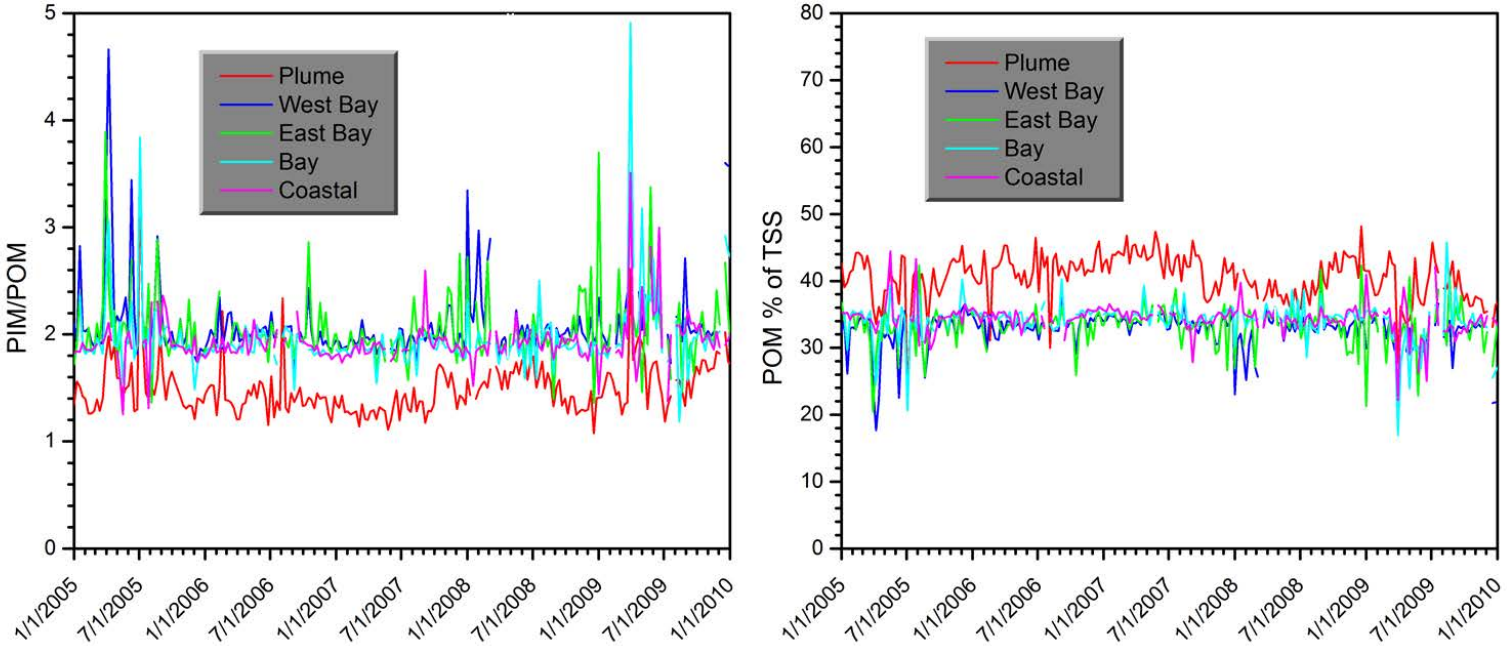

Figure 3-25. Time-series analysis. Weekly averages for 5-years, within-bay variability, Pensacola Bay. PIM/POM ratio and % of TSS represented by organic matter (POM % of TSS).

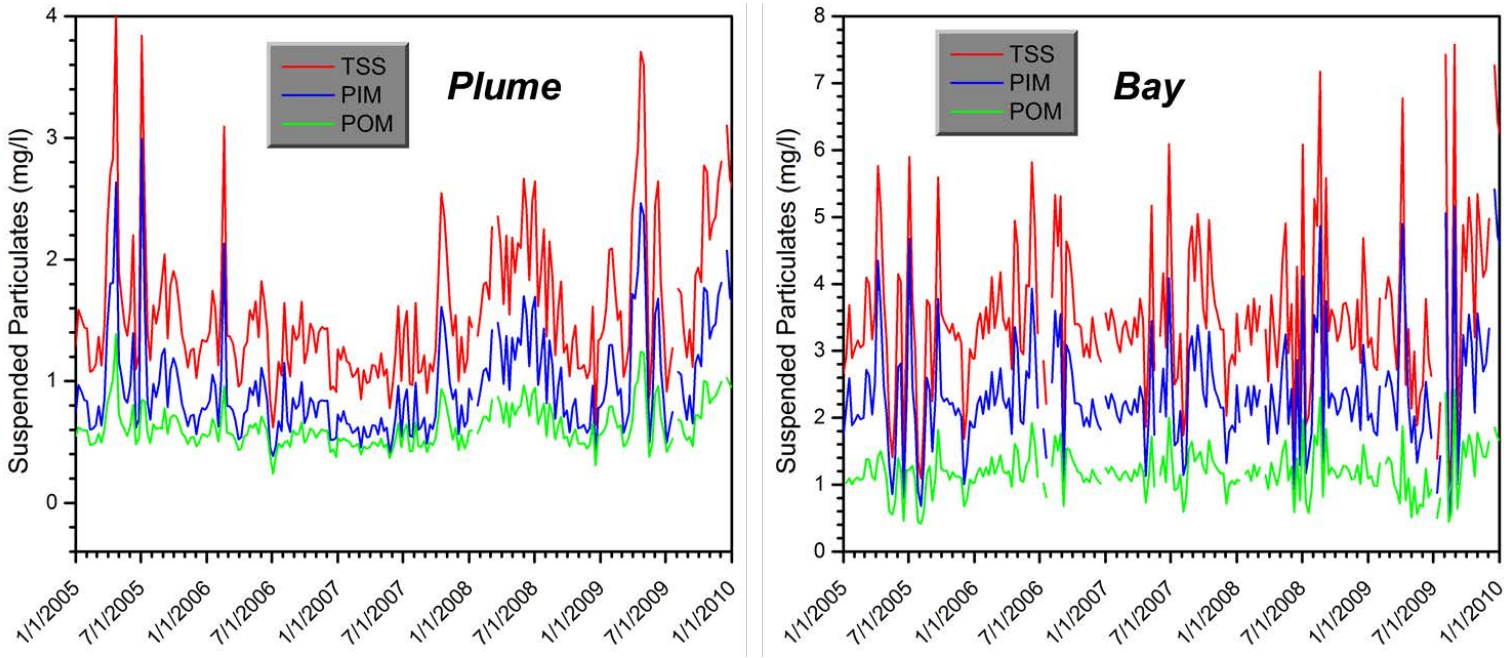

Figure 3-26. Time-series analysis. Weekly averages for 5-years, within-bay variability, Pensacola Bay. Comparison of suspended particulate loads in the plume and Bay.

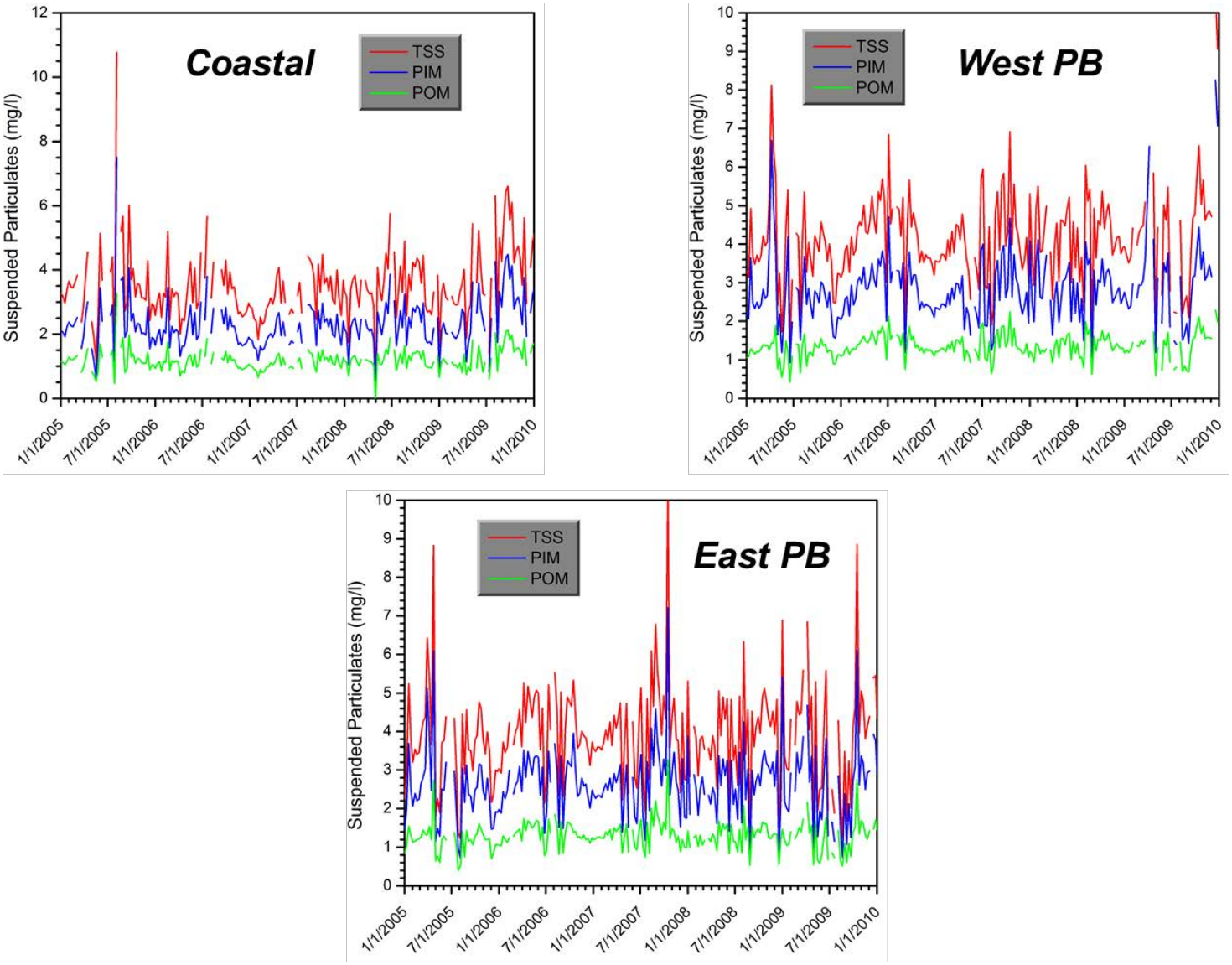

Figure 3-27. Time-series analysis. Weekly averages for 5-years, within-bay variability, Pensacola Bay. Comparison of suspended particulate loads in the coastal, West Bay, and East Bay subregions.

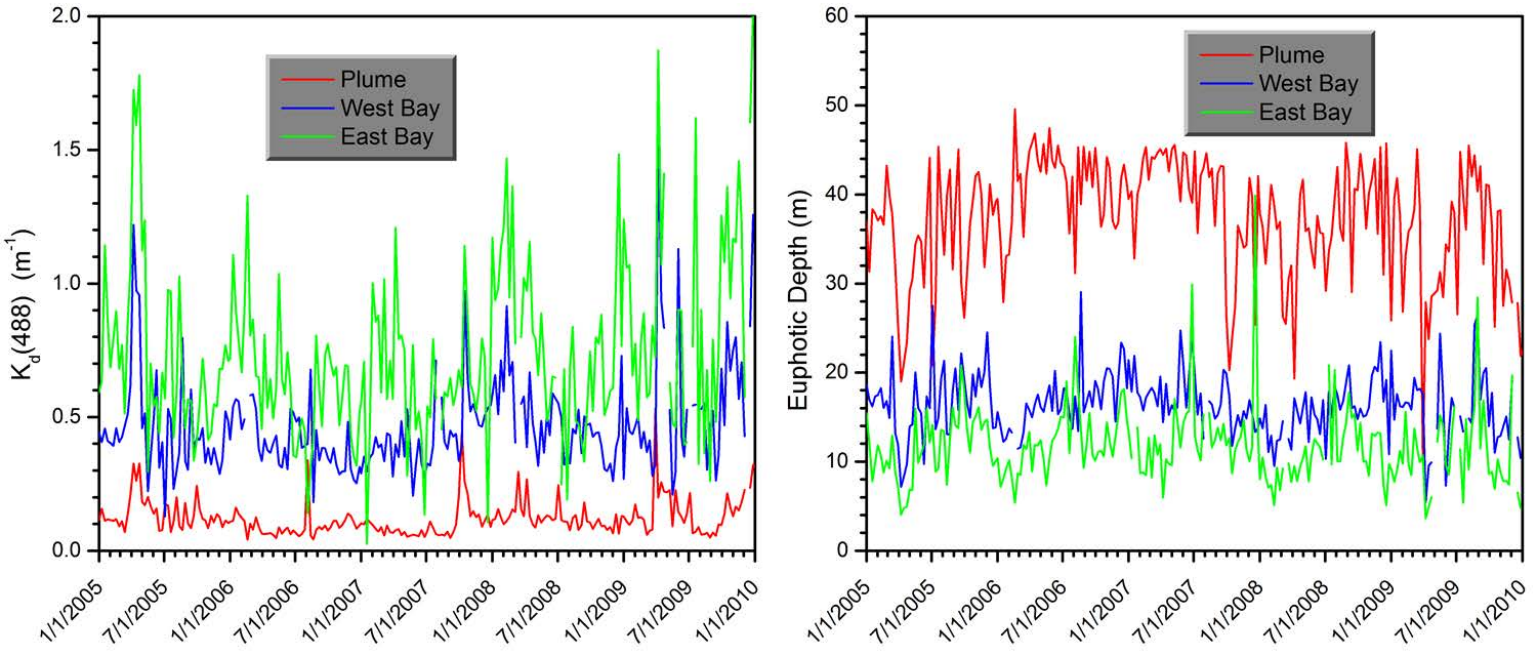

Figure 3-28. Time-series analysis. Weekly averages for 5-years, within-bay variability, Choctawhatchee Bay. Diffuse attenuation coefficient, $K_d(488)$ and euphotic depth, Z_{eu}.

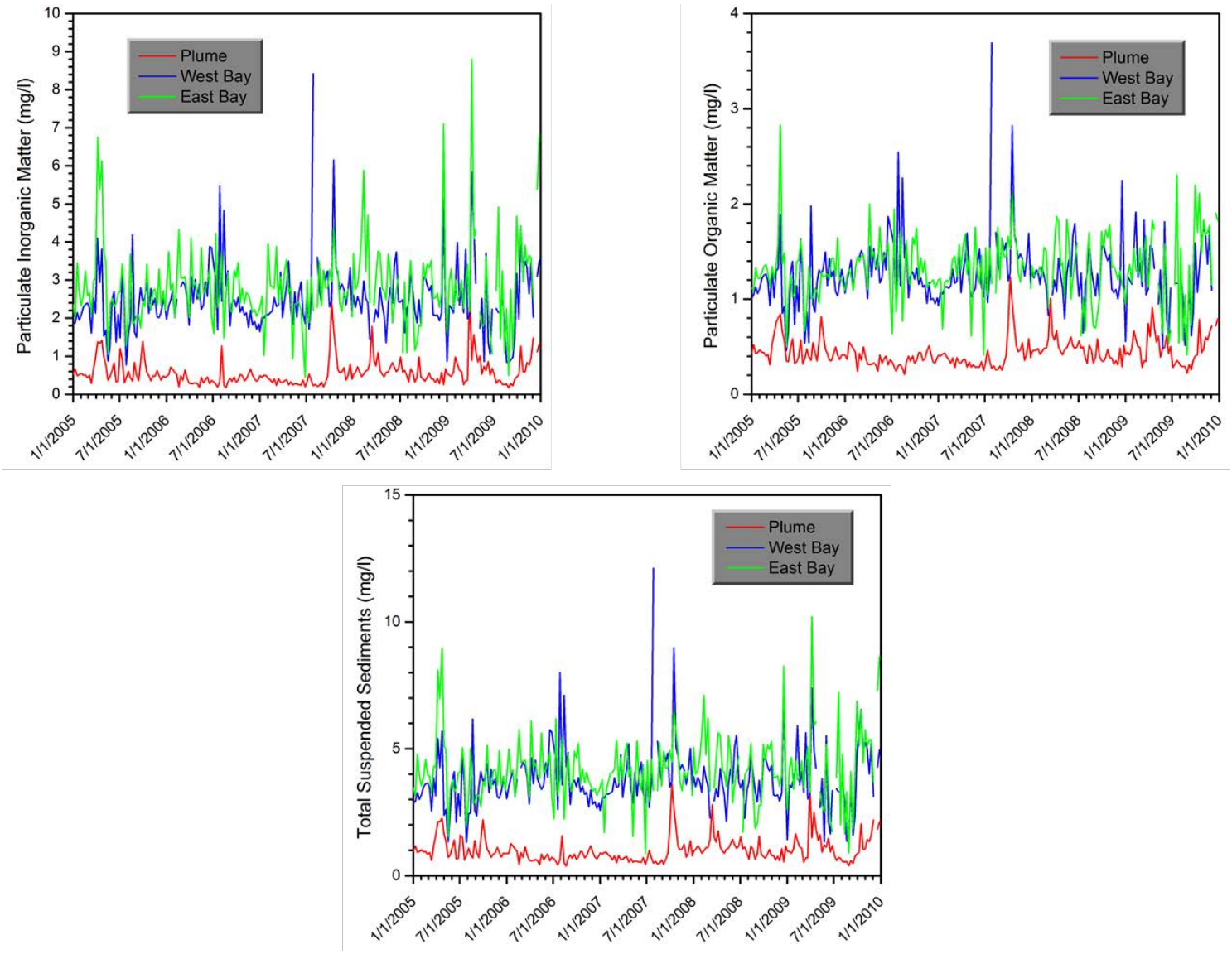

Figure 3-29. Time-series analysis. Weekly averages for 5-years, within-bay variability, Choctawhatchee Bay. Particulate Inorganic Matter (PIM), Particulate Organic Matter (POM), and Total Suspended Solids (TSS) concentrations.

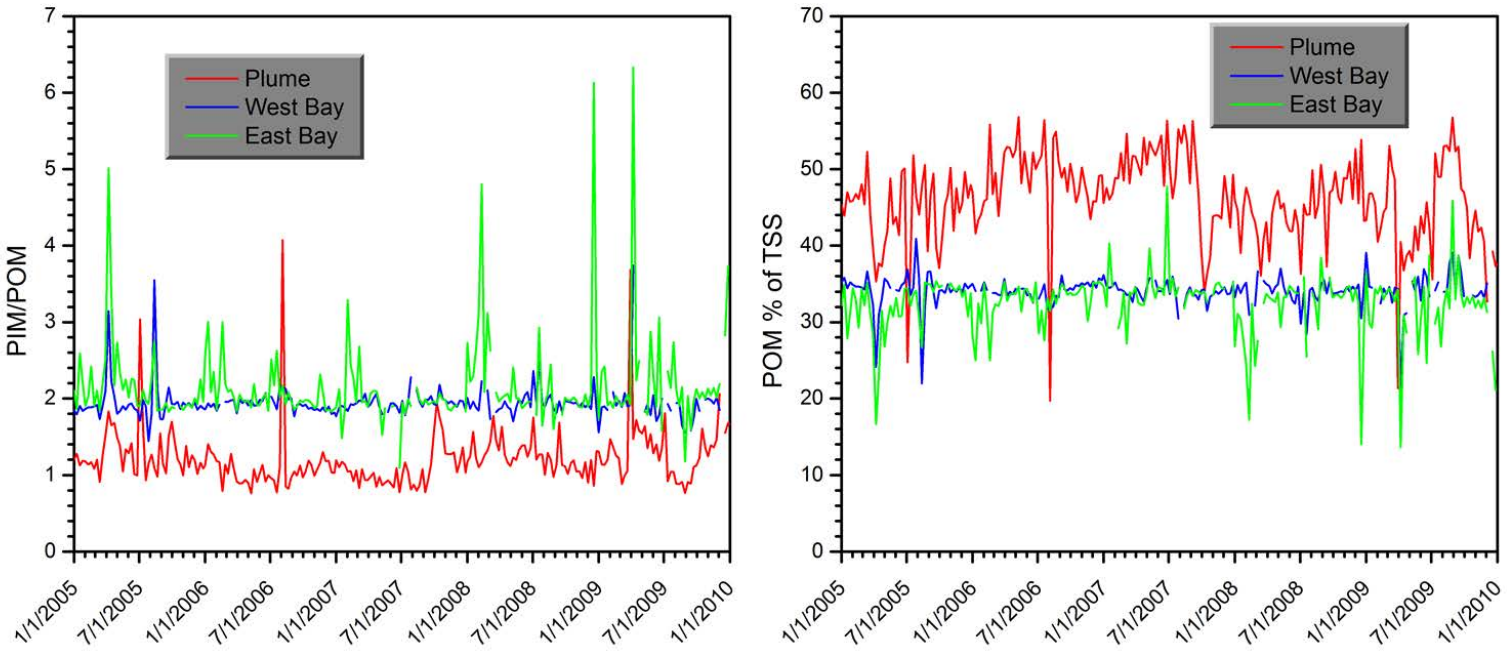

Figure 3-30. Time-series analysis. Weekly averages for 5-years, within-bay variability, Choctawhatchee Bay. PIM/POM ratio and % of TSS represented by organic matter (POM % of TSS).

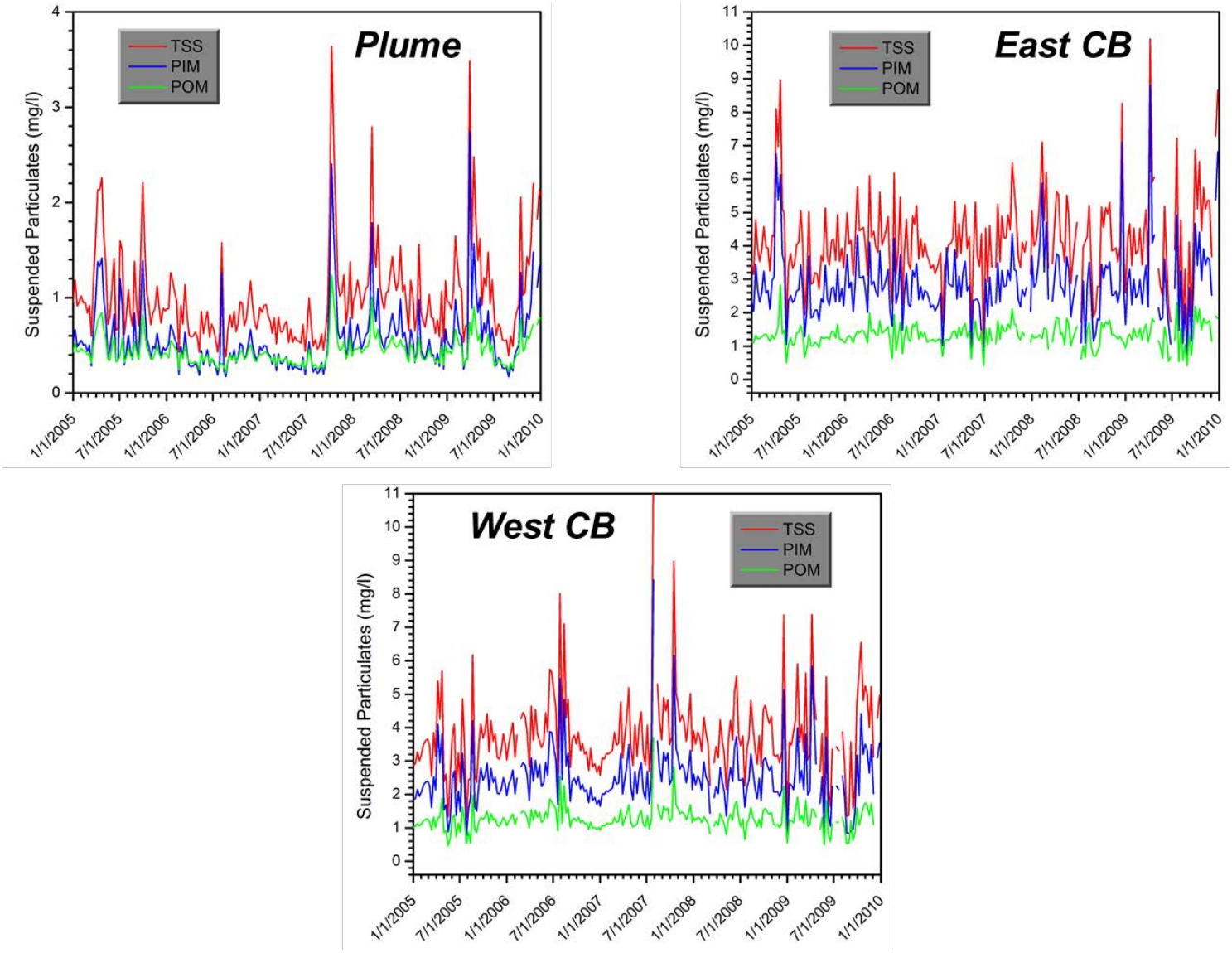

Figure 3-31. Time-series analysis. Weekly averages for 5-years, within-bay variability, Choctawhatchee Bay. Comparison of suspended particulate loads in the plume, East Bay, and West Bay subregions.

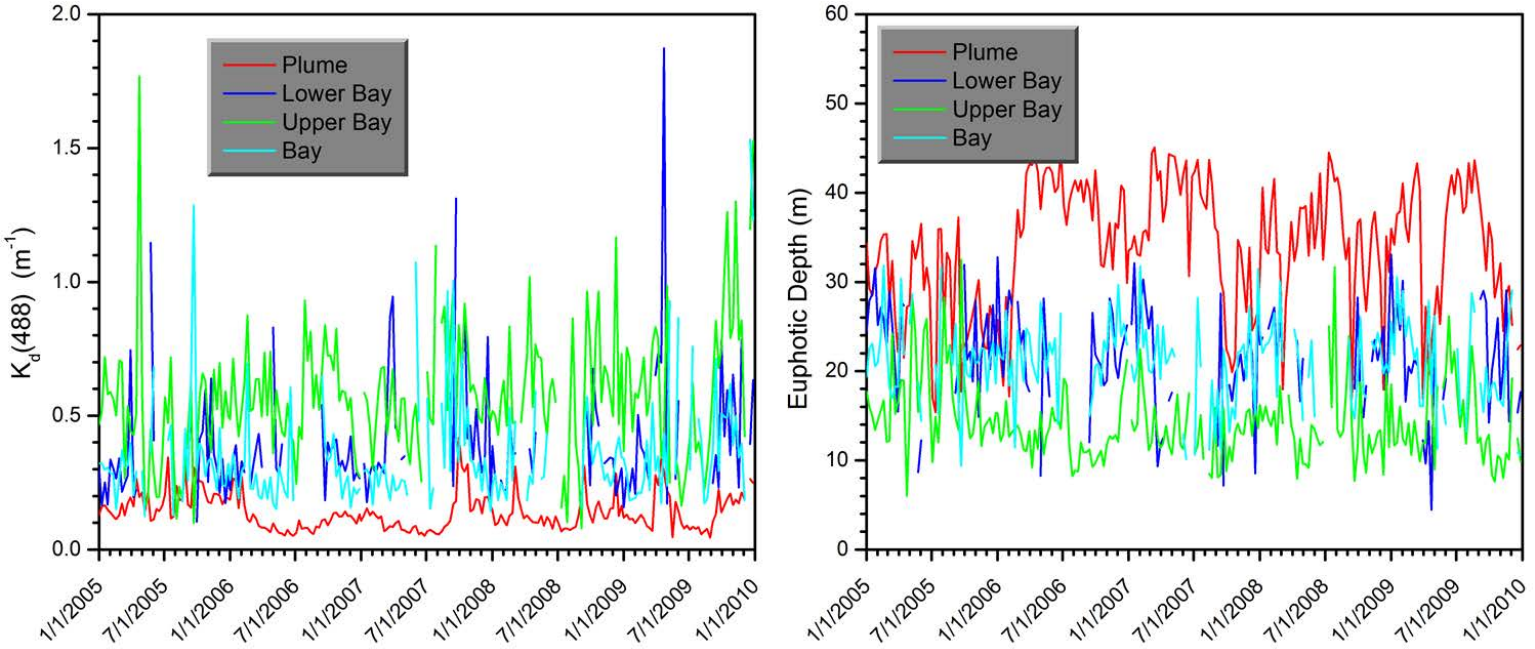

Figure 3-32. Time-series analysis. Weekly averages for 5-years, within-bay variability, St. Andrews Bay. Diffuse attenuation coefficient, $K_d(488)$ and euphotic depth, Z_{eu}.

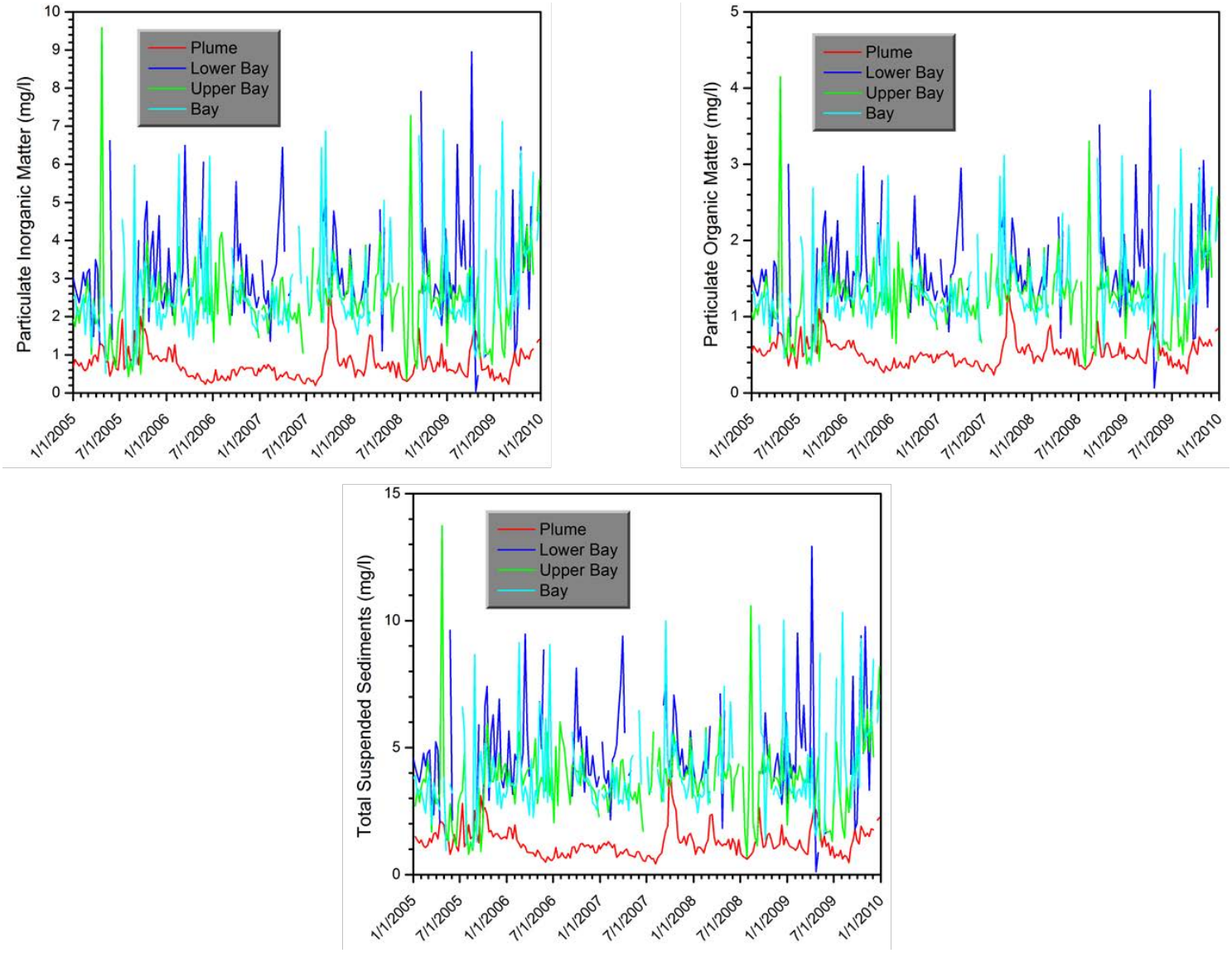

Figure 3-33. Time-series analysis. Weekly averages for 5-years, within-bay variability, St. Andrews Bay. Particulate Inorganic Matter (PIM), Particulate Organic Matter (POM), and Total Suspended Solids (TSS) concentrations.

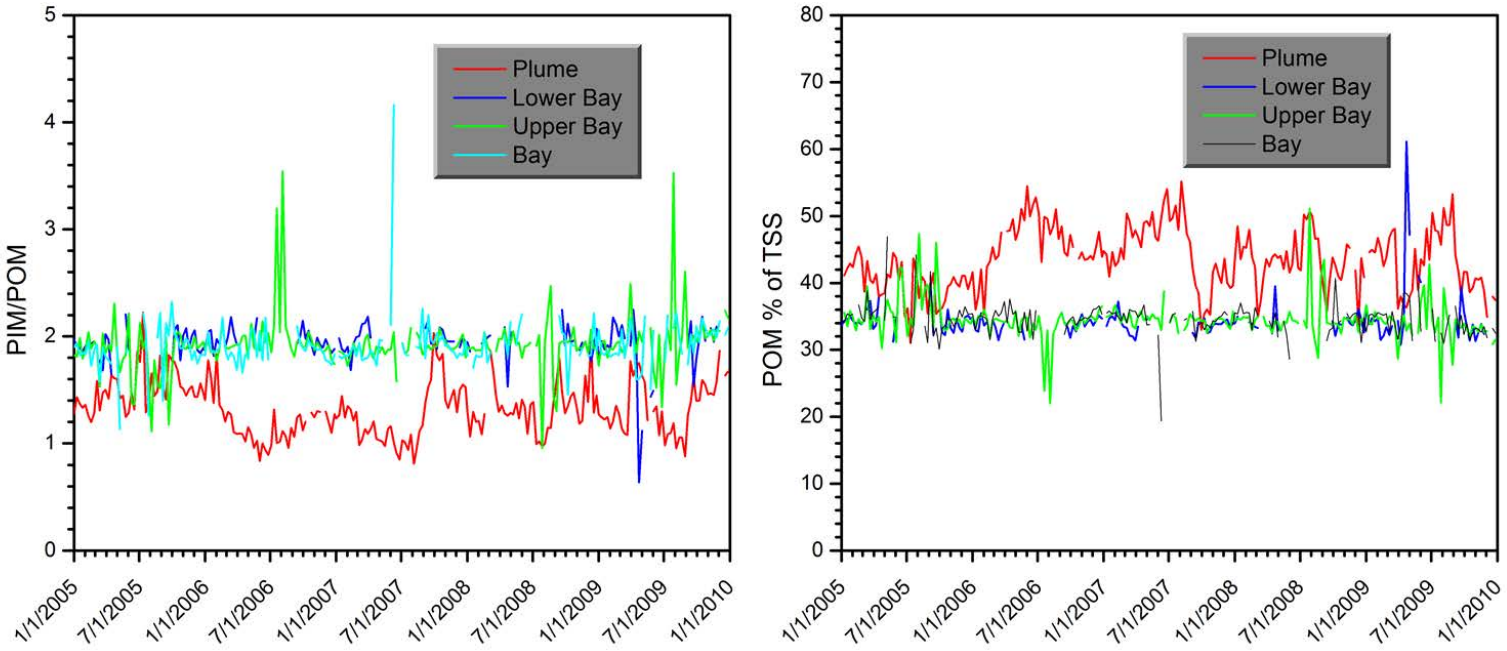

Figure 3-34. Time-series analysis. Weekly averages for 5-years, within-bay variability, St. Andrews Bay. PIM/POM ratio and % of TSS represented by organic matter (POM % of TSS).

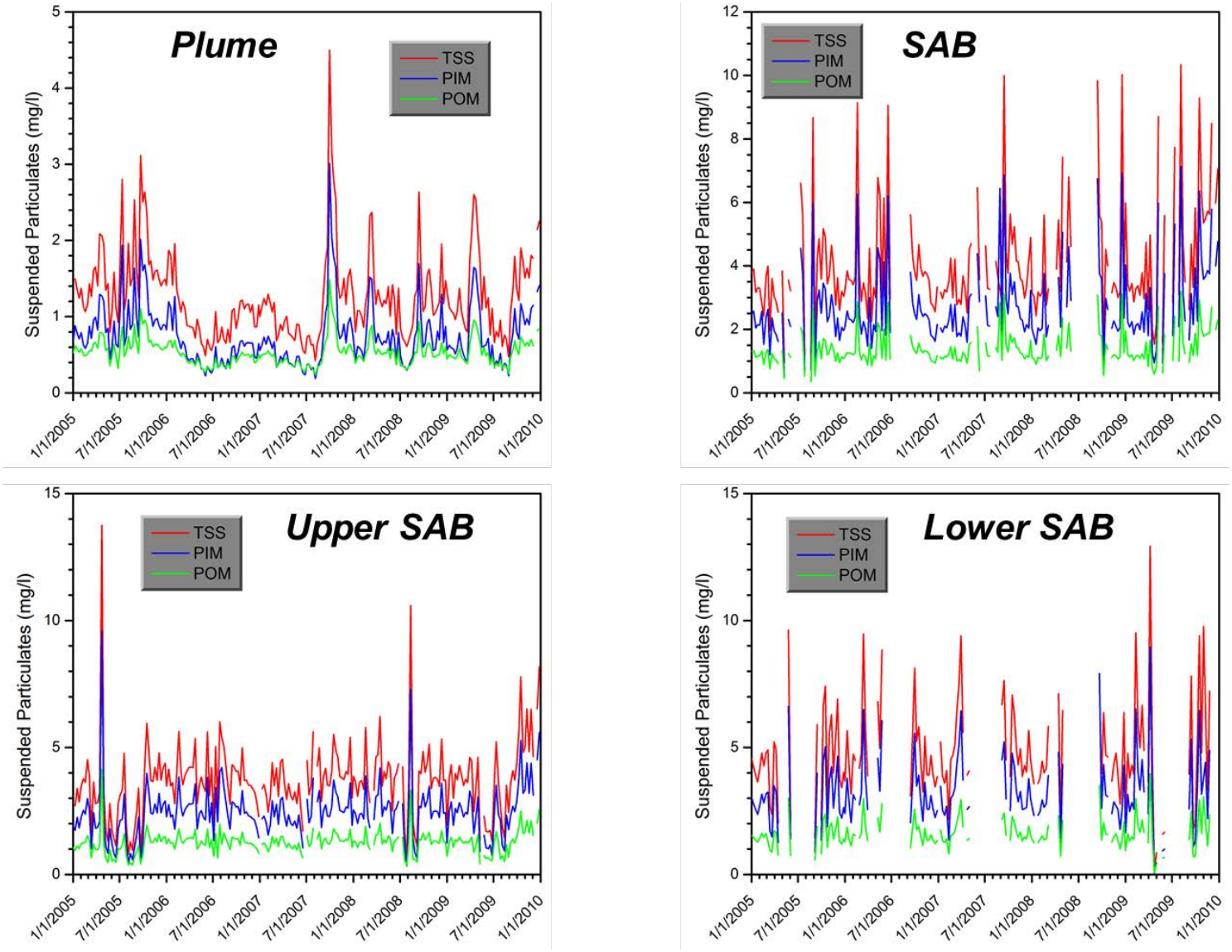

Figure 3-35. Time-series analysis. Weekly averages for 5-years, within-bay variability, St. Andrews Bay. Comparison of suspended particulate loads in the plume, Bay, Upper Bay, and Lower Bay subregions.

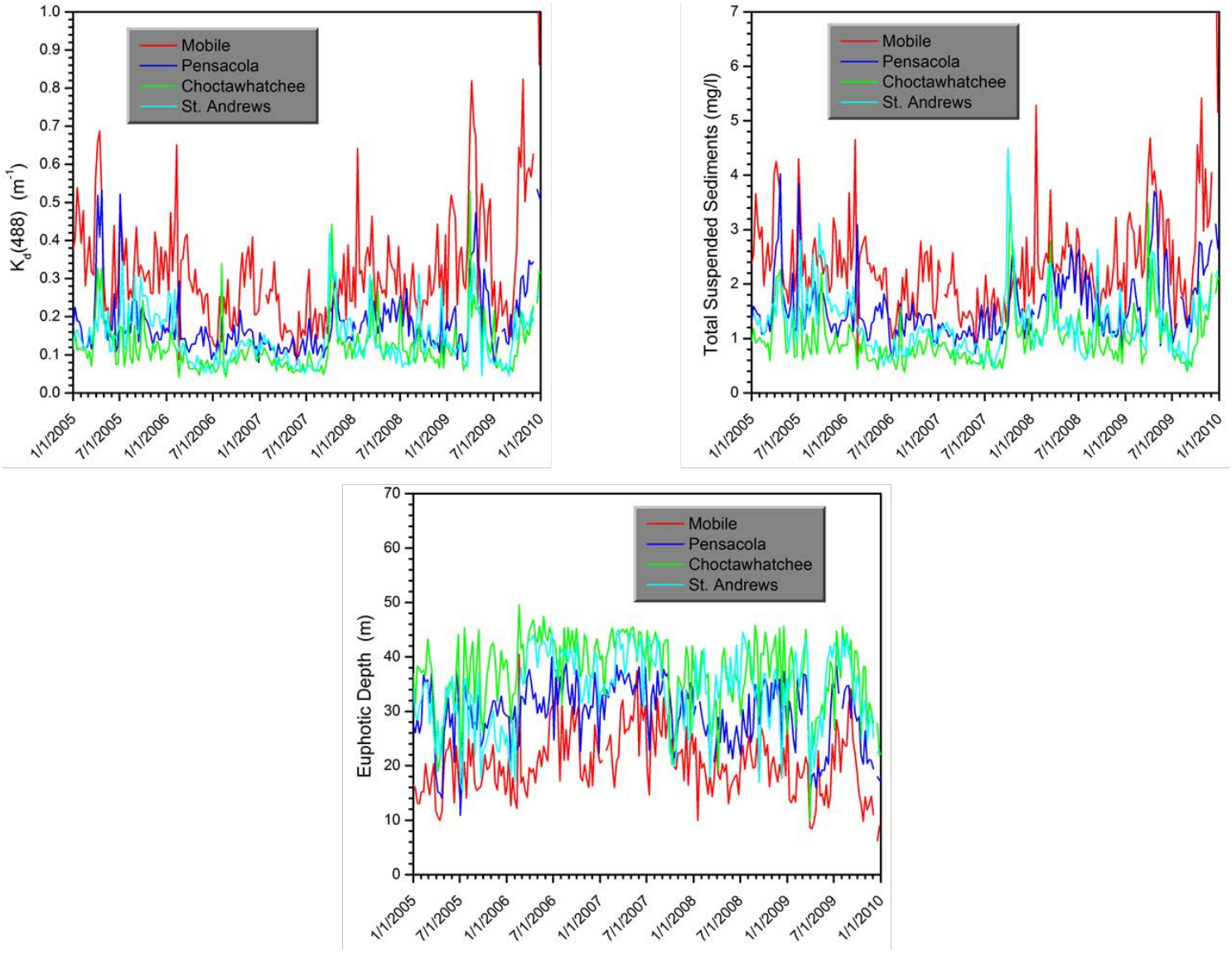

Figure 3-36. Time-series analysis. Weekly averages for 5-years, between-bay variability (plume subregions). Diffuse attenuation coefficient, $K_d(488)$, Total Suspended Solids (TSS), and euphotic depth, Z_{eu}.

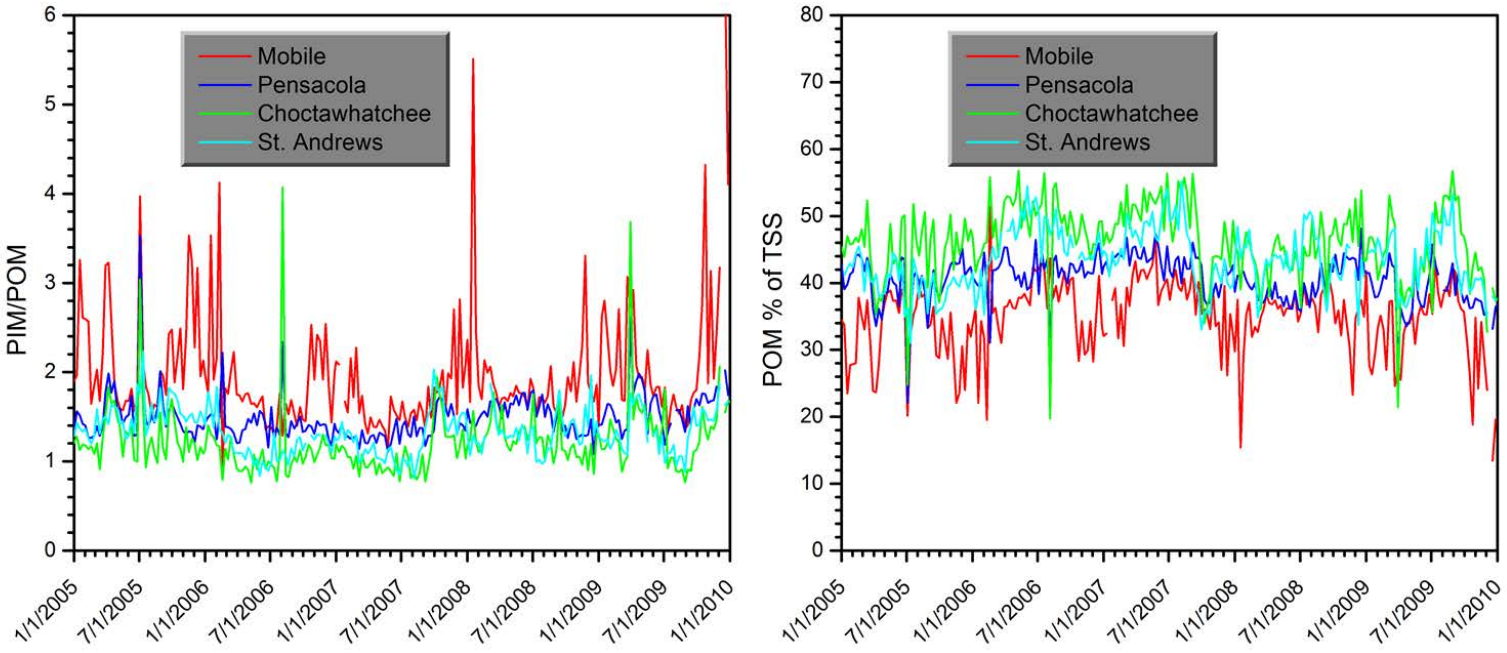

Figure 3-37. Time-series analysis. Weekly averages for 5-years, between-bay variability (plume subregions). PIM/POM ratio and % of TSS represented by organic matter (POM % of TSS).

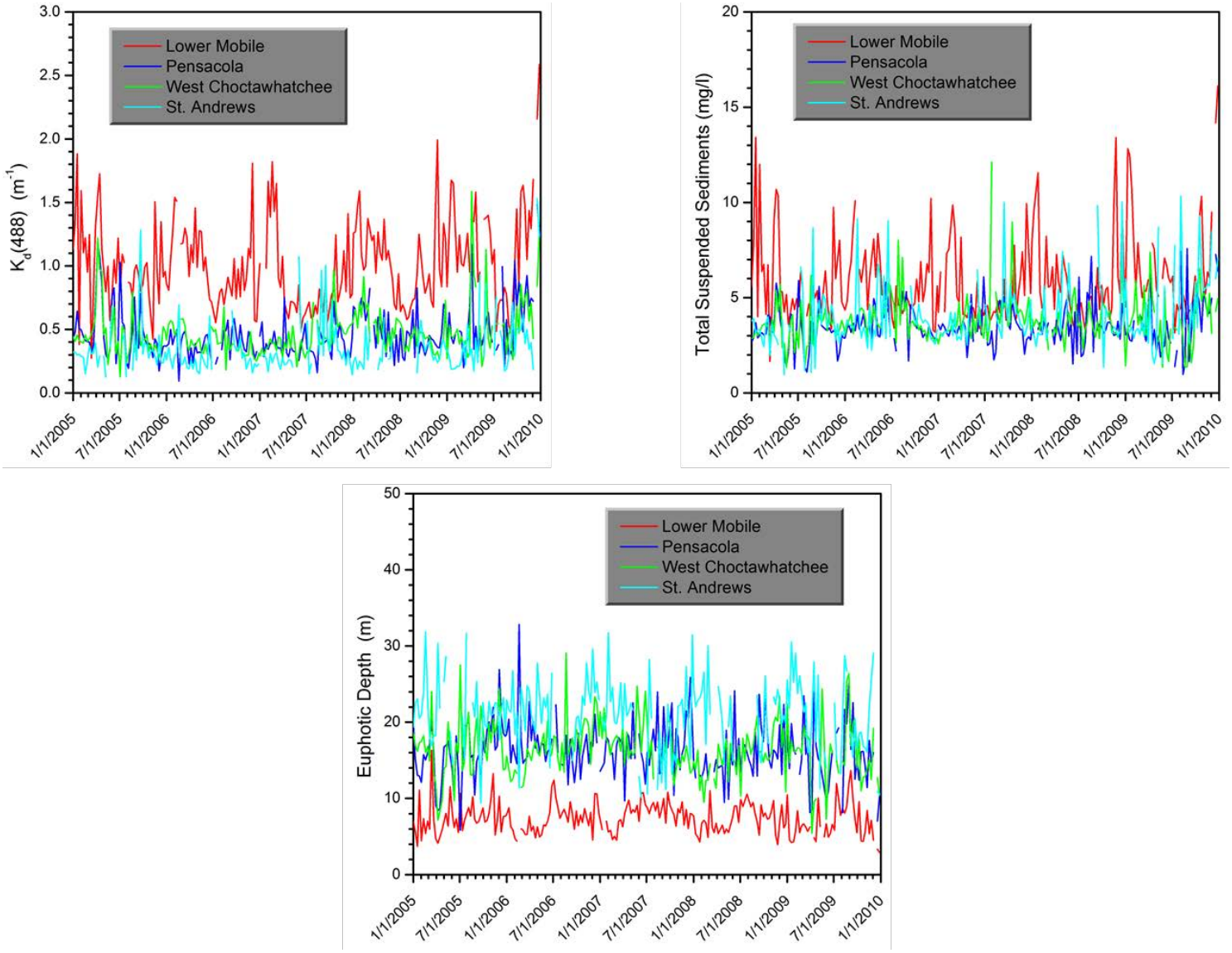

Figure 3-38. Time-series analysis. Weekly averages for 5-years, between-bay variability (bay subregions). Diffuse attenuation coefficient, $K_d(488)$, Total Suspended Solids (TSS), and euphotic depth, Z_{eu}.

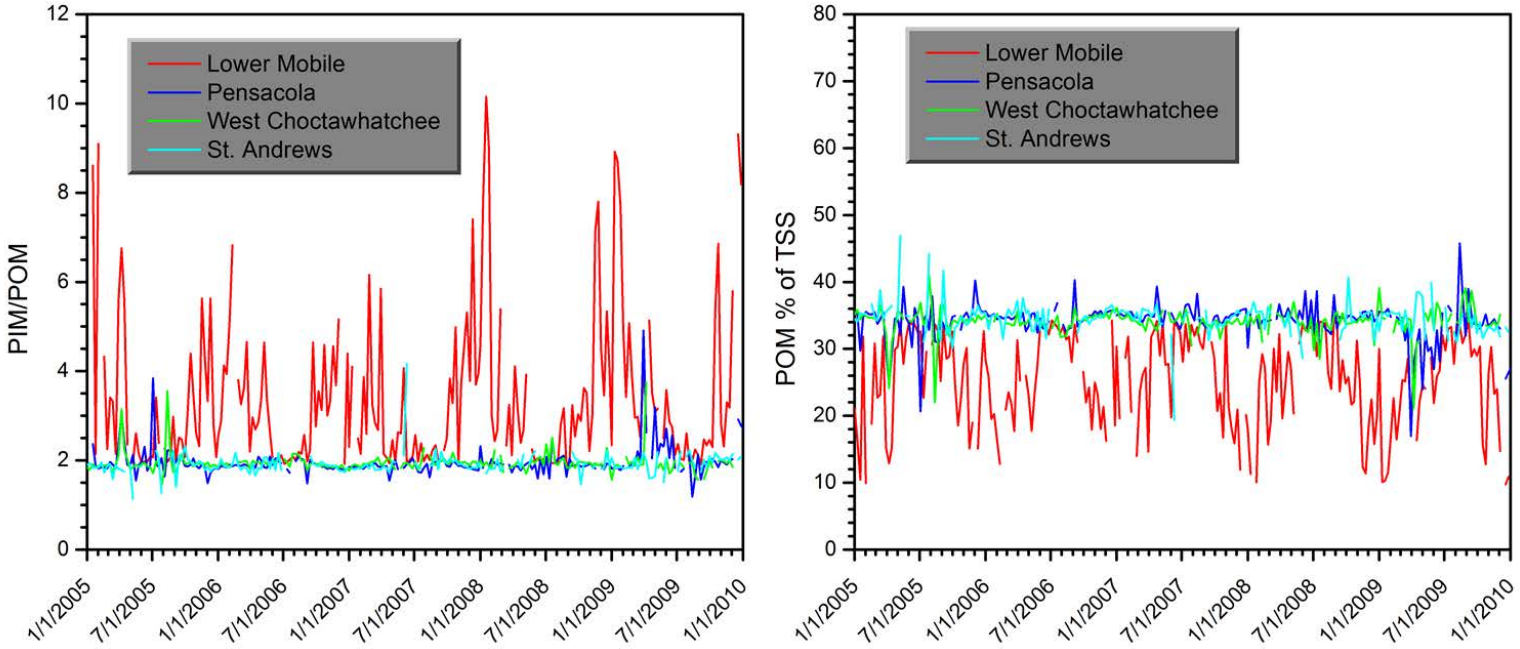

Figure 3-39. Time-series analysis. Weekly averages for 5-years, between-bay variability (bay subregions). PIM/POM ratio and % of TSS represented by organic matter (POM % of TSS).

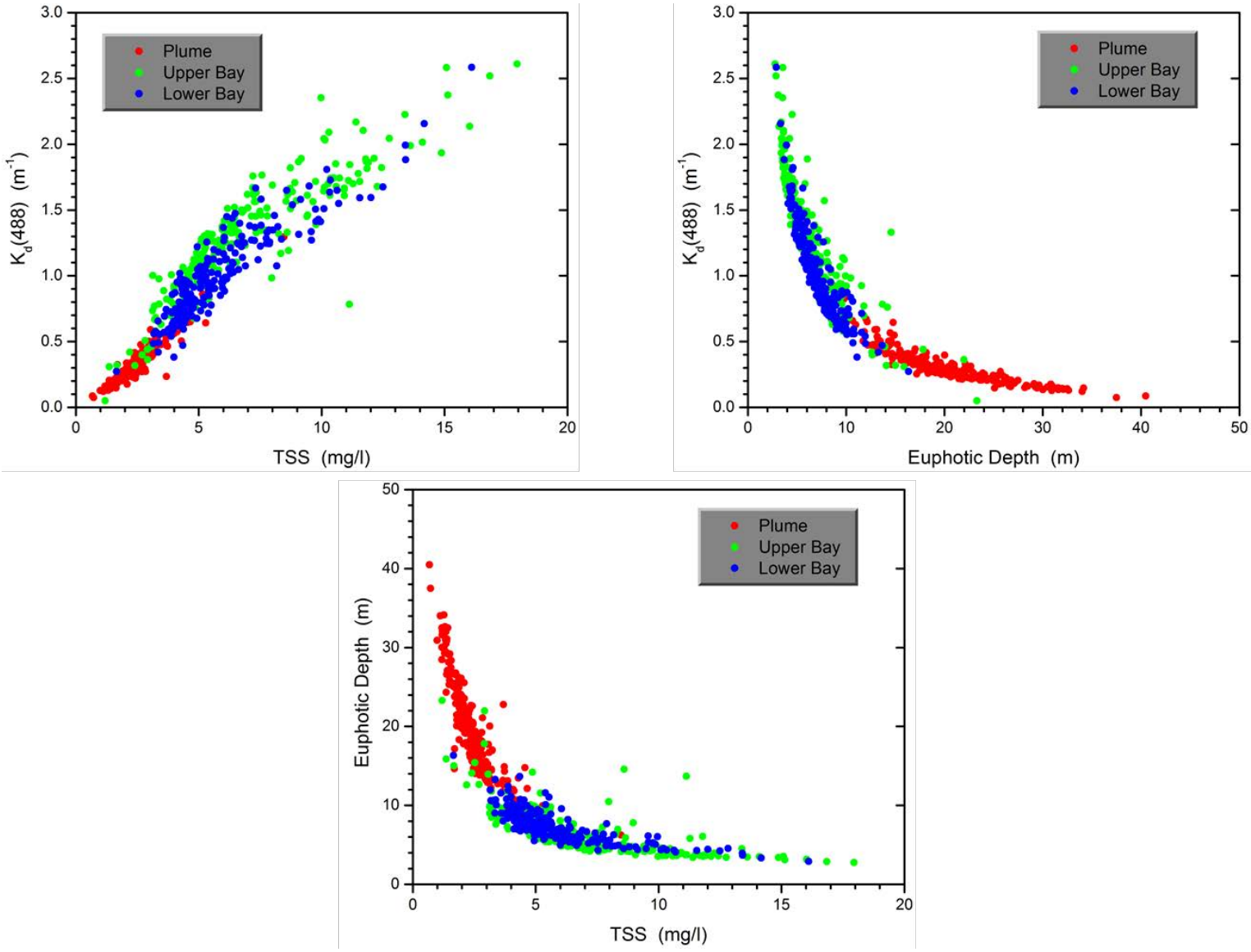

Figure 3-40. Bio-Optical Property Relationships. Weekly averages for 5-years, within-bay variability, Mobile Bay. $K_d(488)$ vs. TSS, $K_d(488)$ vs. Z_{eu}, Z_{eu} vs. TSS.

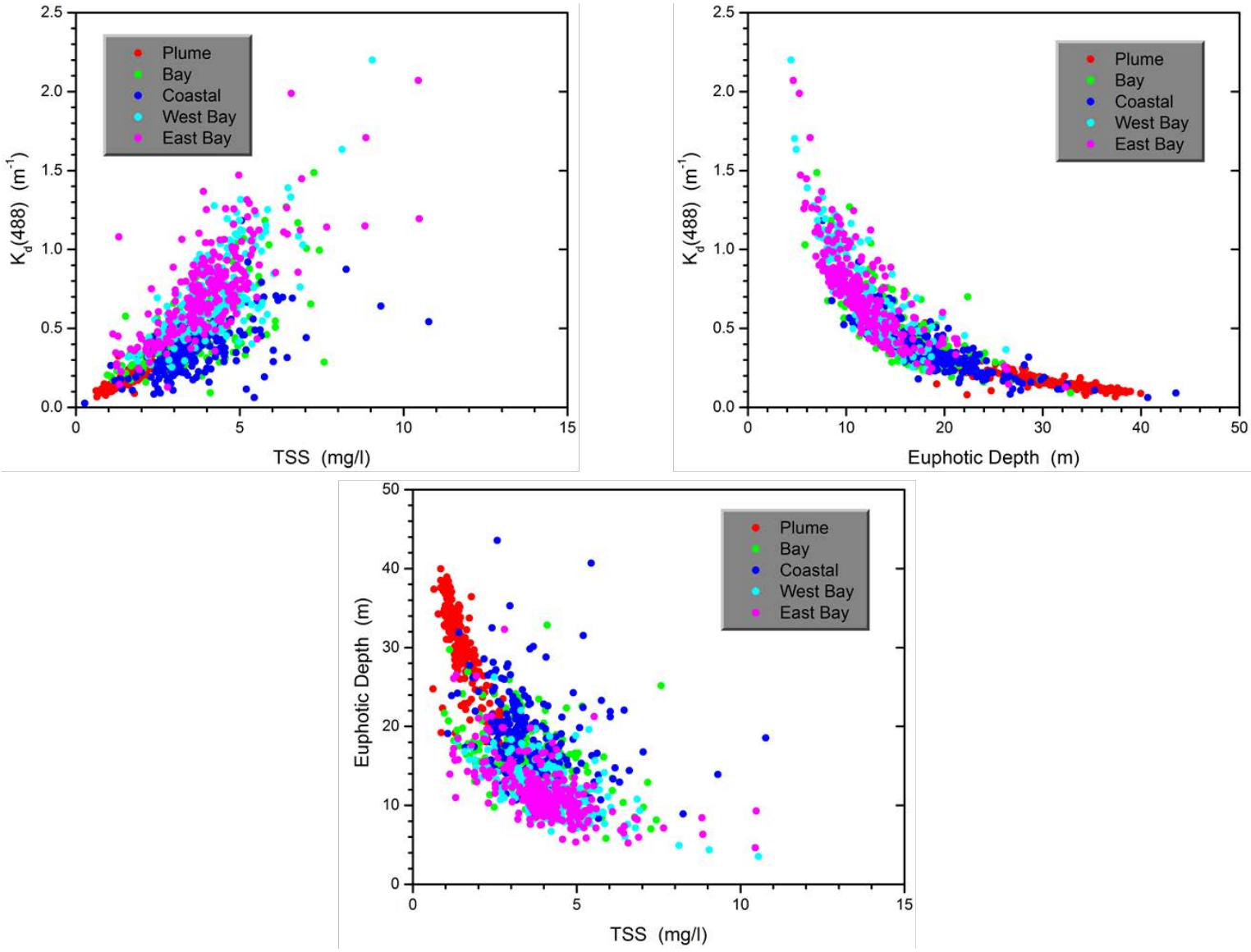

Figure 3-41. Bio-Optical Property Relationships. Weekly averages for 5-years, within-bay variability, Pensacola Bay. $K_d(488)$ vs. TSS, $K_d(488)$ vs. Z_{eu}, Z_{eu} vs. TSS.

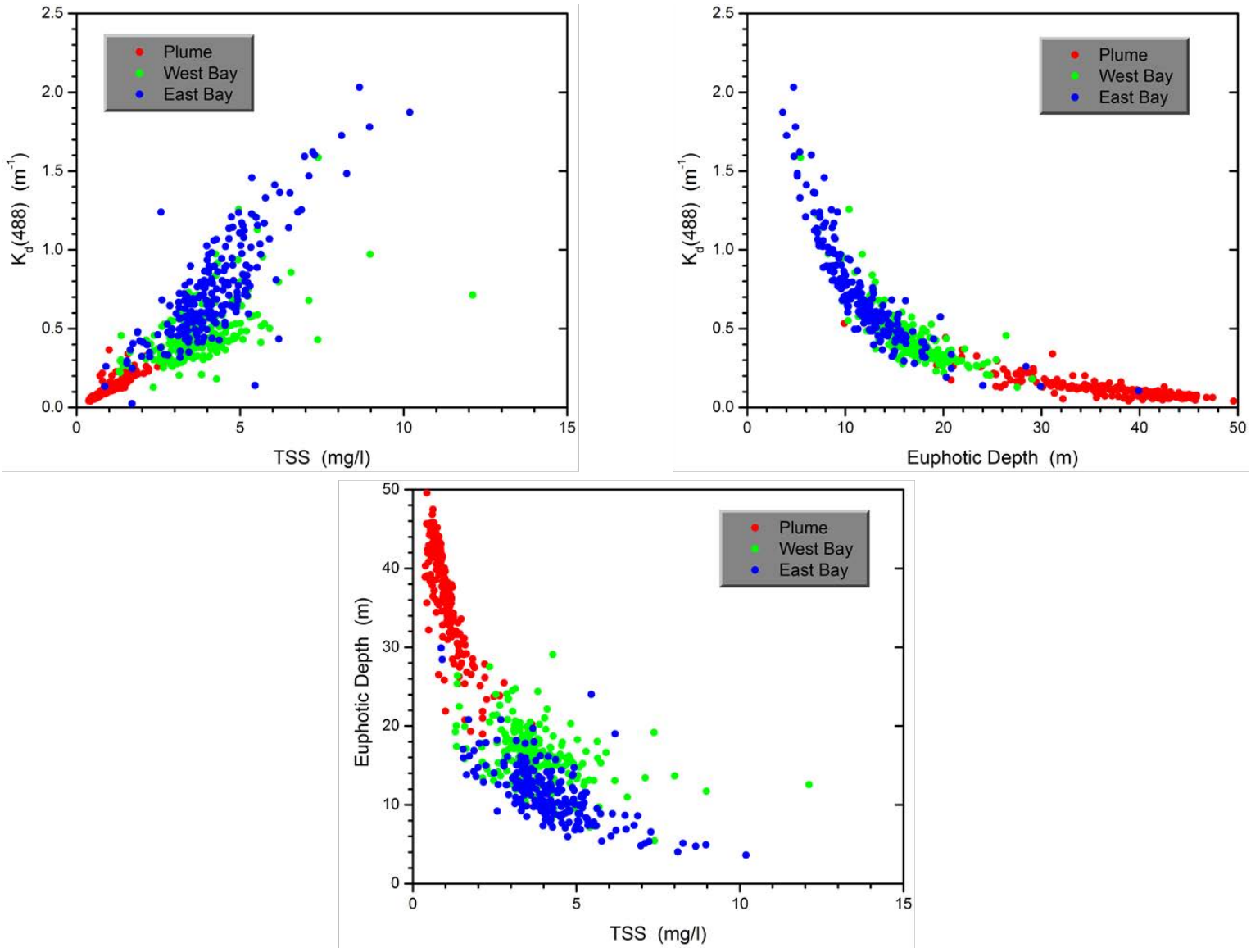

Figure 3-42. Bio-Optical Property Relationships. Weekly averages for 5-years, within-bay variability, Choctawhatchee Bay. $K_d(488)$ vs. TSS, $K_d(488)$ vs. Z_{eu}, Z_{eu} vs. TSS.

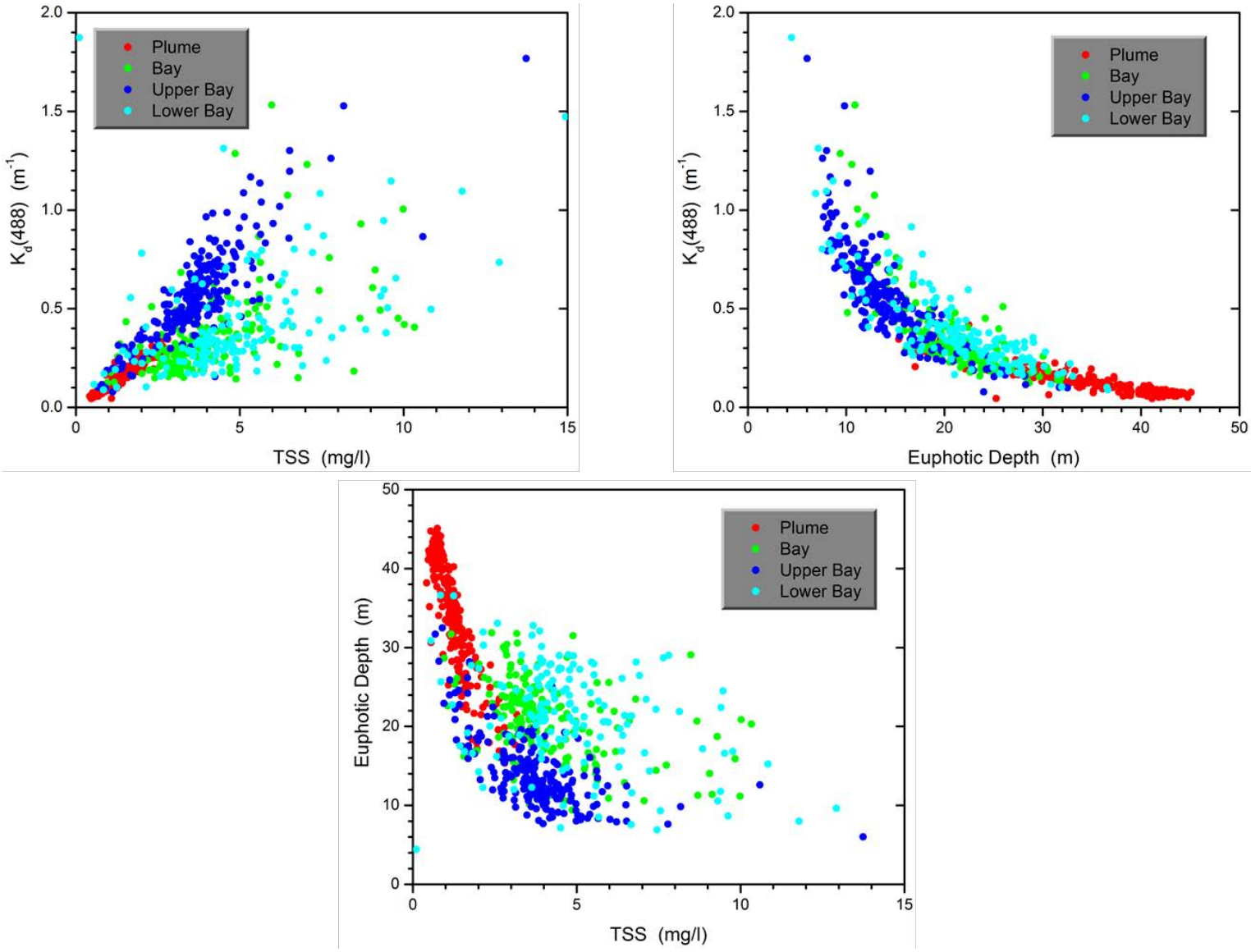

Figure 3-43. Bio-Optical Property Relationships. Weekly averages for 5-years, within-bay variability, St. Andrews Bay. $K_d(488)$ vs. TSS, $K_d(488)$ vs. Z_{eu}, Z_{eu} vs. TSS.

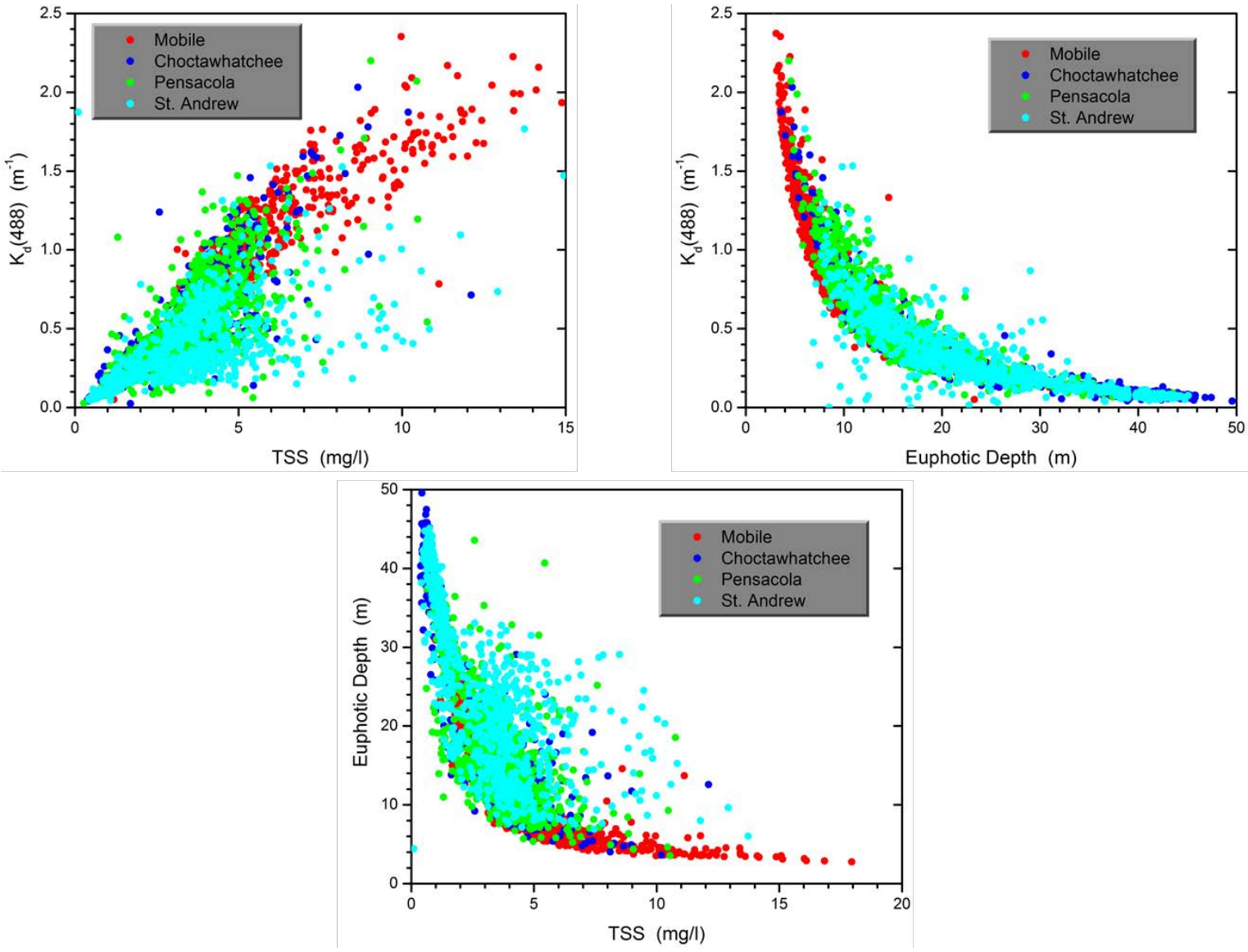

Figure 3-44. Bio-Optical Property Relationships. Weekly averages for 5-years, between-bay variability (all subregions in each bay included). $K_d(488)$ vs. TSS, $K_d(488)$ vs. Z_{eu}, Z_{eu} vs. TSS.

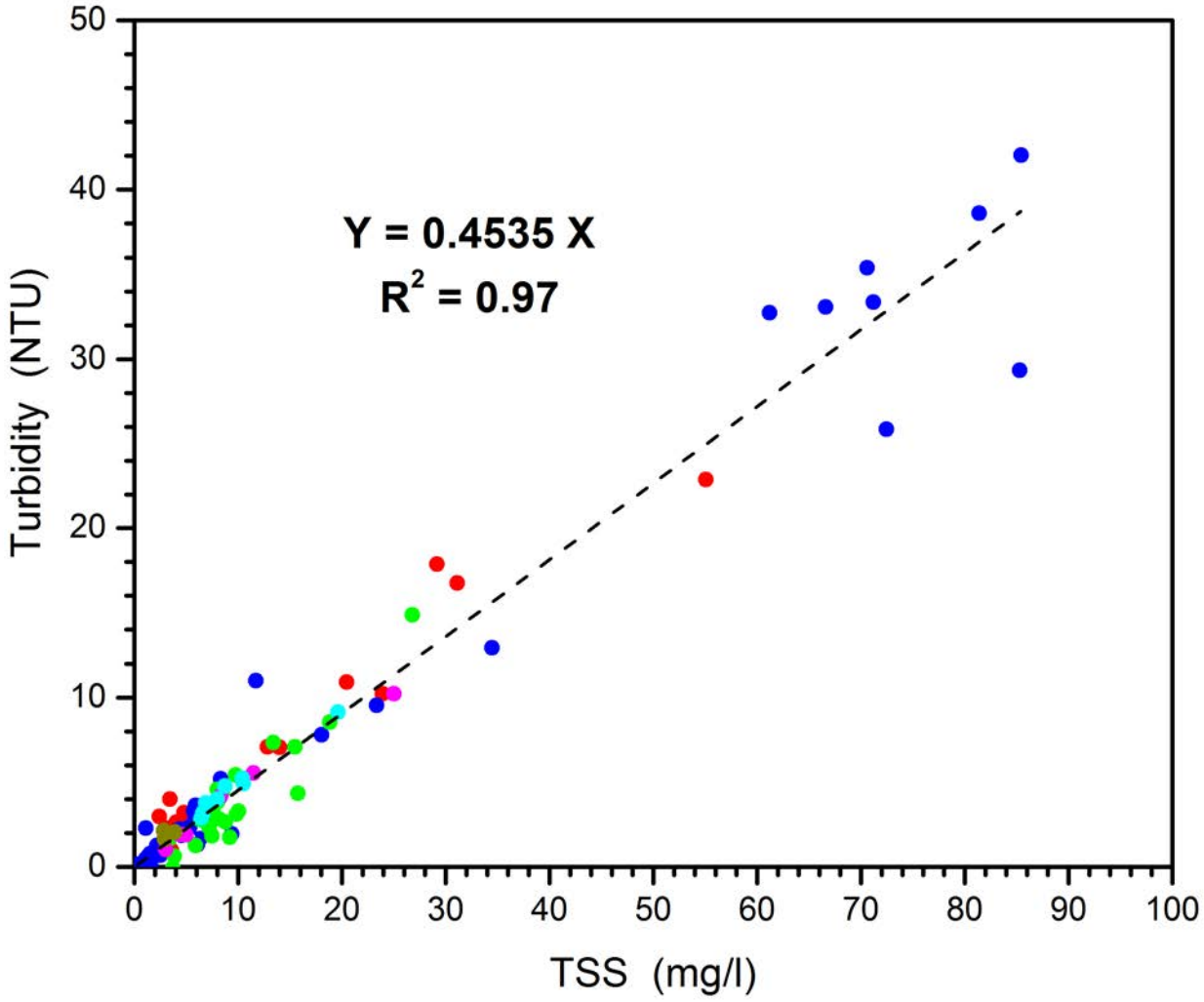

Figure 3-45. Turbidity (NTU) vs. TSS. In situ data from 6 cruises in the Mississippi Bight and Mobile Bay areas. For converting from satellite TSS values to alternative units (Nephelometric Turbidity Units, NTU) frequently used by USACE.

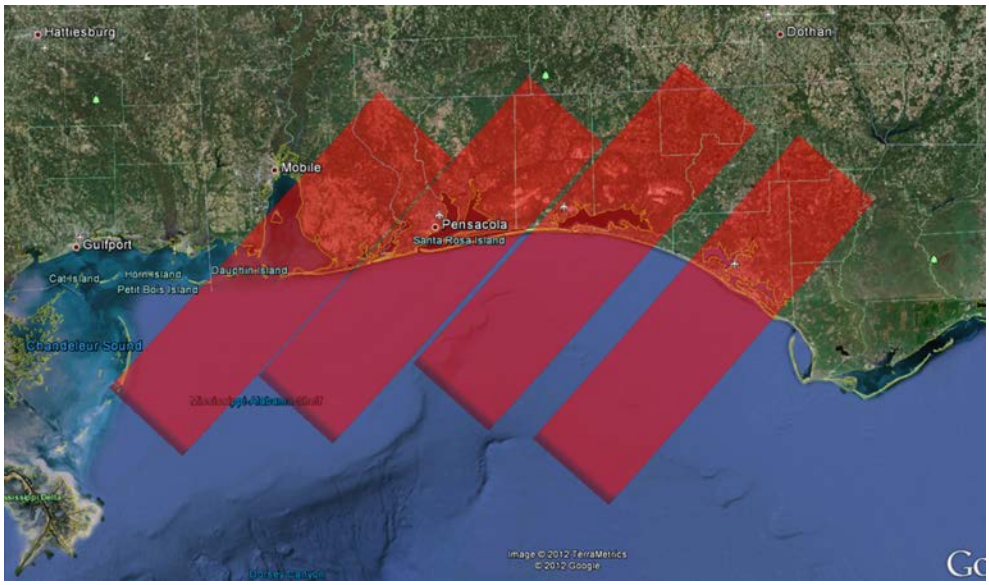

Figure 3-46. HICO targets covering the bays of interest (ascending passes; descending pass coverage not shown).

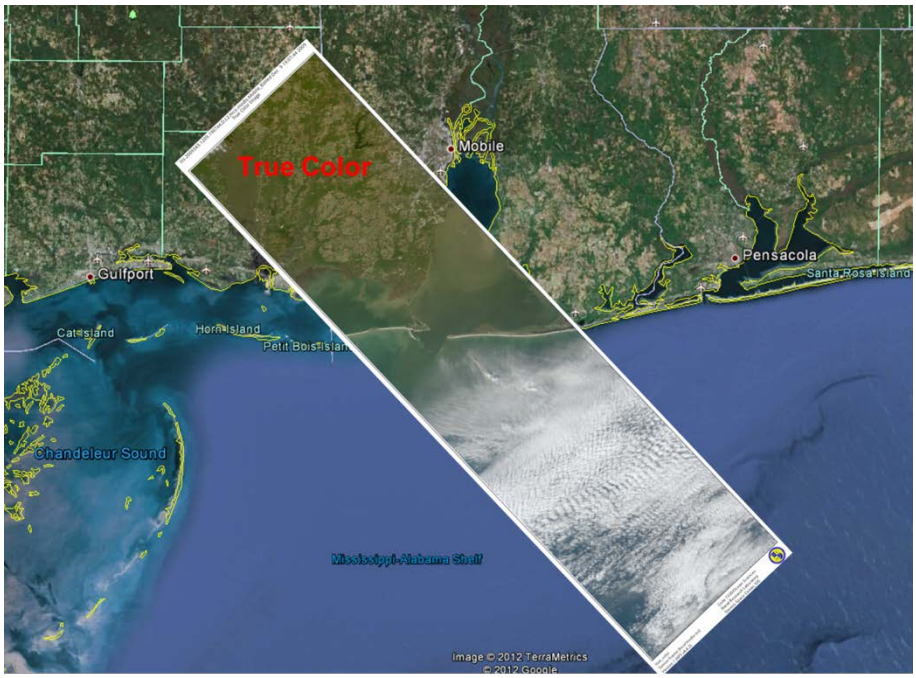

Figure 3-47. HICO image, 9 December 2009, Mobile Bay, AL. True color image.

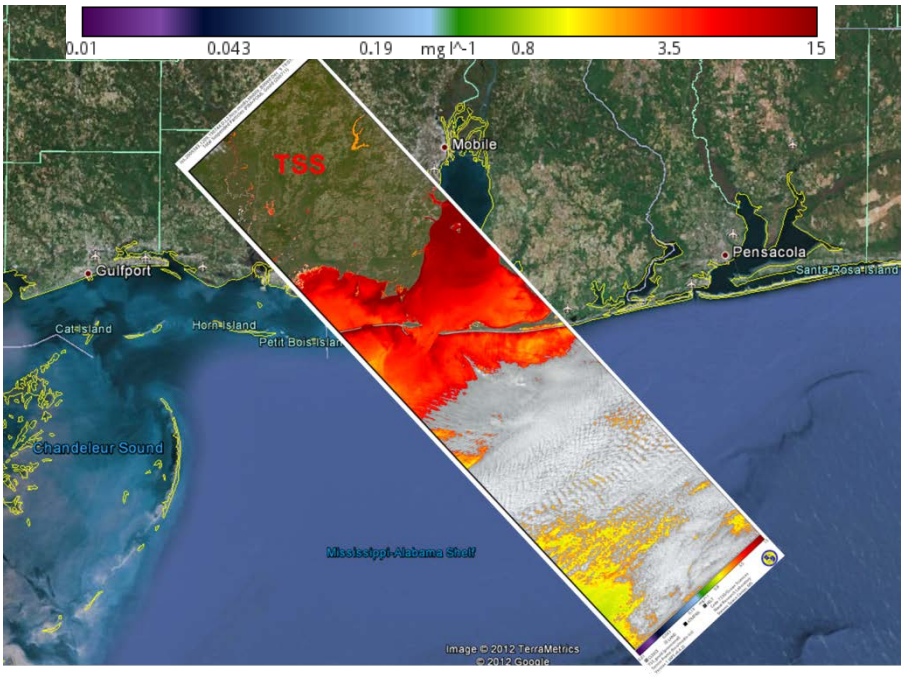

Figure 3-48. HICO image, 9 December 2009, Mobile Bay, AL. Total Suspended Solids (TSS) concentration.

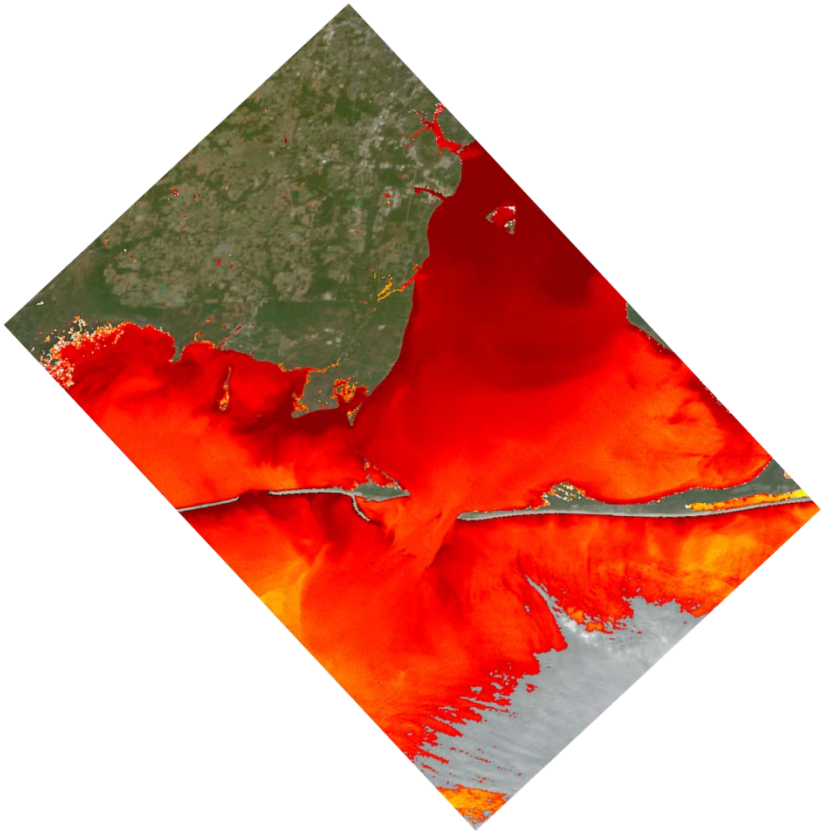

Figure 3-49. Zoomed image of Figure 3-48, showing coastal details. Total Suspended Solids (TSS) concentration.

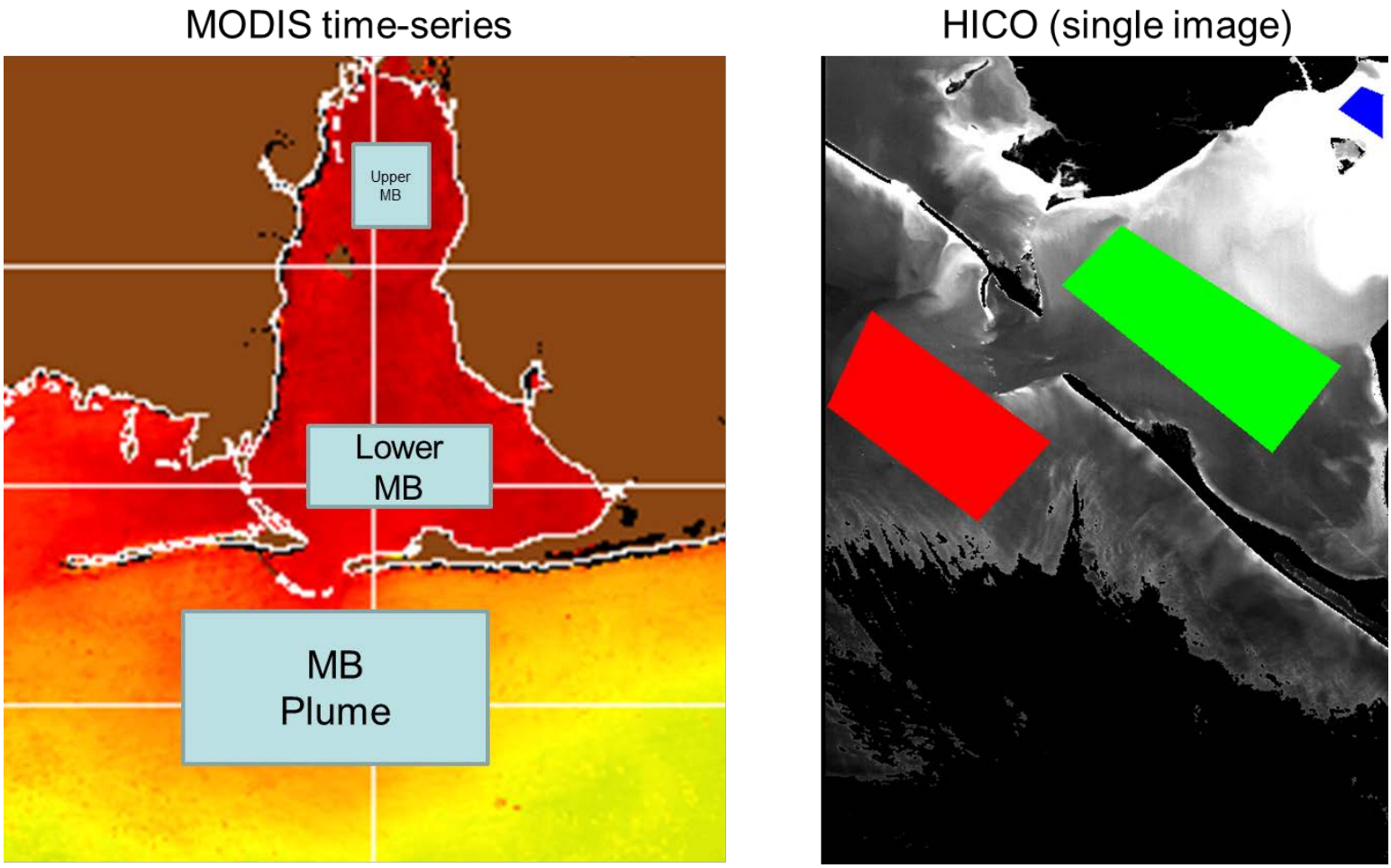

Figure 3-50. Locations of extracted pixels from MODIS weekly composite (12/3-12/10/2009) and HICO image(12/9/2009), for comparisons in Figure 3-51. All pixels in the subregions were averaged. Note that the same geographic areas are not exactly covered by the corresponding subregions in the two images.

MODIS (weekly mean, 12/3-12/10/2009) vs. HICO (12/9/2009)

Region	Property	MODIS time-series	HICO	|% Difference| (HICO – MODIS)
Plume	TSS	4.0	4.7	*17.5*
	PIM	3.1	3.9	*25.8*
	POM	1.0	0.7	*30.0*
	Zeu	11.0	9.0	*18.2*
	$K_d(488)$	0.63	0.61	*3.2*
Lower Bay	TSS	9.5	6.5	*31.6*
	PIM	8.1	5.6	*30.9*
	POM	1.4	0.8	*42.8*
	Zeu	4.5	6.6	*46.7*
	$K_d(488)$	1.68	0.96	*42.8*
Upper Bay	TSS	11.8	17.7	*50.0*
	PIM	10.4	16.7	*60.6*
	POM	1.4	1.0	*28.6*
	Zeu	6.1	3.1	*49.2*
	$K_d(488)$	1.89	2.14	*13.2*

generally increasing differences

TSS (mg/l) *PIM (mg/l)* *POM (mg/l)* *Zeu (m)* *K_d (m^{-1})*

Figure 3-51. Comparison of satellite-retrieved bio-optical properties from MODIS and HICO. MODIS values were extracted from the weekly composite image covering the day of the HICO image. Pixels extracted from the subregions shown in Figure 3-50. For each set of corresponding property values, differences between the two sensors generally increased northward from the plume to the Upper Bay.

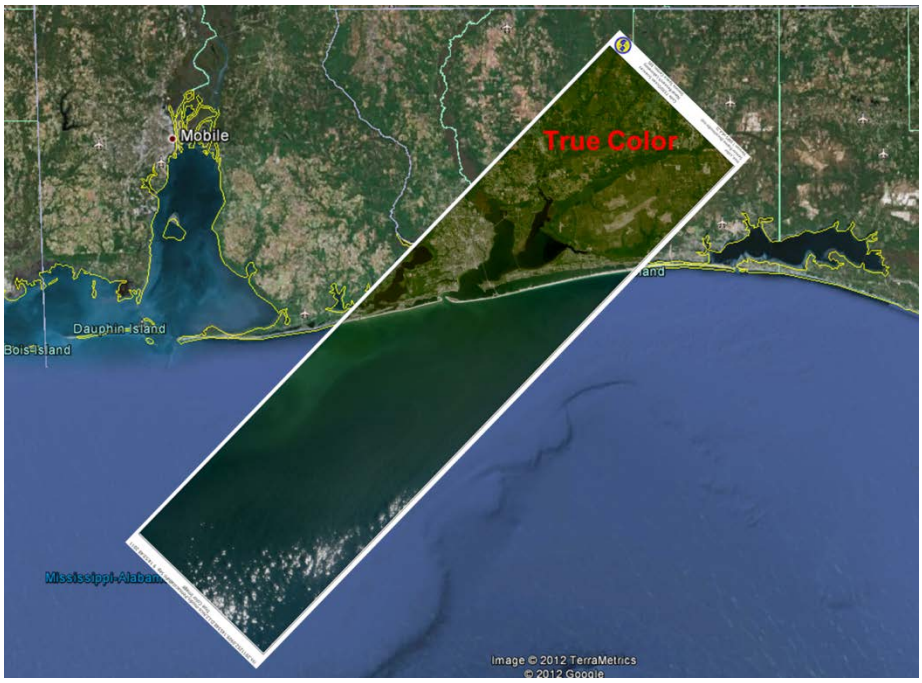

Figure 3-52. HICO image, 11 September 2011, Pensacola Bay, FL. True color image.

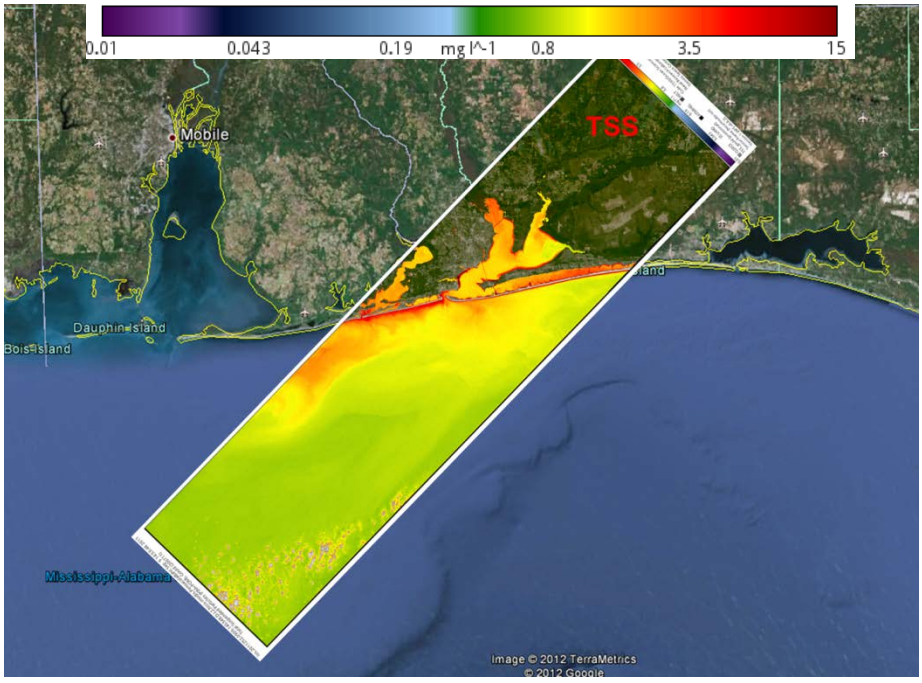

Figure 3-53. HICO image, 11 September 2011, Pensacola Bay, FL. Total Suspended Solids (TSS) concentration.

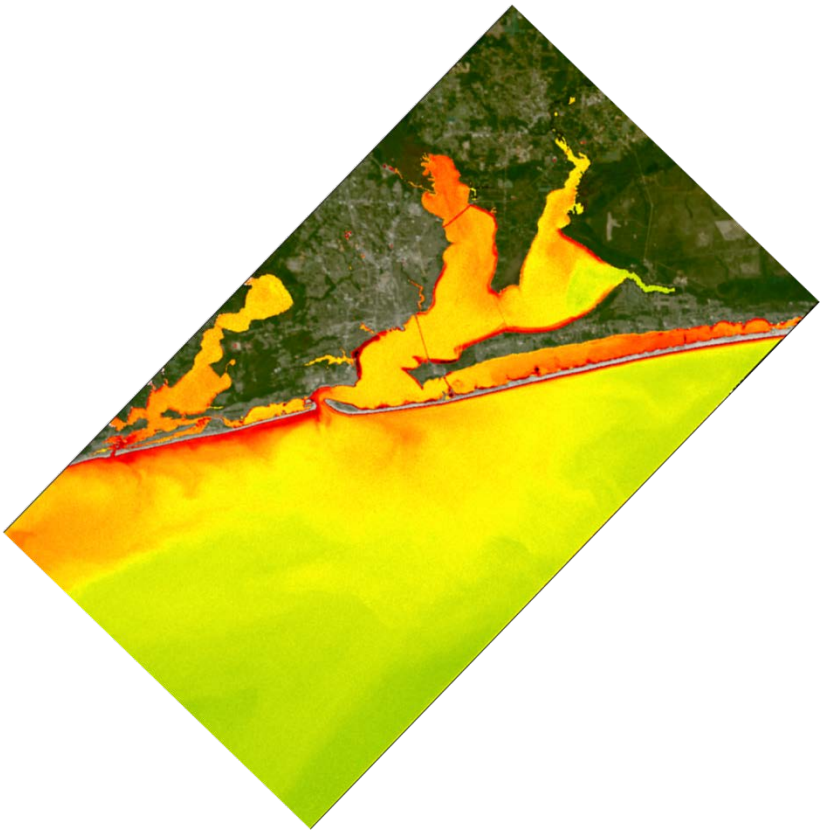

Figure 3-54. Zoomed image of Figure 53, showing coastal details. Total Suspended Solids (TSS) concentration.